

**BEHAVIOUR OF PARTIALLY ENCASED COMPOSITE
SLENDER COLUMNS**

By

Saima Ali

Student No.: 0409042328

A Thesis Submitted in Partial Fulfillment for the
Requirements of the Degree of
Master of Science in Civil Engineering



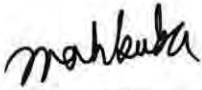
Department of Civil Engineering
Bangladesh University of Engineering and Technology, Dhaka

November, 2012

CERTIFICATION

The thesis titled “Behaviour of Partially Encased Composite Slender Columns” submitted by Saima Ali bearing student number 0409042328(P), session: April 2009 has been accepted as satisfactory in partial fulfillment of the requirement for the degree of Master of Science (Civil and Structural) on 17 November 2012.

BOARD OF EXAMINERS



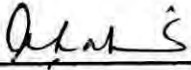
Dr. Mahbuba Begum
Associate Professor
Department of Civil Engineering
BUET, Dhaka-1000

Chairman
(Supervisor)



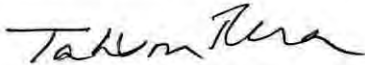
Dr. Md. Mujibur Rahman
Professor and Head
Department of Civil Engineering
BUET, Dhaka-1000

Member



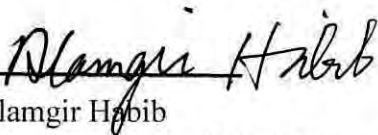
Dr. Ahsanul Kabir
Professor
Department of Civil Engineering
BUET, Dhaka-1000

Member



Dr. Tahsin Reza Hossain
Professor
Department of Civil Engineering
BUET, Dhaka-1000

Member



Dr. Alamgir Hossain
Ex-Professor, Dept. of Civil Engg. (BUET)
Professor (MIST)
Apartment 2A, House No. 124
BL.dg.Urban Heights, 9A, Dhanmondi, Dhaka

Member
(External)

CANDIDATES DECLARATION

It is hereby declared that this thesis or any part of it has not been submitted elsewhere for the award of any degree or diploma.

Saima

Saima Ali

ACKNOWLEDGEMENT

The work described in this thesis is carried out under the supervision of Dr. Mahbuba Begum, Associate Professor of Civil Engineering Department, Bangladesh University of Engineering and Technology, Dhaka. The author wishes to express her indebtedness and gratitude to her for her constant supervision, continuous guidance, helpful criticism, invaluable suggestions and unfailing encouragement given throughout the course of this work.

The author expresses her gratefulness to the Head, Department of Civil Engineering, BUET for providing all the computation facilities to materialize this work.

The author acknowledges the co-operation and help of the members of staff of Civil Engineering Department, BUET. Above all, the author expresses her gratitude to Allah to whom belongs ALL GLORY, WHO has wished this work to bring to reality.

Saima Ali

ABSTRACT

Partially Encased Composite (PEC) Columns consist of thin-walled built-up H-shaped steel sections with links welded near the flange tips and concrete cast between the flanges. This study presents the behaviour of slender partially encased composite (PEC) columns under eccentric axial load causing symmetrical single curvature bending. The load to deflection response of slender partially encased composite column is formulated using the Newmark's iterative procedure. The performance of the proposed numerical method is demonstrated by simulating the three slender PEC column tests from the literature. The ultimate capacity of the test columns are compared to that obtained numerically. The proposed numerical method is observed to predict the experimental results with good accuracy.

A parametric study is conducted using this method to identify the potential variables that can significantly affect the behaviour of slender partially encased composite column. Both the major and minor axis bending is considered to observe the significance of the selected parameters. The geometric properties that can greatly affect the behaviour of PEC columns include the column cross-sectional dimensions, length of the column, longitudinal spacing of the transverse links, thickness of the steel flange plates and initial load eccentricity. The effects of these parameters on the axial capacity, mid-height deflection and interaction diagram of the slender PEC column are studied. Among material properties, variation of concrete strength is considered.

The axial capacity of a partially encased composite columns are found to decrease significantly as the overall slenderness ratio increases, particularly for columns with slender plates. The effect of the ratio of initial load eccentricity to the overall depth of the column cross-section is observed to increase the lateral displacement of slender columns significantly and is found more pronounced for columns with higher L/d ratio. Besides, a reduction in load carrying capacity has been found with increasing the flange plate slenderness ratio. On the other hand, link spacing-to-depth ratio has negligible effect on the axial capacity and lateral deflection of slender PEC column. The axial capacity drops significantly in weak axis bending since lower stiffness is achieved here. Effect of overall column slenderness ratio, flange plate slenderness ratio and concrete strength are also studied on the P-M curve of the slender PEC column.

CONTENTS

Declaration	i
Acknowledgement	ii
Abstract	iii
Contents	iv

Chapter 1

INTRODUCTION

1.1 Background	1
1.2 Objectives of the Study	3
1.3 Scope of the Study	3
1.4 Organization of the Thesis	4

Chapter 2

LITERATURE REVIEW

2.1 Introduction	5
2.2 Behaviour of Short PEC Column	5
2.2.1 Experimental Investigations	5
2.2.2 Numerical Investigations	13
2.2.3 Capacity Prediction Models	20
2.2.3.1 Axial Capacity	20
2.3 Behaviour of Slender PEC Column	21
2.3.1 Experimental Investigation	21
2.3.2 Numerical Investigation	23
2.4 Conclusions	24

Chapter 3

METHODOLOGY TO FORMULATE LOAD DEFLECTION AND INTERACTION CURVE

3.1 Introduction	26
3.2 Behaviour and Analysis of Slender Column	26
3.3 Newmark's Method to Compute Second Order Deflection	29

3.3.1	Subdivision of Slender Column	29
3.3.2	Assumption of Deflection	29
3.3.3	Calculation of Total Moment	29
3.3.4	Determination of Curvature	31
3.3.4.1	Calculation of Effective Stiffness	31
3.3.5	Determination of Equivalent Nodal Force	33
3.3.6	Determination of Slope of the Deflected Columns	36
3.3.7	Determination of Lateral Deflection of Columns	36
3.4	Formulation of Load Deflection Curve and Ultimate Axial Load for Slender PEC Column	37
3.4.1	Load to Mid Height Deflection Curve	39
3.4.2	Formulation of Interaction Diagram for Short Column	40
3.4.3	Ultimate Axial Load	41
3.5	Formulation of Interaction Diagram for Slender PEC Column	42
3.6	Verification of Applied Numerical Method	43
3.7	Limitations of the Numerical Study	45
3.8	Conclusions	46

Chapter 4

PARAMETRIC STUDY ON PEC COLUMN UNDER STRONG AXIS BENDING

4.1	Introduction	47
4.2	Design of Parametric Study	47
4.2.1	Effect of Load Eccentricity Ratio (e/d)	48
4.2.2	Effect of Overall Column Slenderness Ratio (L/d)	54
4.2.3	Effect of Flange Plate Slenderness Ratio (b/t)	58
4.2.4	Effect of Link Spacing to Depth Ratio (s/d)	60
4.2.5	Effect of Slenderness Ratio on P-M Curve	62
4.2.6	Effect of Flange Plate Slenderness Ratio on P-M Curve	63
4.2.7	Effect of Concrete Strength on P-M Curve	64
4.3	Summary	65

Chapter 5

PARAMETRIC STUDY ON PEC COLUMN UNDER WEAK AXIS BENDING

5.1	Introduction	67
5.2	Design of Parametric Study	67
5.2.1	Effect of Load Eccentricity Ratio (e/d)	67
5.2.2	Effect of Overall Column Slenderness Ratio (L/d)	73
5.2.3	Effect of Flange Plate Slenderness Ratio (b/t)	76
5.2.4	Effect of Link Spacing to Depth Ratio (s/d)	78
5.2.5	Effect of Slenderness Ratio on P-M Curve	80
5.2.6	Effect of Flange Plate Slenderness Ratio on P-M Curve	81
5.2.7	Effect of Concrete Strength on P-M Curve	82
5.3	Conclusions	83

Chapter 6

CONCLUSIONS AND RECOMMENDATIONS

6.1	Introduction	85
6.2	Conclusions	86
6.2.1	Parametric Study under Strong Axis Bending	86
6.2.2	Parametric Study under Weak Axis Bending	87
6.3	Design Recommendations	87
6.4	Recommendations for Future Research	89
	References	90
	Appendix	92

LIST OF FIGURES

Figure 1.1	Typical cross-sections of composite columns	1
Figure 1.2	Cross-section and 3D view of partially encased composite column	2
Figure 2.1	Finite element mesh developed by Begum et al. (2007)	16
Figure 2.2	Experimental and numerical load to strain behaviour for concentric columns	18
Figure 2.3	Comparison of numerical and experimental failure modes for long PEC column	24
Figure 3.1	Forces in a deflected column	28
Figure 3.2	Load and moment in a column	28
Figure 3.3	Deflected shape of slender PEC column	30
Figure 3.4	Bending moment diagram of a column subjected to eccentric loading	30
Figure 3.5	Curvature diagram for slender PEC column	33
Figure 3.6	Equivalent nodal force at extreme corner point	33
Figure 3.7	Equivalent nodal force at interior point	34
Figure 3.8	Equivalent nodal force at mid height of slender column	35
Figure 3.9	Curvature diagram and equivalent nodal force on slender column	35
Figure 3.10	Slope of the deflected shape of column	36
Figure 3.11	Deflection of slender PEC column	37
Figure 3.12	Cross-section of a typical PEC column	38
Figure 3.13	Load deflection curve of slender PEC column	39
Figure 3.14	Determination of ultimate moment at a given eccentricity	41
Figure 3.15	Formation of interaction diagram of slender PEC column	42
Figure 3.16	Cross-section of PEC column	43
Figure 4.1	Effect of e/d ratio on axial load to lateral deflection curve of column P_b with L/d ratio of 15	51
Figure 4.2	Effect of e/d ratio on axial load to lateral deflection curve of	51

	column P_b with L/d ratio of 25	
Figure 4.3	Effect of e/d ratio on axial load to lateral deflection curve of column P_d with L/d ratio of 15	52
Figure 4.4	Effect of e/d ratio on axial load to lateral deflection curve of column P_d with L/d ratio of 15	52
Figure 4.5	Effect of e/d ratio on axial load of PEC column	53
Figure 4.6	Effect of e/d ratio on mid-height deflection of PEC column	53
Figure 4.7	Effect of L/d ratio on axial load to lateral deflection curve of column P_a with e/d ratio of 0.2	56
Figure 4.8	Effect of L/d ratio on axial load to lateral deflection curve of column P_b with e/d ratio of 0.2	56
Figure 4.9	Effect of L/d ratio on axial load to lateral deflection curve of column P_d with e/d ratio of 0.4	57
Figure 4.10	Effect of L/d ratio on axial capacity of PEC column	57
Figure 4.11	Effect of L/d ratio on mid-height deflection of PEC column	58
Figure 4.12	Effect of b/t ratio on axial load to lateral deflection curve of column P_a with e/d 0.2 and L/d 20	60
Figure 4.13	Effect of b/t ratio on axial load to lateral deflection curve of column P_a with e/d 0.3 and L/d 25	60
Figure 4.14	Effect of s/d ratio on axial load to lateral deflection curve of P_b column with e/d 0.2 and L/d 15	61
Figure 4.15	Effect of overall column slenderness ratio on interaction diagram of slender PEC column	62
Figure 4.16	Effect of flange plate slenderness ratio on interaction diagram of slender PEC column	63
Figure 4.17	Effect of concrete strength on interaction diagram of slender PEC column	64
Figure 5.1	Effect of e/d ratio on axial load to lateral deflection curve of column P_b with L/d ratio of 15	70
Figure 5.2	Effect of e/d ratio on axial load to lateral deflection curve of column P_b with L/d ratio of 25	71
Figure 5.3	Effect of e/d ratio on axial load to lateral deflection curve of column P_d with L/d ratio of 15	71

Figure 5.4	Effect of e/d ratio on axial load to lateral deflection curve of column P_d with L/d ratio of 15	72
Figure 5.5	Effect of e/d ratio on axial load to lateral deflection curve P_a with L/d ratio of 25	72
Figure 5.6	Effect of L/d ratio on axial load to lateral deflection curve of column P_a with e/d ratio of 0.2	74
Figure 5.7	Effect of L/d ratio on axial load to lateral deflection curve of column P_c with e/d ratio of 0.3	75
Figure 5.8	Effect of L/d ratio on axial load to lateral deflection curve of column P_d with e/d ratio of 0.2	75
Figure 5.9	Effect of L/d ratio on axial capacity of PEC column	76
Figure 5.10	Effect of L/d ratio on mid-height deflection of PEC column	76
Figure 5.11	Effect of b/t ratio on axial load to lateral deflection curve of column P_b with e/d 0.2 and L/d 30	78
Figure 5.12	Effect of b/t ratio on axial load to lateral deflection curve of column P_c with e/d 0.3 and L/d 25	78
Figure 5.13	Effect of s/d ratio on axial load to lateral deflection curve of P_b Column with e/d 0.2 and L/d 25	79
Figure 5.14	Effect of overall column slenderness ratio on interaction diagram of slender PEC column	80
Figure 5.15	Effect of flange plate slenderness ratio on interaction diagram of slender PEC column	81
Figure 5.16	Effect of concrete strength on interaction diagram of slender PEC column	82

LIST OF TABLES

Table 3.1	Geometric properties of slender PEC test columns	44
Table 3.2	Material properties of slender PEC test columns	44
Table 3.3	Comparison of experimental and numerical ultimate capacities of slender PEC columns	45
Table 4.1	Geometric properties of reference column	48
Table 4.2	Effect of load eccentricity ratio at slenderness ratio 15	49
Table 4.3	Effect of load eccentricity ratio at $L/d = 25$	50
Table 4.4	Effect of load eccentricity ratio at $L/d = 15$	50
Table 4.5	Effect of load eccentricity ratio at $L/d = 25$	50
Table 4.6	Effect of overall slenderness ratio on column P_a at $e/d = 0.2$	55
Table 4.7	Effect of overall slenderness ratio on column P_b at $e/d = 0.2$	55
Table 4.8	Effect of overall slenderness ratio on column P_d at $e/d = 0.4$	55
Table 4.9	Effect of flange plate slenderness ratio on column P_a	59
Table 4.10	Effect of flange plate slenderness ratio on column P_b	59
Table 4.11	Effect of link spacing to depth ratio on column P_b	61
Table 5.1	Effect of load eccentricity ratio at slenderness ratio 15	69
Table 5.2	Effect of load eccentricity ratio at $L/d = 25$	69
Table 5.3	Effect of load eccentricity ratio at $L/d = 15$	69
Table 5.4	Effect of load eccentricity ratio at $L/d = 25$	70
Table 5.5	Effect of load eccentricity ratio at $L/d = 25$	70
Table 5.6	Effect of overall slenderness ratio on column P_a at $e/d = 0.2$	73
Table 5.7	Effect of overall slenderness ratio on column P_c at $e/d = 0.2$	74
Table 5.8	Effect of overall slenderness ratio on column P_d at $e/d = 0.4$	74
Table 5.9	Effect of flange plate slenderness ratio on column P_b	77
Table 5.10	Effect of flange plate slenderness ratio on column P_c	77
Table 5.11	Effect of link spacing to depth ratio on column P_b	79

LIST OF SYMBOLS

A_c	Cross-sectional area of concrete
A_s	Cross-sectional area of steel shape
A_{se}	Effective cross-sectional area of steel shape
b/t	Width to thickness ratio of flange plate
b	Unsupported flange width
b_e	Full effective flange width
b_f	Full flange width
d	Depth of column cross-section
e	Initial load eccentricity
e/d	Initial load eccentricity ratio
E_c	Modulus of elasticity for concrete
E_s	Modulus of elasticity for steel
f_c	Compressive stress of concrete
L	Column length
L/d	Overall column slenderness ratio
M	Total moment at any segment
P_u	Peak load of the parametric column
s	Link spacing
s/d	Link spacing to depth ratio
t	Plate thickness
Δ	Second order deflection due slenderness of column
φ	Curvature corresponding to the total moment
I_s	Moment of inertia of steel shape
I_c	Moment of inertia of the concrete section
EI_{eff}	Effective stiffness of the composite section
λ_p	Column slenderness parameter
ν_s	Poisson's ratio of steel
n	Empirical factor used to relate effective flange width to actual flange width
R	Equivalent nodal force at station

f_{cu}	Measured uniaxial compressive strength of concrete
ϵ_{cu}	Axial strain of concrete at f_{cu}
F_{sh}	Stress at the onset of strain hardening of steel
F_u	Ultimate strength of steel plate
ϵ_y	Yield strain of steel
ϵ_{sh}	Strain at the onset of strain hardening of steel
ϵ_u	Strain at the ultimate strength of steel



CHAPTER ONE

INTRODUCTION

1.1 BACKGROUND

An innovative structure may be composed of various types of building materials. As building materials, steel has high tensile strength and ductility and concrete has high compressive strength, stiffness and good resistance to corrosion. With the method of composite construction, it is now possible to combine the positive features of steel construction and structural concrete, without having to accept the drawbacks. Steel-concrete composite columns can substantially improve the behaviour and cost efficiency of steel columns used in the construction of mid-rise and high-rise buildings. A steel concrete composite column is a compression member, comprising either a concrete encased hot-rolled steel section or a concrete filled tubular section of hot-rolled steel and is generally used as a load-bearing member in a composite framed structure. Typical cross-sections of composite columns with fully and partially encased steel sections and concrete filled tubular sections are illustrated in Fig. 1.1.

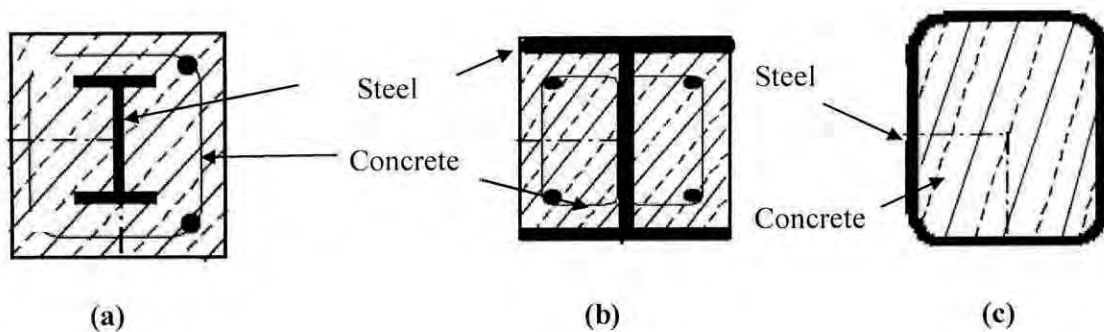


Fig.1.1: Typical cross-sections of

(a) Fully encased composite column (FEC), (b) Partially encased composite column (PEC) and (c) Concrete filled tubular sections (CFT)

Steel-concrete composite columns are very effective in providing the required stiffness to limit the lateral drift of the building to the acceptable level as well as to resist the lateral seismic and wind loads. The introduction of steel rolled shapes and high strength concrete has made it possible to design columns of large slenderness.

Partially encased composite (PEC) columns consisting of thin walled built up steel section with concrete infill cast between the flanges, is a relatively new concept in composite construction. Transverse links are provided between the flanges at regular intervals to enhance the resistance to local instability of the thin steel plates. Typical cross-section and 3D view of the steel skeleton of a PEC column is shown in Fig. 1.2. Additional longitudinal and tie rebars are sometimes provided in the encased concrete of this composite column to enhance the ductility of the column under cyclic loading.

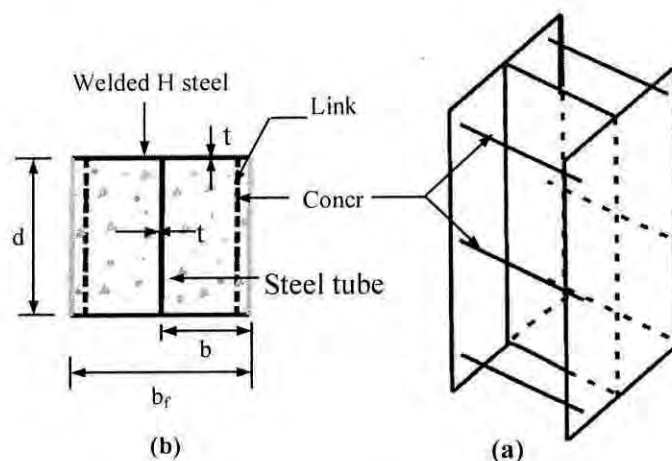


Fig.1.2: Partially encased composite columns, (a) cross section and (b) 3D view of the steel configuration

This innovative composite system reduces the cost of construction using relatively low-cost concrete by minimizing the use of higher cost steel. Besides, it also helps to overcome the complexities related to erection and design of connections of more commonly used composite columns. Several research works performed by Fillion (1998); Tremblay et al. (1998); Bouchereau & Toupin (2003); Prikett & Driver (2006); Begum et al. (2007) and Chicoine et al. (2002) on partially encased composite columns are manifested. Their research includes both numerical and experimental works. Their objective is to establish the behaviour and the design provisions for this new type of composite column under

various loading conditions. Short (length-to-depth ratio of 5) column behaviour of partially encased composite column section is the major focus included in these research works. Nevertheless, a few long column tests (length-to-depth ratio of 20) are carried out by (Chicoine et al. 2002) under static loading condition. This test database is not sufficient to establish design guidelines for slender PEC columns. Therefore, extensive research work is required to fully understand the behaviour of slender PEC columns under eccentric loading.

1.2 OBJECTIVES OF THE STUDY

The objectives of the study can be listed as,

1. To formulate the load to mid-height deflection curve for slender partially encased composite (PEC) columns using Newmark's numerical iterative procedure.
2. To construct the load to maximum moment curve and column strength curve (Interaction diagram) for slender PEC column, under symmetric single curvature bending.
3. To conduct a parametric study with a range of various geometric and material properties of this composite section under eccentric loading conditions.

1.3 SCOPE OF THE STUDY

The scope of the study are as follows:

1. In the analysis of slender partially encased composite column, cross-section of the column is taken as 450mm × 450mm.
2. To conduct a parametric study of this composite section under eccentric loading conditions, the column slenderness ratio is varied between 10 to 30 with intermediate values of 10, 15 and 25.
3. A wide range of load eccentricity ratio is considered to observe the significant effect of this parameter on the behaviour of slender PEC column. The values considered are 0.1, 0.2, 0.3, 0.4 and 0.5.
4. The eccentricities are applied about major as well as minor axis of the steel section of the composite column. This enables to cover the effect of second order moment on PEC columns about both major and minor axis bending, under single curvature bending.

1.4 ORGANISATION OF THE THESIS

The thesis is composed of six chapters. They are as follows:

- Chapter 1 provides an introduction to steel-concrete composite columns along with the objectives and scope of the research.
- Chapter 2 presents a comprehensive review on the literature related to both short and slender PEC column. This chapter elaborately focuses on the experimental and numerical research works carried out on PEC columns with thin walled built-up steel sections.
- Chapter 3 includes the detailed description of Newmark's method which is used as a numerical tool for the analysis of slender PEC column. This chapter also describes the formulation of load-deflection curve and the formation of interaction diagram for slender PEC column. Moreover, the performance of the developed nonlinear numerical iterative procedure for predicting the behaviour of slender PEC column is presented in this chapter.
- Chapter 4 presents the detailed parametric study conducted with the developed numerical tool to cover the range of several geometric and material parameters on the behaviour of slender PEC column. The detailed study presented herein is carried for bending about the strong axis of slender PEC column.
- Chapter 5 includes the parametric study regarding bending about weak axis of slender PEC column. In this chapter, similar geometric and material parameters are considered as in the previous chapter. The findings of the parametric study along with a comparative observation with the major axis bending are demonstrated in this chapter.
- Chapter 6 summarises the study performed, gives the important conclusions based on of major findings of the research and finally recommendations for future work is also provided in this chapter.

LITERATURE REVIEW

2.1 INTRODUCTION

A partially encased composite (PEC) section is referred to as H-shaped steel section with concrete infill between the flanges. To better understand the behaviour of the PEC column with a thin walled steel section, on which the current study is being conducted, a review of the experimental investigations related to this composite system is presented in this chapter. Besides, a brief review of the literature on PEC columns conducted by finite element analysis of PEC columns is also included to achieve a complete picture of the works on this type of composite section.

2.2 BEHAVIOUR OF SHORT PEC COLUMN

2.2.1 Experimental Investigations

Extensive experimental research is conducted on thin walled short PEC columns with built up section by several research groups. Among these the work carried out by Fillion (1998), Tremblay et al. (1998), Chicoine et al. (2000, 2003), Bouchereau and Toupin (2003), Prikett and Driver (2006) has been remarkable. A large number of tests were performed on short PEC columns constructed with normal strength concrete subjected to eccentric and axial loads, including static and cyclic conditions. Short PEC columns with high performance concrete were also tested under pure axial compression as well as combined axial and flexural compression.

The first series of test on short PEC columns was performed by Fillion (1998) and Tremblay et al. (1998) on specimens with 300mm × 300mm and 450mm × 450mm cross-sections. The specimens were of a length of five times the cross-section dimension and were loaded under axial compression. The test program included ten tests on bare steel

column and seven tests on composite columns with different transverse link spacing and flange slenderness ratios.

To study the possible size effect on the behaviour of short PEC columns, Chicoine et al. (2000) tested five 600mm × 600mm concentrically loaded columns and compared them with the first series of test on short PEC specimens which was performed by Tremblay et al. (1998). They also varied the transverse link spacing and flange slenderness ratio to study their influences on column behaviour. One of the five composite specimens was provided with additional reinforcement in the form of longitudinal and transverse rebars in the concrete. Local flange imperfections between the transverse links were measured on the steel section of these test specimens. It is observed that the inward imperfection measurements outnumbered the outward ones with a ratio of 18:1 on the 600mm specimens. The tendency of the flange to bow inward was attributed to the fabrication process used for the specimens, which is influenced by the shrinkage of the web to flange welds. The maximum amplitude of the measured local imperfections in these test specimens varied from 0.39mm to 2.02mm. The residual stresses in the steel plate of these test specimens were also evaluated before the test.

The results of these tests showed that the bare steel PEC columns failed due to local buckling in the flanges and the web, while the failure of the composite columns occurred by a combination local buckling of the steel flanges between the transverse links, yielding of the steel and crushing of the concrete. Usually local buckling occurred at or near the peak load, depending on the slenderness of the flange plates and link spacing. For columns with relatively wider link spacings, local buckling was observed to occur between 75% and 80% of their ultimate loads.

The load to deformation responses was studied for the test specimens to evaluate the influence of the column size, plate slenderness ratio, link spacing and additional reinforcements. The test results on 300mm, 450mm and 600mm short column specimens with equal plate slenderness and link spacing, demonstrated that the 450mm and 600mm specimens behaved in a similar manner while the 300 mm specimens exhibited a more gradual failure with the same post-peak response. It was also reported that the specimens with higher b/t and s/d ratios exhibited a faster degradation of post-peak strength than columns with lower b/t ratios and smaller link spacings. However, the load to deformation

response before the ultimate load did not vary much from one specimen to another since it remained elastic until near the peak. The additional rebar had a negligible impact on the ultimate capacity of the column, but significant improvements were observed in the ductility of the post-peak response. During the tests, the longitudinal and transverse strains in the steel shape and transverse links were measured from which the corresponding stresses were calculated. The strain measurement in the flanges indicated that the flanges were bending outward slightly between the links and the web. However, the transverse stresses in the flanges and the web of the steel shape due to the lateral expansion of concrete were found to be small and did not affect the axial capacity of the column. On the other hand, the lateral expansion of concrete was observed to induce high tensile stresses in the transverse links. The stresses in the links were observed to be doubled when the link spacing was halved, as a result of the better confinement of concrete near the exposed face. Chicoine et al. (2000) reported weld failure between the transverse links and the flanges in three of the composite test specimens. It was recommended that the links be welded to the flanges to develop their full yield capacity.

Chicoine et al. (2003) investigated the effects of construction loading sequence and long term loading on the behaviour of PEC columns by testing seven short composite columns with $300\text{mm} \times 300\text{mm}$ and $450\text{mm} \times 450\text{mm}$ cross-sections. Four of these specimens were loaded for 150 days, following a typical construction sequence. The rest were without any long term loading since they were used to assess the effect of shrinkage strain in the steel and concrete. The specimens under long-term loading, showed similar behaviour to that observed in the short term loading tests by Chicoine et al. (2000). The stress conditions before loading to failure was observed to have no influence on the ultimate capacity and failure mode of these columns.

Bouchereau and Toupin (2003) conducted tests to investigate the behaviour of short PEC columns subjected to axial compression and bending under monotonic and cyclic loading conditions. A total of 22 tests on 2250mm long columns and two tests on 5000mm long beams were performed. Two types of specimens were used, one without additional reinforcement and the other with reinforcing steel in the form of longitudinal and transverse rebars. Both types had a square cross-section of $450\text{mm} \times 450\text{mm} \times 9.53\text{mm}$. A link spacing of 300mm was used in all the test columns. The loading conditions imposed in the tests were selected based on the flexural demand on PEC columns when used in

concentrically braced structures subjected to design level earthquake motions. To evaluate this demand, a nonlinear seismic dynamic analysis was carried out by the researches on a 16 and 24 storey braced frame building. The results of this study revealed limited flexural demand on gravity columns with considerably larger bending moments on the columns of the bracing bents.

The test program was mainly designed to simulate the conditions of a column of the bracing bents subjected to monotonic and cyclic eccentric axial loads. In each case, the effect of strong and weak axis bending was investigated for two different values of load eccentricity. The effect of cyclic lateral loading with monotonic axial load on PEC columns was also explored for both strong and weak axis. In addition, two columns were tested under monotonic concentrated loading only, the results of which were used as reference values for other tests performed by Bouchereau and Toupin (2003). They reported that the occurrence of local buckling and concrete crushing was essentially simultaneous in all of the eccentrically loaded test specimens. The specimens with weak axis bending exhibited brittle and explosive failures as compared to other specimens. However, the presence of additional reinforcement in the specimens under weak axis bending is observed to improve the behaviour of these columns significantly. The additional reinforcement was also increased the ultimate capacity of the PEC columns by an average of 8% as observed by Bouchereau and Toupin (2003). Comparing the results of cyclic tests to corresponding monotonic tests, no significant differences in the column behavior were observed.

Bouchereau and Toupin (2003) reported that the cycles of loading was no deleterious effect on the ultimate capacity. It improved the capacity obtained under monotonic loading conditions by about 4%. No significant differences were observed in the post-peak load to displacement response between cyclically and statically loaded PEC columns. Bouchereau and Toupin (2003) also constructed load-moment interaction diagrams for PEC columns with normal strength concrete and validated the curves against test results. The interaction diagrams were developed using the methods typically adopted for reinforced concrete columns, assuming a linear strain distribution across the cross-section. They did not include the effect of local flange buckling, residual stresses in the steel section or confinement of concrete in calculating the load-moment interaction diagrams for PEC columns with normal strength concrete. Very good agreement was observed between the

test and predicted capacities. However, the capacities of two test columns with weak axis bending without additional rebars were lower than the predicted from the interaction diagram by 10 to 15%. They explained this inconsistency by noting the sensitivity of these columns to unexpected test conditions such as accidental eccentricity, improper installation or defects during the fabrication process.

Prikett and Driver (2006) conducted a comprehensive experimental research project to study the behaviour of thin walled PEC columns made with high performance concrete. The study included 11 short PEC columns measuring 400mm × 400mm × 2000mm, with the primary variables being the concrete type, link spacing and load eccentricity. The plate slenderness ratio was constant ($b/t = 25$) for all of the test columns. The specimens were divided into two groups. The first group consisted of seven specimens subjected to axial compression only. Three different link spacing and three types of concrete (normal strength, high strength and high strength steel fiber reinforced concrete) were used in these specimens. Two normal strength concrete columns with different link spacings were used as reference specimens. Steel fibers were used to observe potential improvement in the failure mode of PEC columns with high strength concrete.

Four identical PEC columns constructed with high strength concrete and subjected to axial compression and bending were tested in the second group of specimens by Prikett and Driver (2006). Bending axis and the amount of load eccentricity were varied to determine the effects of these parameters on the column behaviour. Initial local imperfections in the flange plate were measured at several locations in the steel sections for all 11 test specimens. The local imperfections in the flanges were observed to be inwards in most locations, with an average maximum amplitude of approximately 1.5mm. Additional measurements of the local flange imperfections were performed after the columns were casted and no significant differences were observed. The column behavior was examined by considering the failure mode, load to strain response and a transverse stresses in the steel plates. The high strength concrete PEC columns failed in a similar manner to the PEC columns with normal strength concrete. Concrete crushing was also combined with local flange buckling. However, the failure of a high strength concrete column was observed to be sudden as compared to an equivalent PEC column with normal strength concrete. Addition of steel fibers in the high strength concrete was found to improve the failure mode of the columns somewhat. They reported no local buckling prior to the peak

load in any of the concentrically loaded test specimens, even for the specimen with a link spacing equal to the depth of the column. However, no of the eccentrically loaded specimen experienced local buckling at 90% of the peak load. The effect of confinement, as revealed by transverse stresses in the steel section, on the capacity of high strength concrete PEC column was similar to that observed for the normal strength concrete PEC columns.

However, the steel section of columns with high strength concrete yielded sooner relative to the peak load as compared to the steel section of the columns with normal strength concrete. The axial capacity of the high strength concrete PEC columns was not significantly affected by the confinement of concrete and therefore Prikett and Driver (2006) recommend that confinement not be accounted for the design of these columns. The maximum stresses in the links were well below the yield stress and therefore it was recommended by the researches that the current design requirements for link cross-sectional area and welding in CSA standard S16-01(CSA 2001) satisfactory for high strength concrete PEC columns under concentric and eccentric loading conditions.

Prikett and Driver (2006) also studied the moment to curvature response and developed load to moment interaction diagrams for the eccentrically loaded specimens. The moment to curvature curves for specimens with strong axis bending showed a gradual decline of the peak moment as compared to the sudden decline observed in the specimens with weak axis bending. To predict the capacity of the eccentrically loaded columns, the load to moment interaction diagrams were developed using the methods used for reinforced concrete columns. The effect of the flange local buckling was included by using an effective area of the steel flange in the compression zone. In general, the interaction curves provided a good and conservative estimate of the ultimate cross-sectional capacities of the eccentrically loaded PEC columns obtained from the tests. Four columns with strong axis bending, the capacities obtained from the test exceeded the predicted capacities by 17 to 27%, whereas for columns with weak axis bending, the predicted capacities were exceeded by only 4 to 9%. Prikett and Driver (2006) attributed this discrepancy to the fact that the concrete confinement, which was neglected in predicting the column capacities, had a more pronounced effect on the column under strong axis bending than on those under weak axis bending. The presence of a steel flange on the face that experiences

maximum compression provided more favorable confinement condition than either columns under weak axis bending or those loaded concentrically.

Deng (2008) researched on a half size two storey one bay steel plate shear wall specimen, with PEC columns as the boundary elements. The test was done under vertical and cyclic lateral loads to study its behaviour. The overall size of the PEC column was 250mm × 250mm, with the same dimension for the flange width and the column depth, which was chosen to provide enough column stiffness for anchoring the tension field in the infill panels. Thickness of the PEC column was 6.35mm and the corresponding flange width to thickness ratio is 19.7. For attachment of perpendicular beams framing into the PEC columns, side plates were welded between the flange tips at each floor level. The thickness of the side plates was 12.7mm and the height of the side plates was designed to simulate real construction so the forms used in the first storey could be re-used in the second storey. Round bars with a diameter of 10mm were used as links welded near the PEC column flange tips to delay local buckling of the column flanges and to provide some confinement for the encased concrete. A relatively large link spacing of 160mm was used in the middle portion of the column. Initial imperfections in the PEC column were treated negligible as the flange deformation was towards the concrete infill between links. To study the behaviour of the PEC columns subjected to both frame action forces and forces due to tension field in the panel, fully plastic moment connections were used at all the beam to column joints. As vertical load, 720kN was applied on each PEC column which was about 26.9% of the factored axial compressive capacity of the composite column or about 19.5% of the unfactored axial compressive capacity. Quasi static, cyclic lateral loading was utilized as the testing technique to conduct the experiment, which means cyclic loads or deformations would be applied on the specimen in a slow, controlled and predetermined manner.

Tearing was initiated from the outside flange tips at the bottom of the columns due to the combination of frame action and anchorage force from the infill panel. Repeated local buckling of the column flanges and loss of concrete in the region was hastened the propagation of the tear through the flange tips towards the web and eventually the tear opened through the entire outside flanges. As the specimen was further loaded, the opening in the column outside flanges tore into the column webs towards the infill panel until the test is terminated. At the end of the test, the width of the opening at the outside

flanges was approximately 20mm for both columns. One additional tear was initiated at the crest of the flange local buckle above the bottom side plate where the flange plate curvature was severe due to extensive localized loss of concrete.

Dastfan (2011) did two large scale tests on steel plate shear walls with built up PEC columns. The research was consisted of an experimental study on the behaviour of two large scale two-storey steel plate shear walls with PEC columns with built up H-shaped steel section. The main objective of the experimental program of was to study the behaviour of PEC columns in the steel plate shear wall system, the columns were subjected to concurrent axial force and bending moment. One of the test specimens was modular and the other one used reduced beam sections in the frame. Another objective of the experimental program was to examine the modular construction method in one of the specimens and the RBS connections in the other specimen.

The modular specimen had an overall height of 4120mm and an overall width of 2690mm, excluding the base plate. Stories were 1900mm high and the column centerline spacing was 2440mm. The thickness of the infill panel was 3mm. The PEC columns were 450mm × 450mm in cross section and the thickness in the flanges and webs of both columns were 6.35mm. As large bending moments were expected at the base of the columns, links were placed closer to postpone the buckling of the flanges. At the base of the column, link spacing was at least 50mm.

Gravity loads were applied to the tops of the columns equally through a cross-shaped distributing beam. A constant gravity load of 600kN was applied on top of each column to represent the service gravity loads during the earthquake. The lateral load was applied through two sets of actuators, which were supported by a reaction wall. To avoid local failure of the PEC column due to the loading mechanism itself, a lateral load transition system was used at each floor to transfer lateral loads from the actuators to the top flanges of the floor beams. Lateral loads were applied to each floor equally.

During the gravity load application, no buckling was detected in the flanges of the columns. The infill plates had an initial out-of-plane displacement in both stories and so there was no buckling visible during the gravity load application. The concrete in the columns did not crack or crush which indicated essentially elastic behaviour in that stage.

The PEC columns fractured in a ductile manner at their base due to the presence of longitudinal reinforcing bars in the columns. Although the specimen suffered from several regions of tearing in the infill plate and the complete tearing of the outer flanges of the columns, there is no sudden decrease in strength of the specimen. Dastfan (2011) recommended that the specimen was highly redundant and capable of changing the load path in case of local failures. Therefore, the specimen configuration was adopted as an excellent option for resisting lateral loads.

The steel plate shear wall with PEC columns and RBS connections showed good overall performance under quasi-static cyclic lateral load. The RBS test specimen exhibited good post-peak performance and ductility. The displacement ductility of the specimen when it reaches its peak strength was 4.0 and 90% of the peak strength in the post-peak stage, the ductility of the specimen is 6.2. The amount of energy dissipated by the RBS specimen increased as the deformation increased throughout the test. Dastfan (2011) recommended that the specimen possessed all the characteristics of an efficient lateral load resisting system. Besides, the failure of PEC columns at the base was gradual and the crushing of concrete happened almost immediately after the specimen reached its maximum strength.

In both the experiments, the presence of longitudinal rebars at the bases of the columns improved the overall behaviour of the specimens. A stress concentration was observed in the concrete at the end of the longitudinal rebars. The outer flanges of the columns buckled in the region during both tests and in the modular test, the concrete crushed in this region. It is recommended by Dastfan (2011) that the link spacing be reduced in this region to improve the performance of this region. In addition Dastfan (2011) recommended that the use of more ductile concrete, like fiber-reinforced concrete, at the bases of the PEC columns might help postpone the crushing of concrete and improve the ductility of the hinge region.

2.2.2 Numerical Investigations

Numerical investigations on short PEC column were done by Maranda (1999), Chicoine et al. (2002) and Begum et al. (2007). All the researchers conducted finite element analysis to study the behaviour of PEC column.

The first reported numerical study on PEC columns with built up steel sections was carried out by Maranda (1999). The finite element model included a quarter of the cross-section between two links and in the modeling, the imperfection of the flanges, residual stresses in the steel section and contact elements between steel and concrete were addressed. The average numerical peak load obtained from this model was more than the experimental study peak loads, as reported by Tremblay et al. (1998). In some cases, the peak load was not reached as the stiffness at the last converged point was observed to be positive.

Chicoine et al. (2002) performed a finite element analysis using ABAQUS to produce numerically the behaviour of the composite column near the peak load, modes of failure and the stresses in the web of the steel shape and in the transverse links. The model was verified and calibrated against the experiments performed on short term load tests on short PEC columns subjected to gravity loading only. The researchers also studied the effects of loading sequence and long term loading on the PEC column using the numerical model by simulating the long term tests on short PEC columns. Chicoine et al. (2002) modeled a quarter of the column cross-section with a length of one link spacing. The finite element model was developed using S8R shell elements for the steel section, C3D20R brick elements for concrete and B32 beam elements for the transverse links. Two node spring elements were used to represent the interaction between steel and concrete at their common surface. The stiffness of these elements was adjusted to simulate the local buckling of the flange and the separation between steel and concrete as the loading progresses. Very high compressive stiffness was defined for the springs to prevent inward buckling of the flange plate due to the presence of the concrete. On the other hand, very low tensile stiffness was given to allow the flange to buckle freely in the outward direction. To simulate the perfect bond between the transverse link and concrete, all nodes of the link were coupled to adjacent concrete nodes in the axial direction of the link.

Steel material behavior was represented by a bilinear stress-strain curve based on the typical stress-strain curves obtained from tension coupon tests of the plates used in the column specimens. The mechanical properties of concrete were defined using an effective compressive strength and an effective elastic modulus.

The cracking model in ABAQUS was used by Chicoine et al. (2002) to represent the concrete material behaviour in PEC columns. The local imperfections were included by

applying a deformed shape corresponding to the first buckling mode obtained from an eigenvalue buckling analysis on the bare steel section with a length of one link spacing. The model also includes the residual stresses defined as initial conditions in the steel plates. Chicoine et al. (2002) used the Riks displacement control technique to simulate the applied loading conditions in the test specimens. Therefore an implicit solution strategy was implemented to trace the overall column behaviour throughout the applied displacement history.

The finite element model developed by Chicoine et al. (2002) provided a very good representation of the ultimate capacity and load to displacement response of short PEC test specimen up to the ultimate load. The mean experimental to numerical peak load ratio is observed to be 1.0 with a standard deviation of 0.03. The numerical model overestimated the experimental strain at peak load by 5% on average. The post peak response of the columns was obtained only over a short deformation range due to convergence problems experienced by the numerical model. This can be attributed to the inadequacy of the implicit solution method for representing the highly nonlinear post-peak behaviour. However, the ultimate point was observed to be passed successfully since the post peak stiffness in all the analysis is negative. The numerical failure mode in axial compression was identical to the experimental one, with local buckling of the flange occurring outwards in a single wave between links.

Begum et al. (2007) developed a more sophisticated mode of the whole PEC column. The model used in the study of the short PEC column is shown in Fig. 2.1. The model was selected based on the observed failure mode in the experiments on concentrically loaded specimens and the symmetric agreement of the transverse links along the height of the column.

Four node finite strain reduced integration shell elements were used to model the flange and web of the steel shape. A sensitivity analysis was performed with this element to optimize the mesh in order to produce proper representations of local buckling of the steel flange. In modeling the web and flange plates of a specimen, seven elements were defined along the half width of the plates. At the corner, narrow elements with a width equal to one-half the thickness of the plates are defined to match the mesh of the steel plates with that of the concrete.

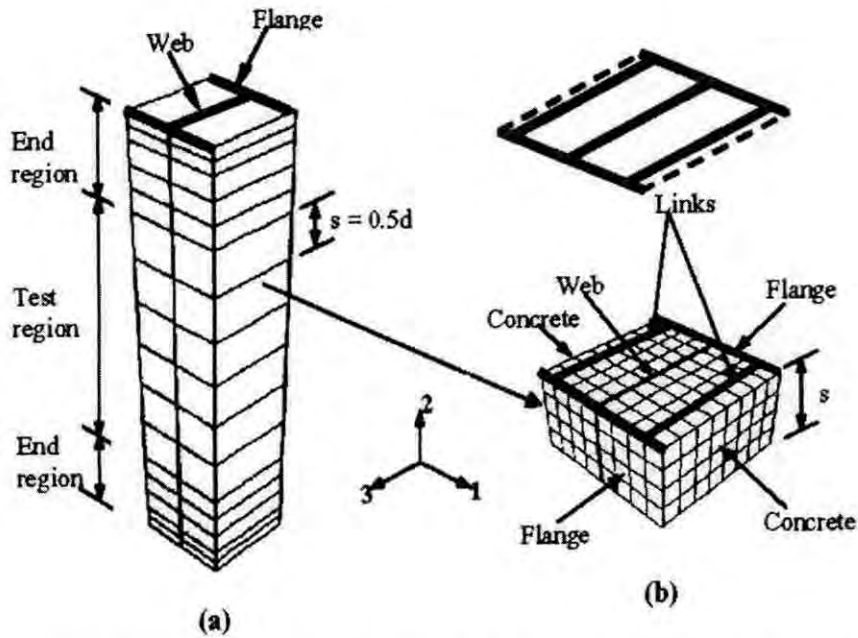


Fig. 2.1: Finite element mesh developed by Begum et al. (2007), (a) Typical short column displaying the parts between consecutive links (b) Mesh configuration of a typical part in the test region of the column

The concrete infill was modeled with eight-node reduced integration brick elements using a 6×6 mesh over the quarter cross section. The number of brick elements in the longitudinal direction was equal to the number chosen for the steel plates. The transverse steel link was modeled using two node beam elements and was meshed in such a way so as to match the nodes of the concrete elements of the column. The extended model of the column was initially in several parts, each with a unique link spacing and compressive strength of concrete. At the common interface between two adjacent parts in the model, the corresponding nodal degrees of freedom were linked using multipoint constraints to ensure compatibility. The interface of the steel flange and the encased concrete was modeled using a friction type master-slave contact. The tensile bond between the contact surfaces was defined as zero. Symmetry boundary conditions are applied along the planes of symmetry of the models. A displacement control technique was used to apply the axial compression to the top surface of the model. To avoid local failure near the top of the column due to the applied loading, no separation was permitted between the flange plate at the top segment of the column and the adjacent concrete surface. Both material and geometric nonlinearities caused by large rotations were accounted for in that finite element model.

A finite element model including the full cross section and full height of the test specimens was developed to produce the combined effect of bending moment and axial load. Four of the eight eccentrically loaded specimens had additional steel reinforcement. The rebars were modeled using two node three dimensional truss elements and were embedded within the concrete. The end plates were modeled using rigid body surfaces. The top and bottom rigid planes were fixed to the adjacent nodes of the composite cross section. The load and the end boundary conditions were applied through the rigid body reference nodes. The damage plasticity model in ABAQUS was used to simulate the concrete material behaviour in the PEC columns. The model was a continuum, plasticity based damage model for concrete. The damage plasticity model used a non-associated plastic flow rule. The uniaxial compressive stress-strain response of concrete was assumed as linear up to 30% of its compressive strength.

Local imperfections in the column were defined as the out-of-straightness of the steel flange between two consecutive transverse links. The inward imperfection of the flange plate was expected to improve the resistance to local buckling of the columns. On the other hand, outward imperfection was expected to decrease the local buckling capacity of the flange plate. The residual stresses in the steel plates were modeled as initial stresses in each element of the flange and web. It is considered constant along the height of the numerical model. To determine the post peak response of the PEC composite system, an explicit dynamic solution strategy was selected. The explicit strategy determined the solution without iteration by explicitly advancing the kinematic state over small time increments. All the test specimens selected in the study are loaded quasi-statically. To simulate the quasi-static process using a dynamic explicit solution method, the load was applied using smooth amplitude displacement history. In full model, a loading rate of 15mm/s was used for columns with strong axis eccentricity and 8mm/s was used for columns with weak axis eccentricity.

To obtain a quasi static response, the duration of applied displacement and the value of mass scaling were chosen through an iterative process. To evaluate whether or not the numerical models were producing a quasi static response, the energy history was studied. The numerical analysis results of the small model were found to be in good agreement with the experimental results in the prepeak zone for concentrically loaded column. For

eccentrically loaded column also the numerical behaviour of the selected specimens was observed to be in good agreement with the experimental response. The mean value of peak load ratios is 0.99. Fig. 2.2 shows the results of concentrically loaded columns.

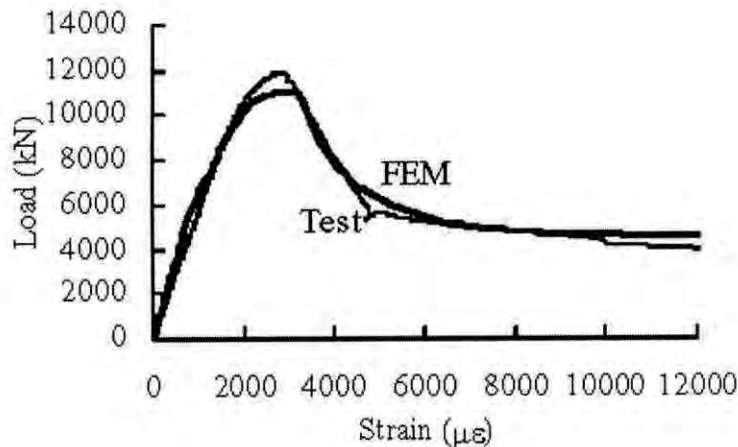


Fig. 2.2: Experimental and numerical load to strain behaviour for concentric column
(Begum et al. (2007))

But near and after the ultimate load, the strains obtained from the model were found to be higher than those obtained experimentally. This was mainly due to the local buckling of the thin flanges followed by separation of concrete and steel surfaces.

For all specimens, after the ultimate point the steel plates carried most of the load as the concrete softened quickly after reaching the crushing strength. Moreover, it was found that the specimen with a link spacing equal to half of the column depth exhibited gradual failure as compared to the specimens with a link spacing equal to the column depth. Besides, when link spacing equal to the depth of the column, inward imperfection with a maximum amplitude of 2mm increased the capacity only 0.36%, whereas the same amplitude of outward imperfection resulted in a 2.03% reduction in the ultimate capacity. When link spacing equal to half of the column depth, inward imperfection of 1mm resulted in a 0.69% increase in capacity and the same amplitude of outward imperfection decreased the capacity by 1.19%. The failure in all the analysis observed in the numerical analysis was due to the initiation of local instability of the flange plate between two transverse links followed by crushing of adjacent concrete. In all cases failure mode is matched with that observed in the experiments.

Deng (2008) conducted a research work on a half size two storey one bay steel plate shear wall specimen, with PEC columns as the boundary elements. A finite element model of the specimen was developed and loaded in a pushover analysis with a dynamic explicit solution strategy in ABAQUS. The finite element model for PEC column developed by Begum et al. (2007) was adopted in the numerical study by Deng (2008).

In finite element analysis, the ultimate capacity of the model was found as 1670kN which is 8% lower than that of the test result. In the model, double curvature was observed in both columns, with the point of contraflexure located at a higher position in the compression column than in the tension column. The model provided good prediction of moment. The internal forces in the columns from the model and the test were close until the first floor deflection reached 21mm. The differences between the internal forces in the columns obtained from the model were affected by the difference in the stress distribution in the panel between the model and the test due to the difference between the monotonic loading with the modified material curve and the cyclic loading with the original material curve.

Dastfan (2011) performed a numerical study on steel plate shear wall with PEC column. A study was done to develop the end-panel flexibility parameter and also the column flexibility parameter. In order to determine the upper limit of the end-panel flexibility parameter, an extensive parametric numerical study was conducted. The numerical study covered various parameters like panel aspect ratio (L/h), infill plate thickness and size effect. In order to investigate the effect of the beam to column connection rigidity on both column flexibility parameter and end panel flexibility parameter, a numerical study was conducted on full-scale models with various panel aspect ratios and infill plate thickness.

A linear elastic model created with SAP2000 showed that the initial stiffness of the first storey of the steel plate shear wall was 158kN/mm. Besides, initial stiffness of the first storey of the frame was 26.5kN/mm. Dastfan (2011) recommended that the contribution of the frame in the overall lateral stiffness of the test specimen was approximately 15% in the initial stage. The contribution of the frame in the overall lateral stiffness of the system reduced as test progressed and the columns suffered from tearing of their flanges and crushing of concrete at their base.

2.2.3 Capacity Prediction Models

The experimental and numerical investigations on PEC columns with built-up sections led to the development of a capacity prediction model for these columns.

2.2.3.1 Axial Capacity

In PEC column with built-up section, compressive cross-sectional strength of the PEC column was calculated using the following expression proposed by Tremblay et al. (1998), with modifications from the work of Chicoine et al. (2002)

$$C_r = (A_{se} F_y + 0.92 \psi A_0 f_{cu} + A_r f_{yr}) \quad (2.1)$$

where, A_{se} is the effective area of the steel shape as defined by Equation (2), F_y is the yield strength of the steel plate, A_0 is the cross sectional area of concrete, f_{cu} is the concrete slender strength and A_r and F_{yr} are the area and yield strength of the longitudinal rebars.

$$A_{se} = (d - 2t + 2b_e)t \quad (2.2)$$

Where, d is the overall depth of the cross-section, t is the thickness of the steel plates and b_e is the total effective width of the flange. To account for the effect of local buckling in the column capacity, b_e is expressed as,

$$b_e = \frac{b_f}{(1 + \lambda_p \frac{2n}{p})^{1/n}} \leq b_f \quad (2.3)$$

$$\lambda_p = \frac{b}{t} \sqrt{\frac{12(1 - \nu_s^2)F_y}{\pi^2 E_s k}} \quad (2.4)$$

$$k = \frac{0.9}{(\frac{s}{b_f})^2} + 0.2(\frac{s}{b_f})^2 + 0.75, \quad (0.5 \leq \frac{s}{b_f} \leq 1) \quad (2.5)$$

In Equation (2.3), b_f is the full width of a flange plate and λ_p is a slenderness parameter calculated using Equation (2.4). E_s and ν_s in Equation (2.4) are the elastic modulus and

Poisson's ratio respectively of steel. The value of the factor n in Equation (2.3) is taken as 1.5 as proposed by Chicoine et al. (2002). Equation (2.1) and (2.4) are included in CSA S16-01 (CSA 2001) for determining the design capacity for axially loaded PEC columns with built-up thin walled shapes, but with a slight modification in the concrete strength reduction factor. For simplicity, the strength reduction factor 0.92ψ in Equation (2.1) is replaced by 0.8 in CSA S16-01. However, these design equations are subjected to certain limitations imposed by the scope of the experimental and numerical research works. The yield strength of the steel plate and reinforcing bar is limited to no greater than 350MPa and 400MPa respectively and concrete strengths only up to 40MPa are allowed. The flange width, b_f must be within 0.9 to 1.1 times the section depth, d and have a slenderness ratio, $b_f/2t$ not greater than 32. The thickness of the web plate must be equal to the thickness of the flanges and the connections between them must be provided by continuous fillet welds designed to develop the shear yield capacity of the web. The spacing of the transverse links is limited to the lesser of 500mm or $0.67d$ and the area of a link must be at least the greatest of 0.63mm^2 , $0.01b_f t$ and 0.5mm^2 per mm of link spacing. Finally, the equations are applicable only to concentrically loaded columns with a clear height to depth ratio of 14. As reported by Prickett and Driver (2006), the design equations for concentrically loaded columns provide conservative estimations of the axial capacity of PEC columns with high strength concrete. Therefore, it was recommended that the current upper limit for the strength of concrete to be increased from 40 to 70MPa.

2.3 BEHAVIOUR OF SLENDER PEC COLUMN

On slender PEC column, limited numbers of experimental and numerical research works were conducted. A brief description of these works is provided in the next section.

2.3.1 Experimental Investigation

Four long columns with a length to depth ratio of were tested by Chicoine et al. (2000) to study the overall buckling behaviour of these columns under monotonic loading. In this test program, one bare steel column and three composite columns were tested with two different link spacings. All columns were of a square cross-section of $450\text{mm} \times 450\text{mm}$ and a flange slenderness ratio of 23.

Additional reinforcement in the form of longitudinal and tie bars were provided in one of the composite specimens. Both local and global geometric imperfections were measured in all specimens before the test took place. The flanges of these specimens were observed to have outward local imperfections, with maximum amplitudes less than 1mm. The global outward straightness was measured about the weak axis and was also found to be small, representing typically about 1/3000 of the total heights of the columns. The long columns were tested under concentric loading, except for one, which was tested with an eccentricity of $0.06d$ about the weak axis. However, Chicoine et al. (2000) reported the presence of significant bending moment in all specimens about the strong and weak axes caused by accidental eccentricity or uneven end bearing. Equivalent strong and weak axes eccentricities are, therefore calculated for each specimen at the bottom, mid-height and top elevations using elastic theory. Chicoine et al. (2000) recommended these computed values of eccentricity be included in the finite element analysis of these test specimens.

The test results demonstrates the brittle and explosive failure mode of the long composite specimens that consisted of global flexural buckling along with local buckling and concrete crushing between two links. The steel only specimen was observed to fail by global buckling followed by local buckling at several link intervals. As reported by Chicoine et al. (2000), no welds of transverse links failed during the tests. The ultimate capacities of the slender column were observed to be about 80% of those of short columns with similar cross-sections and link spacings. The initial weak axis eccentricity of $0.06d$ applied in one of the tests decreased the column capacity by 20% when compared with the specimen having similar geometric and material properties. The transverse stresses on the flange plates were observed to be higher on the compression side and lower on the tension side, with intermediate values in the web. The additional reinforcement was observed to provide no improvement in the ductility of the long composite column, as opposed to the beneficial effect observed in the short composite columns. However, a direct comparison between the two long specimens with and without additional reinforcements was not possible due to the presence of accidental eccentricity in the test specimens.

2.3.2 Numerical Investigation

Begum et al. (2007) conducted comprehensive finite element analysis on PEC columns. Three 9.0m long PEC columns with a cross-section of $450\text{mm} \times 450\text{mm} \times$

9.75mm tested by Chicoine et al. (2000) were selected for finite element simulation to predict the global buckling behaviour of slender PEC column. In the test regions of these columns, two types of link spacing were used. One is equal to the depth of column and another is half of the depth of column. Additional reinforcements were provided only in the third specimen. Among these three specimens, one was intended to have eccentric loading. In the case, the load was applied at an eccentricity of 28mm, resulting in bending about the weak axis. However, bending moment was found in the concentrically loaded columns due to accidental eccentricity. To represent these bending moments, both strong and weak axis equivalent eccentricities were calculated from the longitudinal strain gauge reading for all three specimens. Two sets of numerical analyses were performed for each of the long test columns, one using the applied eccentricity and other using the measured eccentricity about the weak axis as reported by Chicoine et al. (2000). The deduced values of weak axis eccentricity used in the numerical analysis of the first specimen were 20mm at the top and 10mm at the bottom end of the column. For second specimen, these values were 45mm and 35mm at top and bottom end of the column respectively, and 35mm and -5mm at top and bottom end respectively for the third specimen.

The ratios of experimental to numerical peak load were found 0.77 and 0.86 for the first and second specimen respectively. However, these values were close to unity when the specimens were analyzed with eccentricities deduced from the measured strains. In the case of third specimen, both of the numerical analyses were observed to give higher peak loads than that obtained experimentally. The slender PEC columns were observed to fail by global buckling as well as local flange buckling. The numerical and experimental failure modes of slender PEC columns are shown in Fig. 2.3.

The axial strains at peak load for long PEC columns were overestimated by the numerical model in both sets of analyses, with better prediction in the analyses including eccentricities deduced from measured strain data.

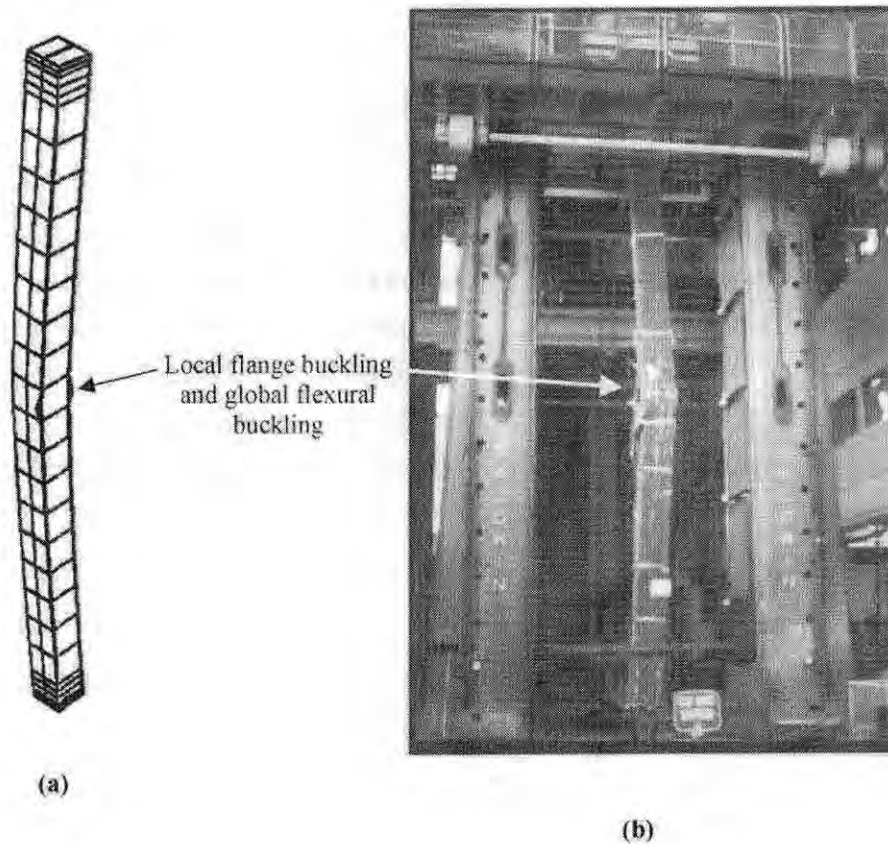


Fig. 2.3: Comparison of numerical and experimental failure modes for long PEC columns, (a) Numerical (Begum et al. 2007) and (d) Experimental (Chicoine et al. 2000)

2.4 SUMMARY

The research on PEC columns with thin walled sections reviewed in this chapter reveals that the behaviour of short PEC column with normal and high performance materials are become relatively well understood from the full scale extensive experimental and numerical investigations. Design guidelines and axial capacity of short PEC column are well established and included in Canadian steel design code (CSA-S16.09). However,

design guidelines for slender PEC columns are not included in the design code due to scarcity of ample research on long PEC columns. Moreover, it is not possible to obtain a complete understanding of various components from experimental investigations only due to high cost and time requirement for full scale testing. No numerical study is not performed yet to explore the behaviour of slender columns under the combined action of axial and flexural loads. In this regard, a numerical analysis needs to be conducted to represent the axial load and moment capacity of this slender column under eccentric loads. Moreover, the influences of several key parameters which could not be studied by the experimental programs, on the behaviour of these columns under axial compression and bending need to be investigated using numerical methods.

METHODOLOGY TO FORMULATE LOAD DEFLECTION AND INTERACTION CURVE

3.1 INTRODUCTION

Experimental research work on slender partially encased composite column is costly and cumbersome. A numerical tool is therefore required to understand the behaviour of slender partially encased composite column. In this regard, Newmark's numerical iterative procedure is selected to develop a numerical model to formulate the load-deflection curve and the corresponding load-moment curve for slender columns. A detailed description of Newmark's method (Newmark's, 1943) is presented in this chapter. Before implementing the Newmark's method, a brief description on the behaviour and analysis of slender column is provided. This is followed by the application of this method in developing the load deflection curve of a typical slender PEC column. This chapter also describes the formation of the interaction diagram of the slender partially encased composite column. The performance of the proposed numerical tool in predicting the ultimate capacity of the column is presented by analyzing the slender column tests performed by Chicoine et al. (2000).

3.2 BEHAVIOUR AND ANALYSIS OF SLENDER COLUMN

A slender column is defined as a column that has a significant reduction in its axial load capacity due to moments resulting from lateral deflections of the column. How the axial load capacity is affected by the lateral deflection, is illustrated in Fig. 3.1 and Fig. 3.2. Fig. 3.1 shows a pin-ended column and subjected to eccentric loads. The moments at the ends of the columns are,

$$M = Pe \quad (3.1)$$

When the loads P are applied, the column deflects laterally by an amount Δ , as shown in Fig. 3.1. For equilibrium, the internal moment at the mid-height must be

$$M = P(e + \Delta) \quad (3.2)$$

The deflection increases the moments for which the column must be designed. In the symmetrical column shown here, the maximum moment occurs at mid-height, where the maximum deflection occurs.

Figure 3.2 shows an interaction diagram for a reinforced concrete column. This diagram gives the combinations of axial load and moment required to cause failure of a column cross section or a very short length of column. The dashed radial line OA is a plot of the end moment on the column in Fig. 3.1. Because this load is applied at a constant eccentricity, e , the end moment, M_e , is a linear function of P , given by Equation (3.1). The curved solid line OB is the moment M at mid-height of the column, given by Equation (3.2). At any given load P , the moment at mid-height is the sum of the end moment, Pe , and the moment due to deflections, $P\Delta$. The line OA is referred to as a load-moment curve for the end moment, while the line OB is the load-moment curve for the maximum column moment.

Failure occurs when the load-moment curve OB for the point of maximum moment intersects the interaction diagram for the cross section. Thus the load and moment at failure are denoted by point B in Fig. 3.2. Because of the increase in maximum moment due to deflections, the axial-load capacity is reduced from A to B . This reduction in axial load capacity results from what is referred to as slenderness effects.

Lateral deflections of a slender column cause an increase in the column moments, as illustrated in Figs. 3.1 and 3.2. These increased moments cause an increase in the deflections, which in turn lead to an increase in the moments. As a result, the load-moment line OB in Fig. 3.2 is nonlinear. If the axial load is below the critical load, the process will converge to a stable position. If the axial load is greater than the critical load, it will not. This is referred to as a second order process, because it is described by a second order differential as,

$$EI \frac{d^2 y}{dx^2} = Py \tag{3.3}$$

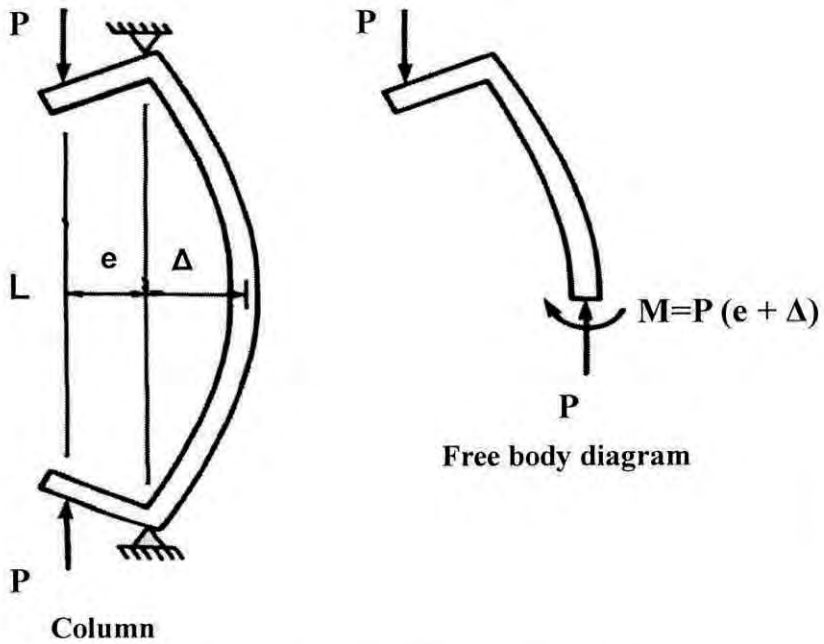


Fig. 3.1: Forces in a deflected column

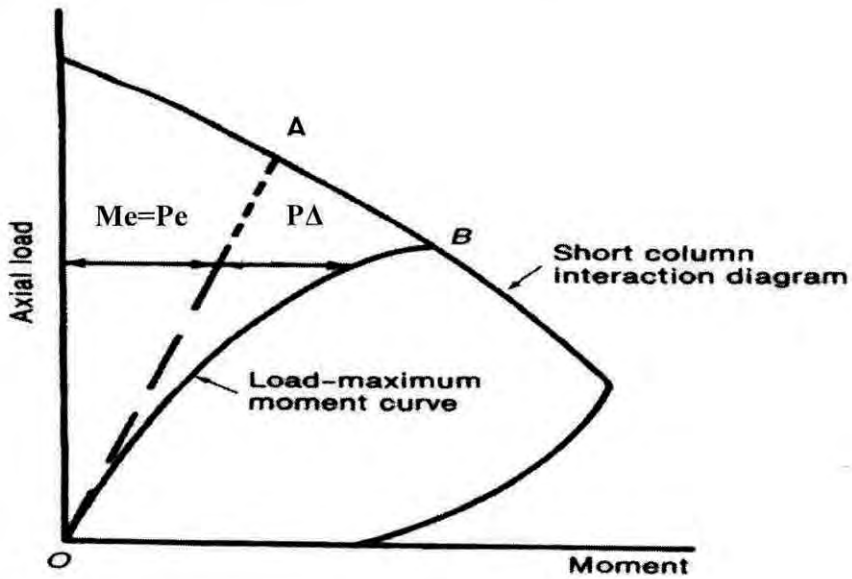


Fig. 3.2: Load and Moment in a Column

3.3 NEWMARK'S METHOD TO COMPUTE SECOND ORDER DEFLECTION

The second order deflection therefore plays a significant role in identifying the strength of slender PEC columns. Newmark's numerical iterative procedure is implemented to compute this second order deflection for slender PEC columns under symmetrical single curvature bending for a given axial load and applied eccentricity. This method is also used by Mirza and Tikka (2005) to simulate the slender column behaviour of fully encased composite columns.

3.3.1 Subdivision of Slender Column

In Newmark's method, the slender column is subdivided into a number of segments or stations. During the subdivision of the slender column, an equal length is maintained for each differential segment of the specific column. In analyzing the slender column, the segmented value is considered as low as possible so that a linear deflected shape can be assumed within each segment (as shown in Fig. 3.3).

3.3.2 Assumption of Deflection (Δ)

Maximum deflection occurs at the mid-height of a slender PEC column. At the ends of the column lateral deflections are zero. Since, the column is divided into differential segments, the shape of the deflection profile of each segment is considered nearly as a straight line instead of a parabolic curve (Fig. 3.3(b)). Unit deflection is assumed at the mid-height of the column. At other points along the length of the deflections are determined by linear interpolation with unit at middle and zero at end. The values are shown in Fig. 3.3(b). Since, the geometry and loading condition is symmetric only half length of the column is considered in this study.

3.3.3 Calculation of Total Moment (M)

The bending moment diagram for a pin ended slender partially encased composite column (Fig. 3.4(a)) of length L , subjected to eccentric axial loading is shown in Fig. 3.4(b), the total bending moment (M) at each station along the length of the column is calculated according to Equation (3.2).

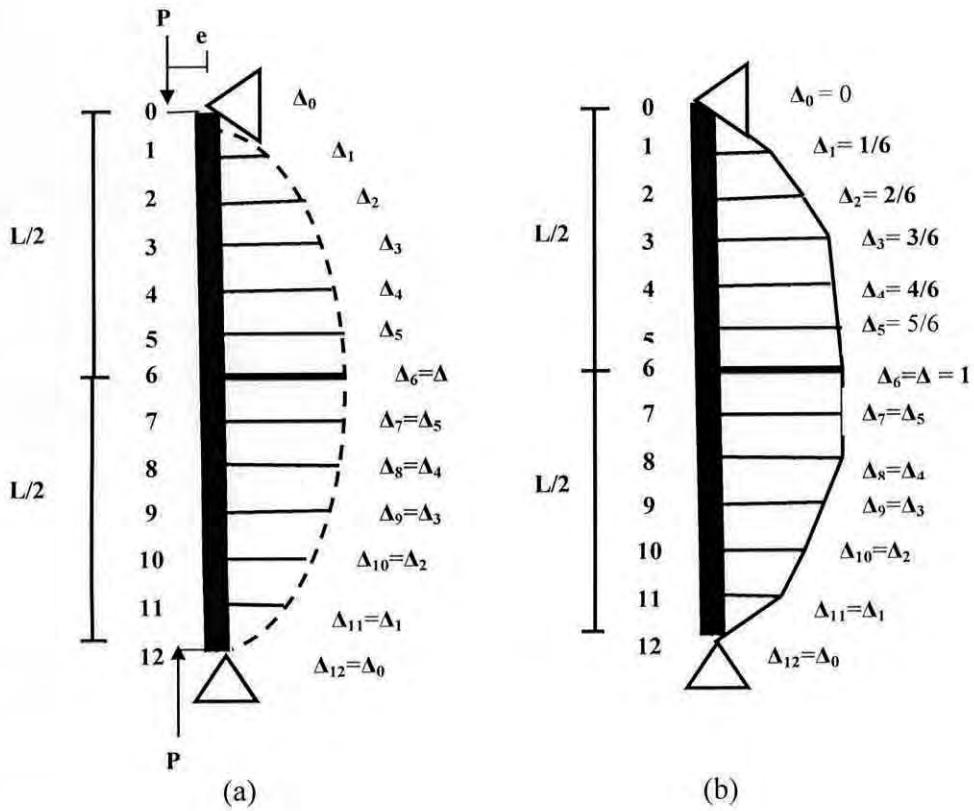


Fig. 3.3: (a) Deflected shape of slender PEC column (b) Identical deflected shape of slender PEC column

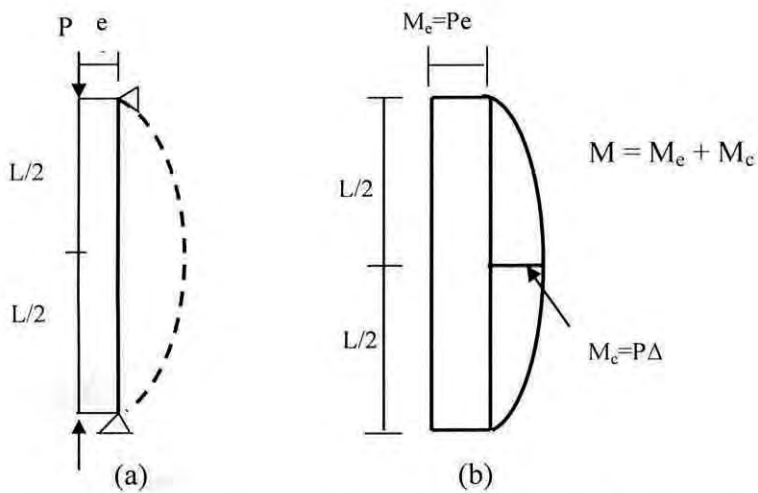


Fig. 3.4: (a) Column subjected to eccentric loading (b) Bending moment diagram of the column

3.3.4 Determination of Curvature

The curvature corresponding to the total moment at each station is retrieved from the cross section moment-curvature curve for the given axial load level in order to define the distribution of curvature along the column length. The following formula is used in determining the curvature,

$$\varphi = \frac{M}{EI_{eff}} \quad (3.4)$$

where,

M = Total moment at any segment

φ = Curvature corresponding to the total moment

EI_{eff} = Effective stiffness of the composite section

3.3.4.1 Calculation of Effective Stiffness

In the analysis of a partially encased composite column, effective stiffness is an important property which entirely depends on the geometric and material properties of the composite section. According to AISC (2005) effective flexural stiffness of composite column can be calculated as,

$$EI_{eff} = E_s I_s + C_1 E_c I_c \quad (3.5)$$

where,

E_s = Modulus of elasticity of steel

E_c = Modulus of elasticity of concrete

I_s = Moment of inertia of steel shape

I_c = Moment of inertia of the concrete section

The co-efficient, C_1 is determined using the effective area of steel as follows:

$$C_1 = 0.1 + 2 \left(\frac{A_{se}}{A_c} + A_{se} \right) \quad (3.6)$$

Again,

$$A_{se} = (d - 2t + 2b_e)t \quad (3.7)$$

where,

d = Overall depth of the cross-section

t = Thickness of the steel plates

b_e = Total effective width of the flange

A_s = Area of steel

A_{se} = Effective area of steel

To account for the effect of local buckling in the column capacity, b_e is expressed as,

$$b_e = \frac{b_f}{(1 + \lambda_p^{2n})^{1/n}} \leq b_f \quad (3.8)$$

$$\lambda_p = \frac{b}{t} \sqrt{\frac{12(1 - \nu_s^2)F_y}{\pi^2 E_s k}} \quad (3.9)$$

$$k = \frac{0.9}{(\frac{s}{b_f})^2} + 0.2(\frac{s}{b_f})^2 + 0.75, \quad (0.5 \leq \frac{s}{b_f} \leq 1) \quad (3.10)$$

where,

b_f = Full width of flange plate

λ_p = Slenderness parameter

ν_s = Poisson's ratio of steel

$n = 1.5$, as proposed by Chicoine et al (2002)

Using the above formulas, curvature is obtained in each segment and curvature diagram is completed as illustrated in Fig. 3.5.

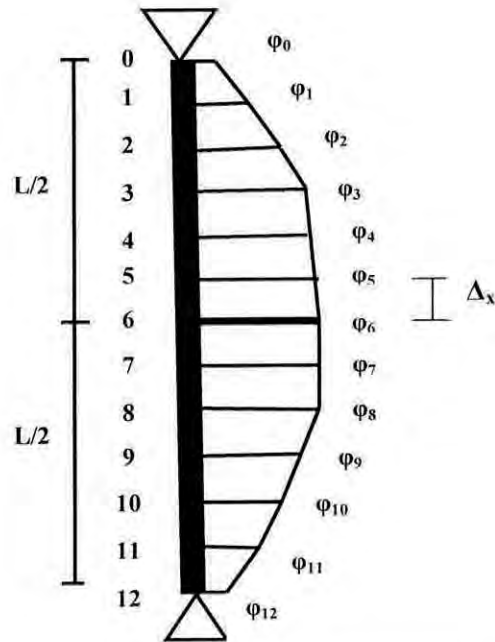


Fig. 3.5: Curvature (M/EI) diagram for slender partially encased composite column

3.3.5 Determination of Equivalent Nodal Force

The conjugate beam method is used to compute the deflection at each of the stations. It is done by determining equivalent nodal force (R) from the M/EI diagram. Equivalent nodal force is taken as the contributing area of the M/EI diagram. The Fig. 3.6 shows the method in details.

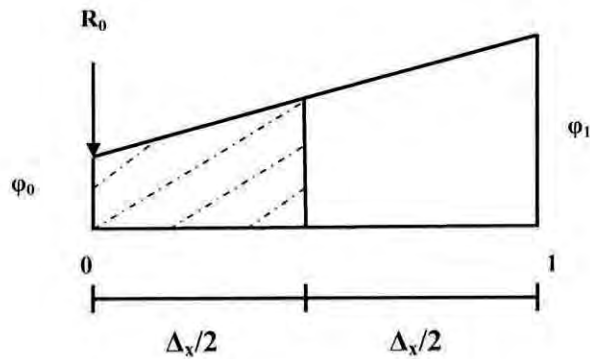


Fig. 3.6: Equivalent nodal force at extreme corner point

At the top point of a slender column, equivalent nodal force is calculated using the contributing area as shown in Fig. 3.6. As the value of curvature at the extreme corner point is very small, the value of equivalent nodal force at that point is approximated as:

$$R_0 = \frac{I}{2} \left(\frac{\varphi_0 + \varphi_1}{2} \right) \left(\frac{\Delta x}{2} \right) \quad (3.11)$$

At the interior points of a slender column, equivalent nodal force is calculated using the contributing area by averaging the adjacent values of curvature diagram. Fig. 3.7 illustrates the calculation clearly.

$$R_1 = \frac{I}{2} \left(\frac{\varphi_0 + 2\varphi_1 + \varphi_2}{2} \right) \left(\frac{\Delta x}{x} \right) \quad (3.12)$$

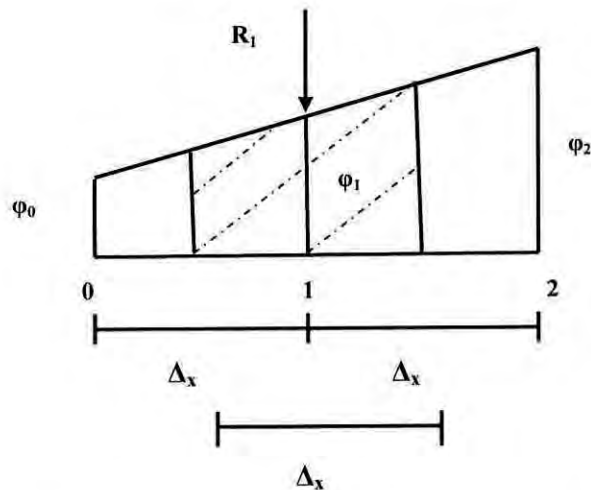


Fig. 3.7: Equivalent nodal force at interior point

At the mid-height of column, the highest value of equivalent nodal force is found. From the curvature diagram, it is noted that the amount of curvatures which are adjacent to the mid-height curvature, is same. Thus, at mid-height location, the value of equivalent nodal force for a slender column is (shown in Fig. 3.8),

$$R_6 = \frac{I}{2} (\varphi_5 + \varphi_6) \left(\frac{\Delta x}{x} \right) \quad (3.13)$$

Here,

R_0, R_1, R_6, \dots = Equivalent nodal force at station 0, 1 and 6 respectively and so on.

Δx = Segmental differential length

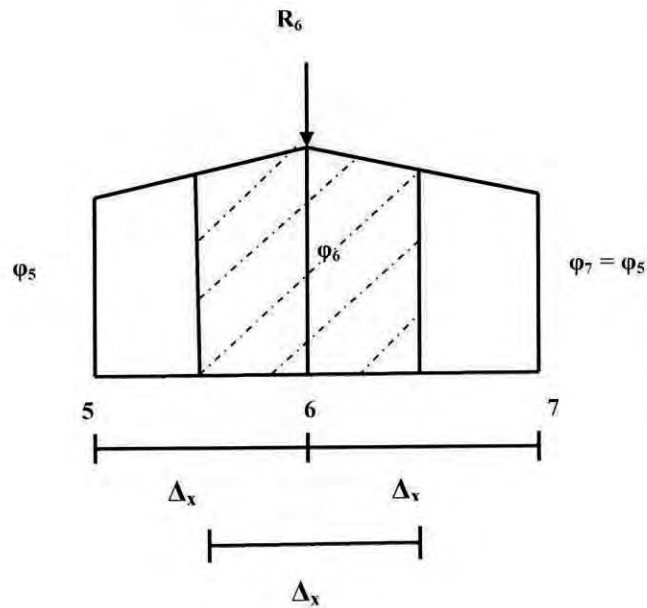


Fig. 3.8: Equivalent nodal force at mid-height of slender column

Using the mentioned formulas, equivalent nodal force is determined up to the mid-height location of slender partially encased composite column. These are the acting point forces on the conjugate beam as shown in Fig. 3.9 (b).

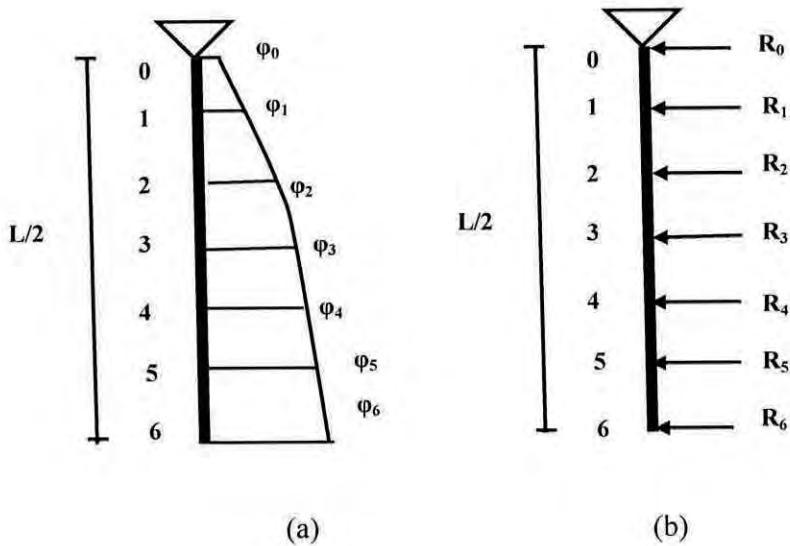


Fig. 3.9: (a) Curvature diagram (b) Equivalent nodal force or point force on slender column or conjugate beam (considering half of column length)

3.3.6 Determination of Slope of the Deflected Columns

In order to determine the slope of the curvature curve, the predetermined equivalent nodal force on slender column is used. In conjugate beam method, the nodal forces are equivalent to the point forces on the conjugate beam. Consequently, the shear forces of the conjugate beam imply the slope for the slender partially encased composite column. The Fig. 3.10 shows the formation of shear force diagram.

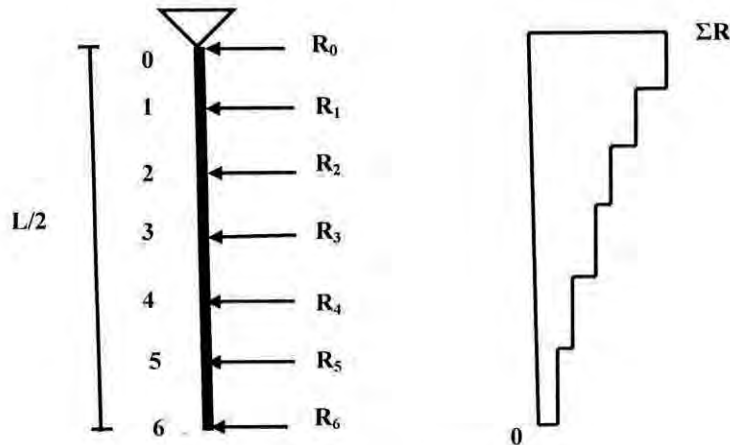


Fig. 3.10: Slope of the deflected shape of column

3.3.7 Determination of Lateral Deflection of Columns

To calculate the deflection of slender partially encased composite column, bending moments of the conjugate beam is to be determined. In conjugate beam method, the slope of the curvature curves are equivalent to the shear forces on the conjugate beam. Consequently, the bending moments of the conjugate beam reveals the lateral deflection for the slender partially encased composite column. Fig. 3.11 shows the conversion of shear force diagram to bending moment diagram for half column length.

After determining the deflection profile for a slender column, the ratio of the assumed deflection and the calculated deflection is determined. If the computed deflections and the initial deflections are within prescribed limits of 0.05%, an equilibrium solution is obtained. If not, the computed deflections are substituted for the assumed deflections and the process is repeated until the deflections converge.

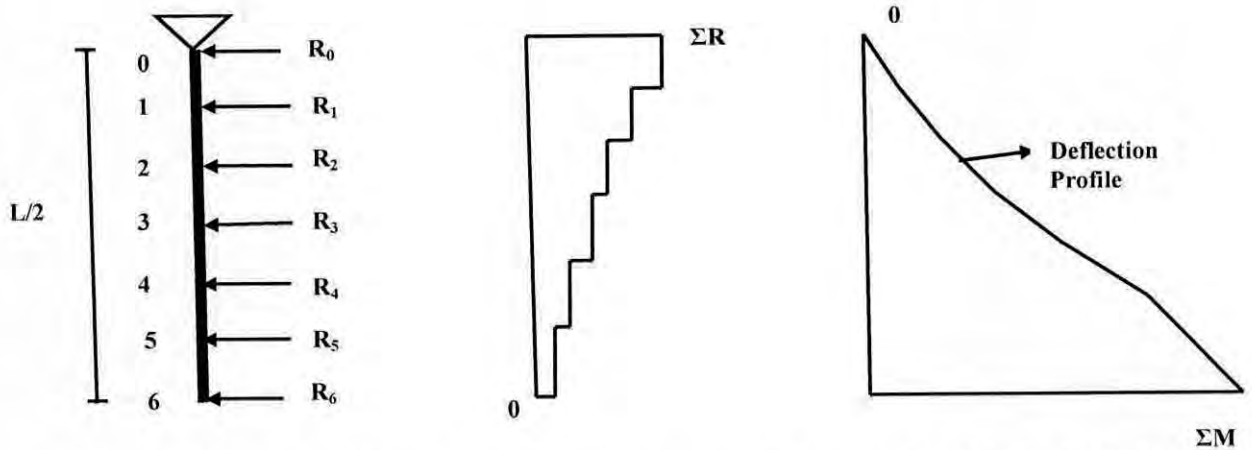


Fig. 3.11: Deflection of slender partially encased composite column (considering half of the column length)

3.4 FORMULATION OF LOAD-DEFLECTION CURVE AND ULTIMATE AXIAL LOAD FOR SLENDER PEC COLUMN

In this section the load to lateral deflection curve and the ultimate capacity for a typical slender PEC column is formulated. A typical PEC column with cross-sectional properties as shown in Fig. 3.12 is selected.

The column has a cross-section of 450mm × 450mm with overall slenderness ratio (L/d) of 25. The flange plate slenderness ratio (b/t) and transverse link spacing to depth ratio (s/d) are selected as 25 and 0.7 respectively. Load eccentricity ratio (e/d) of this eccentrically loaded column is taken as 0.2. Normal strength concrete of 30MPa is used to construct the column. Grade of steel is assumed to be 350MPa with a modulus of elasticity of 200GPa. The effective flexural stiffness and effective steel area are calculated using Equations (3.3) and (3.5), respectively.

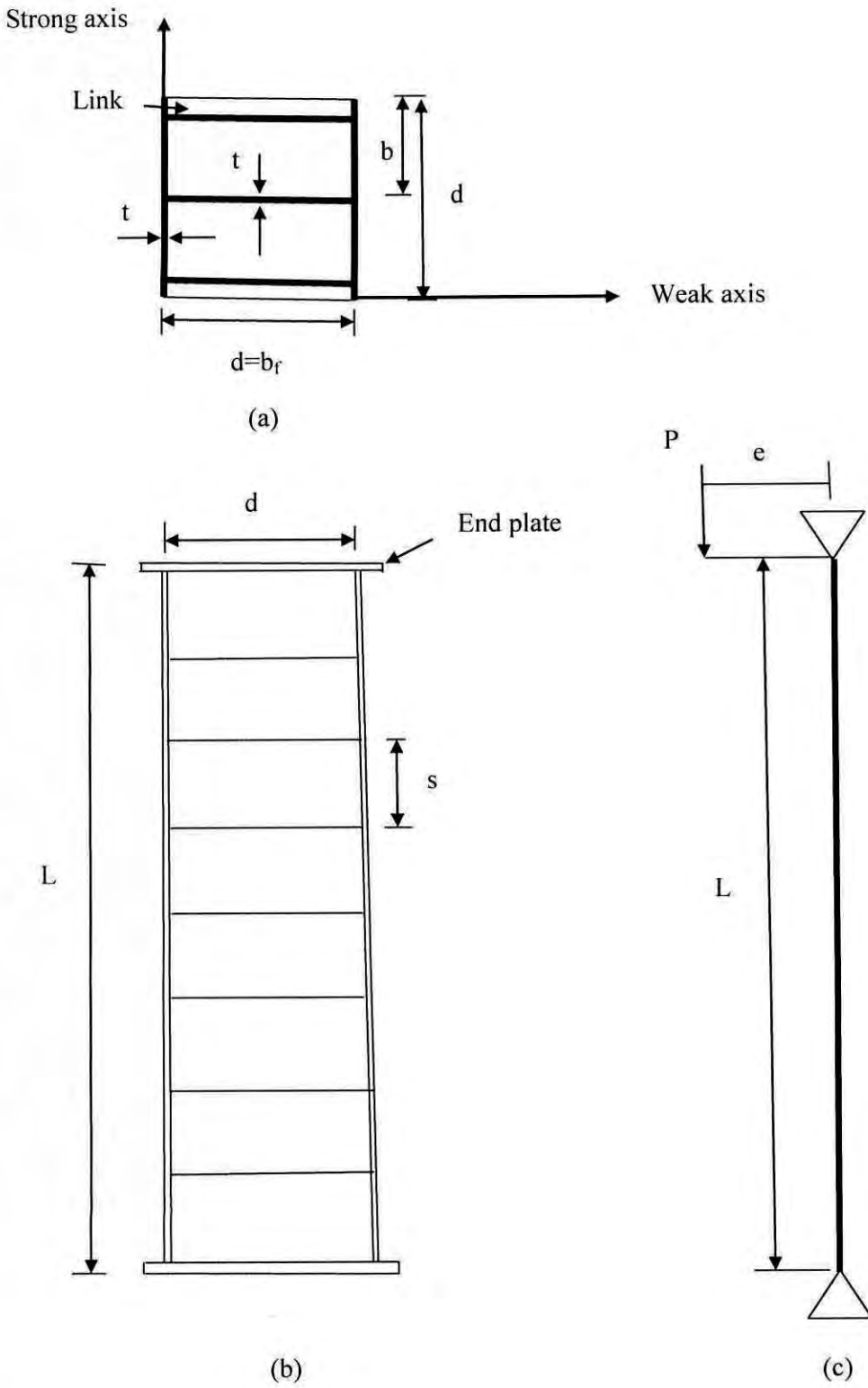


Fig. 3.12: Geometry of slender PEC column and forces on column
 (a) Cross-section (b) Elevation (c) Loading on PEC column

3.4.1 Load to Mid Height Deflection Curve

To formulate the load-deflection curve, few values of axial loads is selected and second order deflection of slender column at its mid-height for each load level is determined using the Newmark's non-linear numerical procedure. The steps followed can be summarized as,

1. The length of the slender column is subdivided into several differential segments. A unit deflection is assumed at the mid-height of the slender column and zero at the ends. The deflection at other stations along the length is determined through linear interpolation.
2. The total moment at each station along the length of the column is evaluated using Equation (3.1) for the selected level of axial load.
3. Using the moments obtained from the previous step the curvature at the selected stations along the length of the column is computed.
4. Using the conjugate beam method the deflection at each station is calculated. This deflection is compared to the assumed deflection.
5. If the computed deflections and the initial deflections are within prescribed limits of 0.05%, an equilibrium solution is obtained. If not, the computed deflections are substituted for the assumed deflections and the process is repeated until the deflections converge.

The details of the calculations and results are presented in Table A.1 to A.4 in Appendix.

The load to mid height deflection curve for the PEC column is shown in Fig. 3.13.

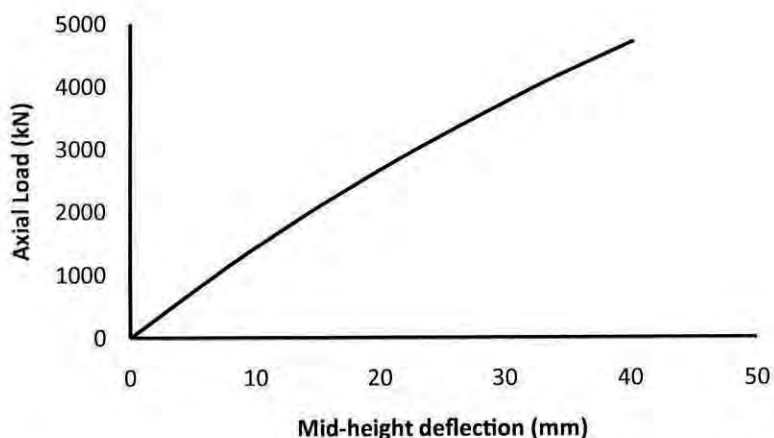


Fig. 3.13: Load- deflection curve of slender ($L/d=25$, $e/d=0.2$) partially encased composite column

3.4.2 Formulation of interaction diagram for short column

The interaction diagram for short column is formulated as followed by Bouchereau and Toupin (2002) and Prickett and Driver (2006). Bouchereau and Toupin (2002) and Prickett and Driver (2006) predicted the capacity of eccentrically loaded columns from load-moment interaction diagrams constructed using a procedure commonly adopted for reinforced concrete columns. A linear strain distribution along the cross-section, based on observations from the strain measurements taken during the test, is implemented for the construction of this diagram. The extreme compressive strain is set at $3500\mu\epsilon$, whereas the extreme tensile strain is varied from 0 to 10 times the yield strain of the steel. For each strain gradient, the ultimate load and moment capacities are calculated from the material and geometric properties of the composite cross-section. The compressive force in the concrete, C_c , is calculated using the following expression, assuming a rectangular stress block,

$$C_c = \alpha_1 f_{cu} b_c \beta_1 c \quad (3.14)$$

where,

b_c = Net width of concrete block (i.e. excluding the web thickness of strong axis bending and excluding the flanges for weak axis bending)

c = Distance between the extreme compression fibre and neutral axis

$$\alpha_1 = 0.85 - 0.0015 f_{cu} \geq 0.67 \quad (3.15)$$

$$\beta_1 = 0.97 - 0.0025 f_{cu} \geq 0.67 \quad (3.16)$$

To calculate the contribution of the steel to the capacity of the composite column, the section is discretised in such a way as to have effectively uniform strain in each individual piece. For strong axis bending, the flanges are considered to be one piece, whereas the web is divided into ten pieces. On the other hand, for weak axis bending, the web is considered as one piece and each flange is discretised into ten pieces. (Prickett and Driver, 2006). The resultant force for each individual piece is calculated by multiplying the area of the piece by its average strain. However, if the strain in the individual piece exceeded the yield strain, the force resultant is determined by multiplying the area of that piece by the yield stress. In calculating the area of a flange piece in compression, the effective width, b_e (using equation 2. With $n=1.5$) is used by (Prickett and Driver, 2006). Finally, the total

load capacity of the composite column is determined by adding the force resultants for concrete and steel and the moment capacity are obtained from the summation of each force multiplied by its distance from the centerline of the column cross-section.

3.4.3 Ultimate Axial Load

The ultimate axial load capacity of a slender column is determined using the cross-sectional column strength curve (load-moment interaction diagram) as well as the slender column load to maximum moment (P-M) curve. The former one is developed using a procedure commonly adopted for reinforced concrete columns. The load to moment curve is plotted using the mid height deflections calculated for each load level in the previous section. The slender column P-M curve is then superimposed on the cross-sectional interaction diagram, as shown in Fig. 3.14. The point of intersection is the ultimate capacity of the column (Wight and MacGregor, 2009). The axial load corresponding to this point is the ultimate capacity of the selected slender PEC column with L/d ratio of 25 and e/d ratio of 0.2.

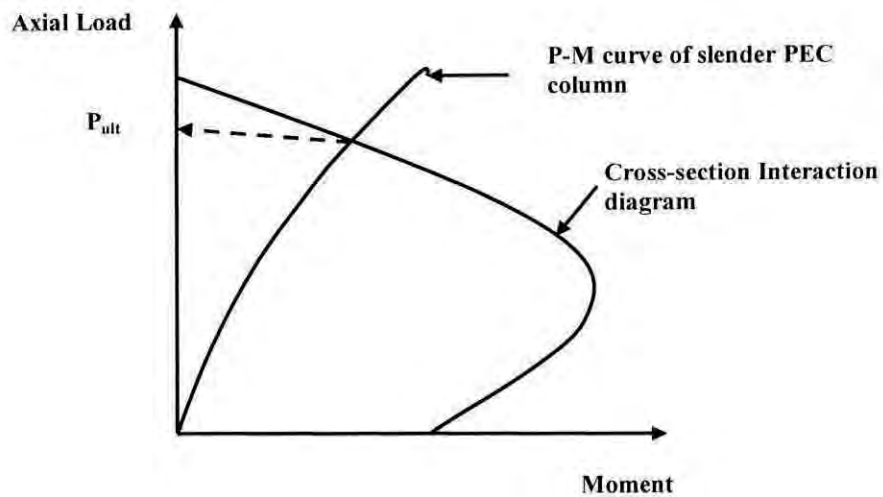


Fig. 3.14: Determination of ultimate moment at a given eccentricity

The moment corresponding to this point is the maximum moment at the mid height of the column.

3.5 FORMULATION OF INTERACTION DIAGRAM FOR SLENDER PEC COLUMN

The interaction diagram or column strength curve of the slender PEC column is constructed using the cross-section interaction diagram and the P-M curves for the column at various levels of e/d ratios as shown in Fig. 3.15. For different e/d ratios ranging from 0.05 to 50, the P-M curves are constructed using the procedure described in section 3.4.1 and 3.4.3. The selected e/d ratios are 0.05, 0.1, 0.2, 0.3, 0.4, 0.5, 0.6, 0.7, 0.8, 0.9, 1.0, 2.5, 5.0 and 50. When the eccentricity depth ratio is 50, the amount of axial load is nearly zero. These curves are superimposed on the cross-section strength curve of the column. The $M=Pe$ diagrams are also plotted for the different values of e/d ratios. Now a horizontal line (BC) is drawn from the intersection point (point B) of the cross-section interaction curve and the nonlinear P-M curve (curve OD) for each eccentricity (e_1 and e_2 are shown). The point of intersection (C) of the horizontal line (BC) and line OA ($M=Pe_1$) represents the axial load and moment at the end of the column at failure. This process is repeated for the selected PEC column ($L/d=25$) for the selected values of e/d ratios and the corresponding failure points are determined. The slender column interaction curve (as shown by dashed line in Fig. 3.15) is then drawn by connecting the failure points (C_1 and C_2) (Wight and MacGregor, 2009). This curve shows the loads and maximum end moments causing failure of the given slender column.

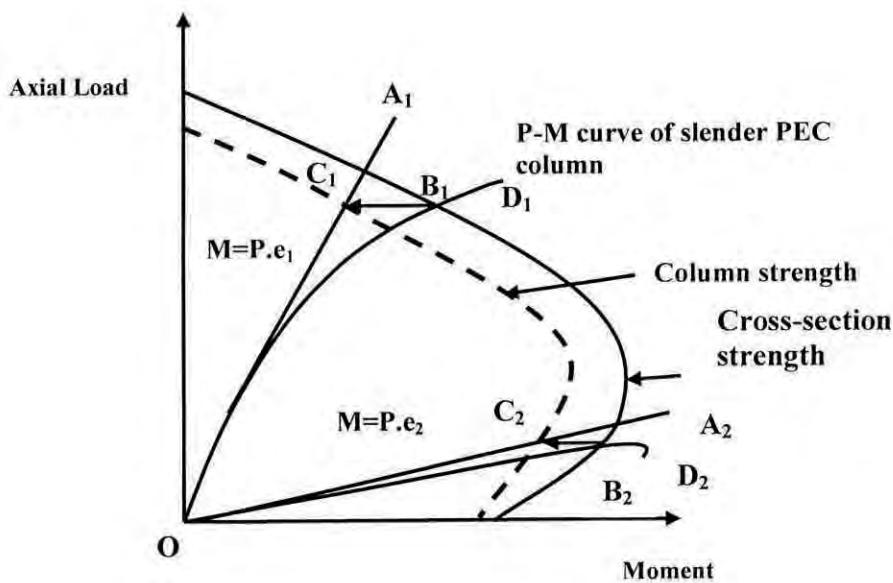


Fig. 3.15: Formation of interaction diagram of slender PEC column

3.6 VERIFICATION OF APPLIED NUMERICAL METHOD

The verification of the applied numerical method in predicting the ultimate axial capacity of slender PEC column is performed by simulating slender PEC column tests performed by Chicoine et al. (2000). Three 9m long PEC columns with a cross-section of $450\text{mm} \times 450\text{mm} \times 9.75\text{mm}$ are tested by Chicoine et al. (2000). The geometric and material properties of these test specimens are presented in Tables 3.1 and 3.2 respectively. The cross-section of a typical test column is shown in Fig. 3.16. In the test, two types of link spacings are used: $1.0d$ in specimens CL1 and CL2 and $0.5d$ in specimen CL3. Additional reinforcements are provided only in specimen CL3, as described in Table 3.1. However, the effect of additional reinforcements are not included in the computation of ultimate capacity for this column in current study, since the effect of additional rebars are found to be negligible on the strength of PEC columns (Chicoine et al, 2000). Among these three specimens, one (specimen CL2) is intended to have eccentric loading, where the load is applied at an eccentricity of 28mm. Though specimens CL1 and CL3 are loaded concentrically, Chicoine et al. (2000) reported the presence of bending moments in these tests, possibly caused by uneven end plates, alignment problems or accidental eccentricity.

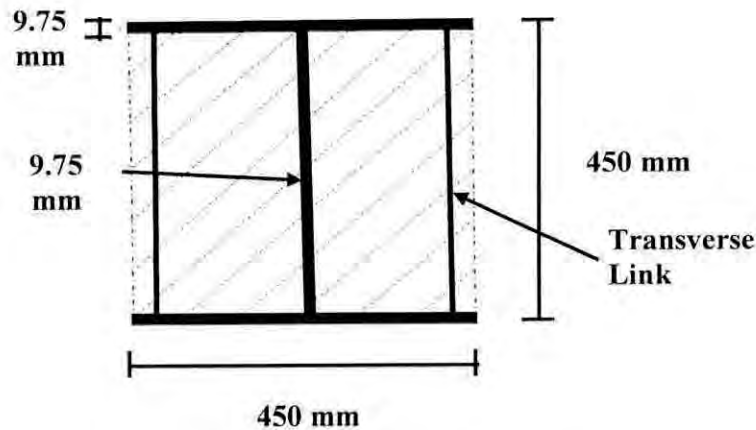


Fig. 3.16: Cross-section of partially encased composite column

Table 3.1: Geometric Properties of Slender PEC Test Columns (Chicoine et al., 2000)

<i>Specimen design.</i>	<i>Plate size</i> $b_f \times d \times t$ (mm)	<i>Length</i> (mm)	<i>Plate slenderness ratio</i> (b/t)	<i>Link spacing to depth ratio</i> (s/d)	<i>Additional reinforcement</i>			<i>Eccentricity</i>	
					<i>Diameters</i> (mm)	<i>Longitudinal bars</i> (mm)	<i>Tie bars</i> (mm)	e_x (mm)	e_y (mm)
CL1	450mm × 450mm × 9.75mm	9000	23	1.0	12.7	–	–	–	–
CL2	450mm × 450mm × 9.75mm	9000	23	1.0	12.7	–	–	–	28
CL3	450mm × 450mm × 9.75mm	9000	23	0.5	12.7	#15	#10	–	–

Table 3.2: Material Properties of PEC Test Specimens (Chicoine et al., 2000)

<i>Specimen design</i> <i>ation</i>	<i>Properties of concrete</i>				<i>Properties of steel plate</i>					
	f_{cu} (MPa)	E_c (MPa)	ϵ_{cu} ($\mu\epsilon$)	ν	F_y (MPa)	F_{sh} (MPa)	F_u (MPa)	ϵ_y (%)	ϵ_{sh} (%)	ϵ_u (%)
CL1	34.6	27900	2050	0.18	345	345	529	0.18	1.95	30.1
CL2	34.6	27900	2050	0.18	345	345	529	0.18	1.95	30.1
CL3	34.6	27900	2050	0.18	345	345	529	0.18	1.95	30.1

The deduced values of weak axis eccentricity used in the numerical analysis of specimen CL1 are 20mm at the top and 10mm at the bottom end of the column. For specimen CL2, these values are 45mm and 35mm at top and bottom end of the column respectively, and 35mm and 5mm at top and bottom end respectively of column CL3. The average values of

the initial eccentricity for columns are 15mm, 40mm and 20mm respectively, as shown in Table 3.3.

Following the procedure as described in section 3.3.1 and 3.3.2, the ultimate capacity of axial load for the slender partially encased composite columns are calculated. The results are shown in Table 3.3. The ultimate axial load capacities obtained from the numerical procedure proposed in this study are compared with the experimental results.

Table 3.3: Comparison of Experimental and Numerical Ultimate Capacities of Slender PEC Columns

<i>Column</i>	<i>Eccentricity (mm)</i>	<i>Ultimate Axial Load (kN)</i>		<i>Ratio of Experimental to Numerical Capacity</i>
		<i>Numerical</i>	<i>Experimental</i>	
CL1	15	7400	7440	1.00
CL2	40	6250	5700	0.91
CL3	20	7650	6670	0.87

The ratios of the numerical to experimental ultimate capacities for these columns are 1.0, 0.91, and 0.87 for columns CL1, CL2 and CL3 respectively.

The results show that the numerical model implemented in this study can predict the capacities of slender PEC columns with reasonable accuracy.

3.7 LIMITATIONS OF THE NUMERICAL STUDY

The numerical procedure implemented in this study is limited to the following assumptions,

- i) Strains between concrete and structural steel are compatible and no slip occurred.
- ii) The strain is linearly proportional to the distance from the neutral axis.
- iii) The confinement of the concrete provided by transverse links and the structural steel section is not considered.

- iv) The effects of residual stresses on steel section are neglected.
- v) The strain hardening of steel is not included.

3.8 CONCLUSIONS

In this chapter the methodology for formulating the load-deflection curve of slender PEC column is presented. Newmark's iterative method is used to conduct the nonlinear analysis to determine the second order deflection of slender PEC column. In addition, the formation of interaction diagram for slender PEC column has also been described. The performance of the proposed numerical method is demonstrated with the help of three slender PEC columns tested by Chicoine et al. (2000). The ultimate capacity of the test columns are compared with the numerical results. The proposed numerical method is observed to predict the experimental capacity of slender PEC columns with reasonable accuracy.

PARAMETRIC STUDY ON PEC COLUMN UNDER STRONG AXIS BENDING

4.1 INTRODUCTION

The behaviour of slender partially encased composite column is studied using Newmark's iterative procedure. In this chapter, a parametric study is conducted using this method to identify the potential variables that can significantly affect the behaviour of slender partially encased composite column subjected to axial compression and bending about strong axis. The variable parameters include load eccentricity ratio (e/d), slenderness ratio (L/d), flange plate thickness ratio (b/t) and link spacing-to-depth ratio (s/d). The only material parameter varied in this study is concrete compressive strength. The effects of these geometric and material parameters are studied by comparing the load deflection response and load-moment curve of the parametric columns. The parametric study demonstrates the effect of the overall column slenderness ratio and load eccentricity ratio in combination with flange plate slenderness ratio and link spacing. Moreover, two different concrete strength values are varied to observe the influence of this material property on the P-M curve of slender PEC column in combination with other parameters.

4.2 DESIGN OF PARAMETRIC STUDY

To conduct the parametric study, the cross-section of slender PEC column is fixed at 450mm x 450mm. Four reference columns are designed with variable plate thickness and link spacing. The properties of these columns are shown in Table 4.1. In each of these columns the above mentioned four geometric properties of PEC column are varied. The global stability of the column is controlled by the overall slenderness ratio, which is defined as the ratio of the length of the column, L , to the depth of the column cross-section, d . Five different slenderness (L/d) ratios— 10, 15, 20, 25 and 30—are employed

in the parametric study to cover the range of short, intermediate and a wide range of slender columns. The load eccentricity ratios which can be obtained by dividing the initial eccentricity, e of the applied axial load by the depth of the column cross-section, d . Different e/d ratios considered in this study are 0.1, 0.2, 0.3, 0.4 and 0.5. The flange plate slenderness ratio (b/t) is selected as 25, 30 and 35. Finally, link spacing-to-depth ratio (s/d) is taken as 0.5 and 0.7. The effects of the selected parameters on the load deflection response, axial capacity and deflection of PEC columns under single curvature bending about major axis are presented in the subsequent sections. Also, the effects of overall column slenderness ratio, flange plate slenderness ratio and concrete strength on the load-moment interaction diagram of slender PEC column have been studied.

Table 4.1: Geometric Properties of Reference Column

<i>Column</i>	<i>Width (b)</i> <i>(mm)</i>	<i>Depth (d)</i> <i>(mm)</i>	<i>Thickness(t)</i> <i>(mm)</i>	<i>Link Spacing (s)</i> <i>(mm)</i>
P _a	450	450	9	225
P _b	450	450	9	315
P _c	450	450	7.5	225
P _d	450	450	7.5	315

4.2.1 Effect of Load Eccentricity Ratio (e/d)

The behaviour of a slender PEC column under bending induced by an eccentrically applied axial load is found to be greatly affected by the initial load eccentricity ratio. Table 4.2 through 4.5 shows the effect of column load eccentricity (e/d) ratio on the axial capacity and mid-height lateral deflection of the reference columns P_b and P_d. These two columns have identical overall cross-sectional size with variable flange plate slenderness (b/t) ratios. Column P_b has a b/t ratio of 25 whereas column P_d has a b/t ratio of 30. This variation in b/t ratio is selected to observe the effect e/d ratio in combination with overall slenderness ratio of 15 and 25.

For column P_b with L/d ratio of 15, changing the e/d ratio from 0.1 to 0.2, 0.3, 0.4 and 0.5 reduces the ultimate load capacity by 19%, 31%, 40% and 47% respectively and increases the lateral deflection by 58%, 100%, 127% and 149% respectively with respect to the base column e/d ratio of 0.1. An average decrease of 15% is found for 10% increase in initial

load eccentricity ratio of this specific slender PEC column. The lateral deflection increases with an average value of 27% with every 0.1d increment in load-eccentricity ratio.

Again, for column P_b with L/d ratio of 25, changing the e/d ratio from 0.1 to 0.2, 0.3, 0.4 and 0.5 decreases the ultimate load capacity by 20%, 32%, 42% and 49% and increases the deflection by 47%, 79%, 99% and 111% respectively. Both of the analysis results show that reduction in ultimate load capacity and increase in lateral deflection increases significantly with the increase in load eccentricity ratio. For slenderness ratio 25, ultimate axial load decreases with an average rate of 14% and the lateral deflection increases at an average rate of 22% for increase of 0.1d in eccentricity. However, the change in lateral deflection is significant within the range of load-eccentricity ratio of 0.1 to 0.2 for both slenderness ratios.

For column P_d with L/d ratio of 15 and 25, for the previous increment, the ultimate load capacity is reduced by 18%, 31%, 40%, 48% and 20%, 33%, 41%, 48% respectively. At the same time, deflection is increased by 60%, 96%, 125%, 141% and 45%, 73%, 94%, 108% respectively. Similar to column P_b , ultimate load capacity is reduced and deflection is increased significantly with increasing the load eccentricity ratio. At slenderness ratio 15, the average reduction rate in axial capacity is found 14% whereas for slenderness ratio 25, this rate is found as 16%. The lateral deflection increases with an average rate of 26% and 21% for slenderness ratio 15 and 25 respectively. In column P_d also, the rate at which the axial load capacity drops or lateral deflection increases becomes significant in the low ranges of load eccentricity ratio compared to the higher range of the load eccentricity ratio.

Table 4.2: Effect of Load Eccentricity Ratio at $L/d = 15$

Col^m	e/d	L/d	b/t	s/d	$P_u(kN)$	$\Delta_u(mm)$	% variation in P_u	% variation in Δ_u
P_b	0.1				6450	8.6	–	–
	0.2				5200	13.6	19	58
	0.3	15	25	0.7	4450	17.2	31	100
	0.4				3850	19.5	40	127
	0.5				3400	21.4	47	149

Table 4.3: Effect of Load Eccentricity Ratio at $L/d = 25$

Col^m	e/d	L/d	b/t	s/d	$P_u(kN)$	$\Delta_u(mm)$	% variation in P_u	% variation in Δ_u
P_b	0.1				5900	27.4	–	–
	0.2				4700	40.2	20	47
	0.3	25	25	0.7	4000	49	32	79
	0.4				3450	54.4	42	99
	0.5				3000	57.7	49	111

Table 4.4: Effect of Load Eccentricity Ratio at $L/d = 15$

Col^m	e/d	L/d	b/t	s/d	$P_u(kN)$	$\Delta_u(mm)$	% variation in P_u	% variation in Δ_u
P_d	0.1				5650	9.9	–	–
	0.2				4650	15.8	18	60
	0.3	15	30	0.7	3900	19.4	31	96
	0.4				3400	22.3	40	125
	0.5				2950	23.9	48	141

Table 4.5: Effect of Load Eccentricity Ratio at $L/d = 25$

Col^m	e/d	L/d	b/t	s/d	$P_u(kN)$	$\Delta_u(mm)$	% variation in P_u	% variation in Δ_u
P_d	0.1				5200	32.7	–	–
	0.2				4150	47.3	20	45
	0.3	25	30	0.7	3500	56.5	33	73
	0.4				3050	63.3	41	94
	0.5				2700	68.1	48	108

Figure 4.1 to 4.4 represents the axial load to mid-height deflection curves obtained by the proposed numerical method for the columns subjected to the selected range of initial load eccentricities.

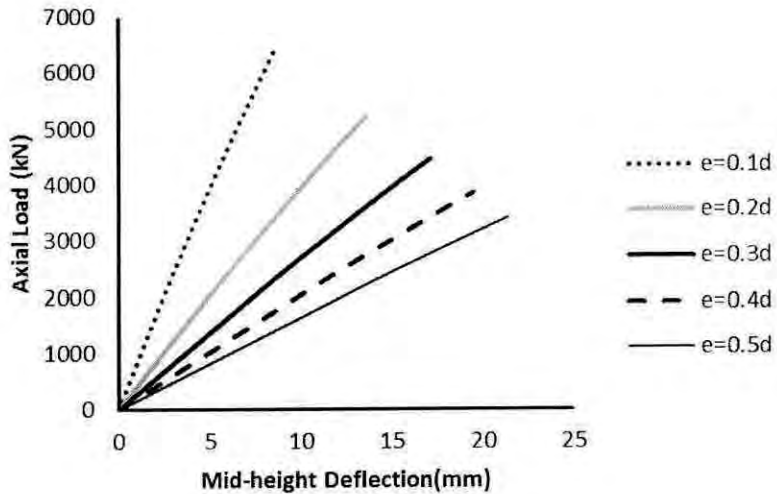


Fig. 4.1: Effect of e/d ratio on axial load to lateral deflection response of column P_b with L/d ratio of 15

Figure 4.1 and 4.2 demonstrates the load to deflection curves for column P_b (which has a b/t ratio of 25) with two different slenderness ratios ($L/d= 15$ and 25). On the other hand Fig. 4.3 and 4.4 show the similar curves for column P_d (b/t ratio of 30) for the similar ranges of L/d ratios. These figures demonstrate that the column capacity is strongly affected by the initial load-eccentricity ratio.

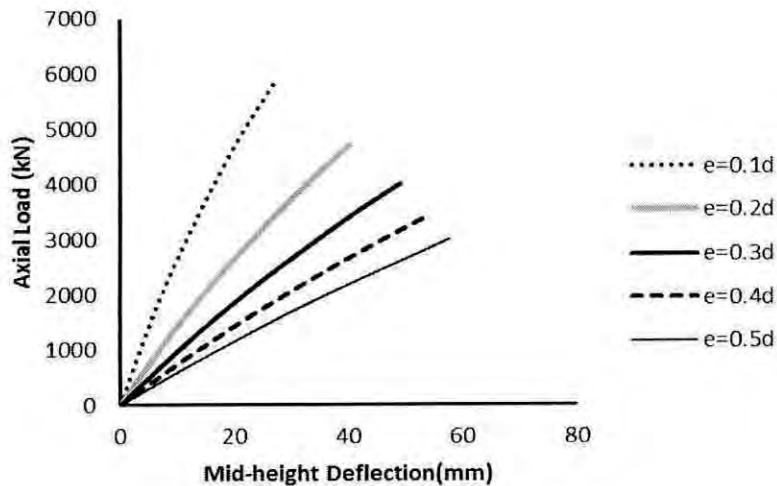


Fig. 4.2: Effect of e/d ratio on axial load to lateral deflection curve of column P_b with L/d ratio of 25

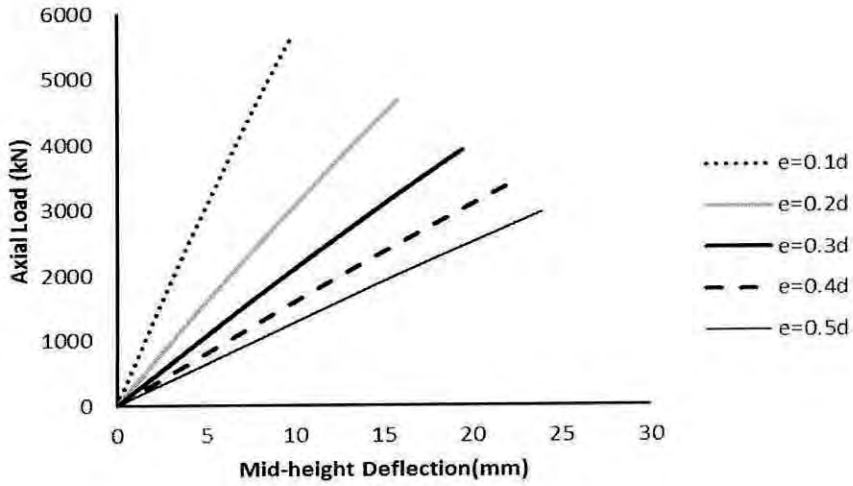


Fig. 4.3: Effect of e/d ratio on axial load to lateral deflection curve of column P_d with L/d ratio of 15

As the eccentricity ratio increases, the load-carrying capacity drops significantly accompanied by an increase in the mid height lateral deflection. For columns with higher slenderness ratio of 25, the load to deflection curves show relatively nonlinear behaviour as compared to the curves for columns with L/d ratio of 15. This is attributed to the increased value of the second order deflection for columns with higher slenderness ratio.

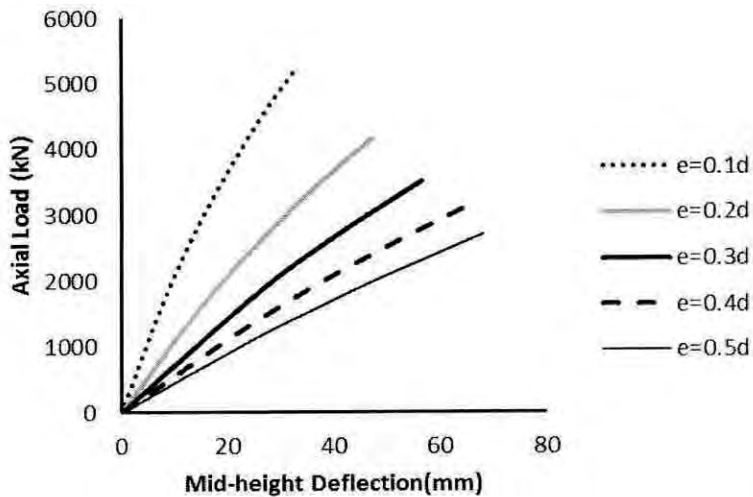


Fig. 4.4: Effect of e/d ratio on axial load to lateral deflection curve of column P_d with L/d ratio of 25

The effect of load eccentricity ratio on the ultimate axial load and corresponding deflection for the four different types of columns are shown in Fig. 4.5 and 4.6 respectively. The effect of e/d ratio on ultimate load of the four columns shows similar trend. However, increase in the deflection at the ultimate point is higher in columns with higher slenderness ratio as shown in Fig 4.6.

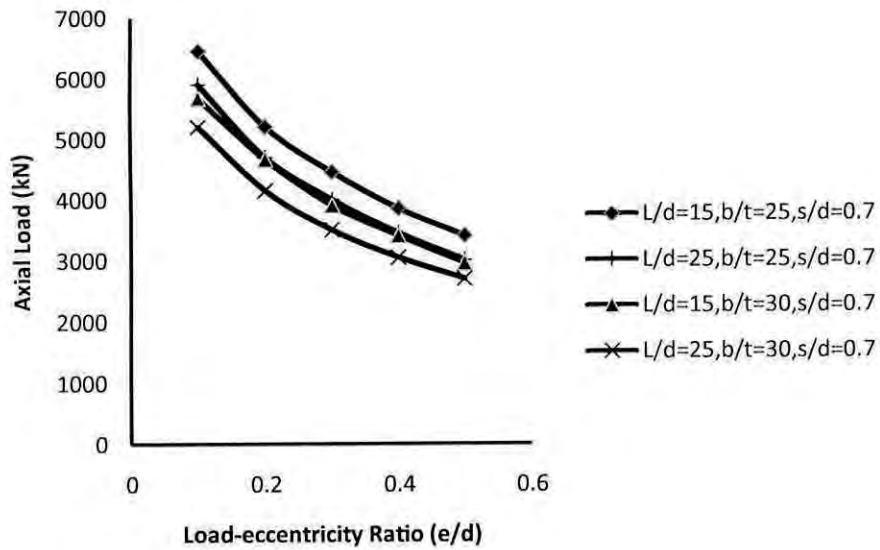


Fig. 4.5: Effect of load eccentricity ratio on axial load of PEC column

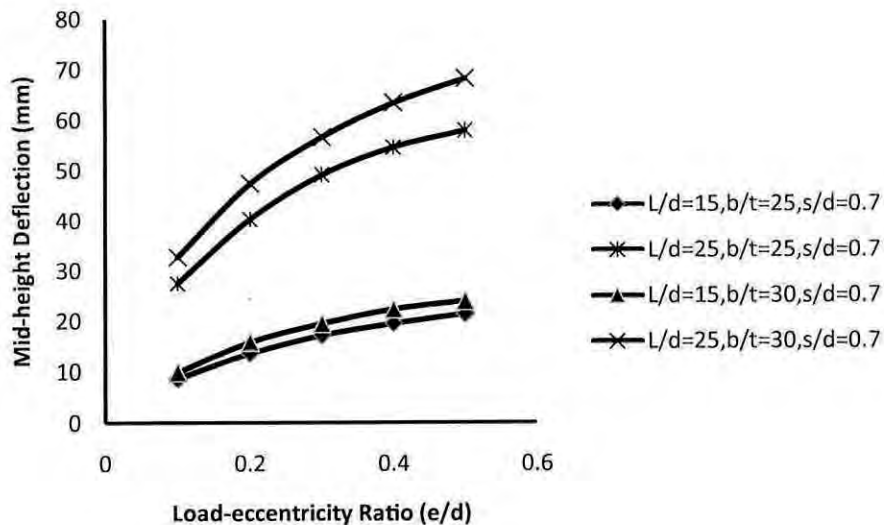


Fig. 4.6: Effect of load eccentricity ratio on mid-height deflection of PEC column

4.2.2 Effect of Overall Column Slenderness Ratio (L/d)

The global stability of the column is controlled by the overall slenderness ratio, which is defined as the ratio of the length of the column, L , to the depth of column cross-section, d . In the parametric study five different slenderness ratios- 10,15,20,25 and 30 are employed. Tables 4.6 through 4.8 show the effects of overall column slenderness (L/d) ratio on the selected output parameters at the peak load point. For column P_a (which has a s/d ratio of 0.5 and a b/t ratio of 25) the ultimate axial load is reduced by 3%, 7%, 13% and 19% respectively with increase in the L/d ratio from 10 to 15, 20, 25 and 30 (Table 4.6).

Again, for column P_b , (which has a b/t ratio of 25 and s/d ratio of 0.7) an increase in the L/d ratio from 5 to 10, 15, 20 and 25 decreases the ultimate load capacity by 3%, 7%, 12% and 18% and increases the deflection by 134%, 329%, 590% and 934% respectively which are almost similar to column P_a (Table 4.7). Both of the analysis results show that reduction in ultimate load capacity and increase in deflection sharply with the increase in slenderness ratio. For column P_a and P_b , main distinguishing feature is the spacing of transverse links. Both columns are analysed for a fixed value of initial load-eccentricity ratio of 0.2.

The axial load capacity variation rate is observed to be similar for these columns within the selected ranges of overall slenderness ratio. In both of the slender PEC column, the average reduction rate in axial load capacity is found to be 5% with the selected increments of slenderness ratio for PEC columns. In column P_a , average increase in lateral deflection is found as 83%. Similarly, for column P_b , lateral deflection increases with an average value of 82%. Therefore, effects of the spacing of the transverse links are found to be negligible on the behaviour of slender PEC columns. For column P_c (with $b/t=30$ and $s/d=0.5$), an increase in the L/d ratio from 5 to 10, 15, 20 and 25 reduces the ultimate load capacity by 3%, 7%, 13% and 20% respectively (Table 4.8). Again, lateral deflections are observed to be increased by 130%, 313%, 556% and 838% respectively.

Table 4.6: Effect of Overall Slenderness Ratio on Column P_a at $e/d=0.2$

Col^m	L/d	e/d	b/t	s/d	$P_u(kN)$	$\Delta_u(mm)$	% variation in P_u	% variation in Δ_u
P_a	10				5650	6.1	–	–
	15				5500	14.2	3	133
	20	0.2	25	0.5	5250	26.3	7	331
	25				4900	42.2	13	592
	30				4600	64.5	19	957

Table 4.7: Effect of Overall Slenderness Ratio on Column P_b at $e/d=0.2$

Col^m	L/d	e/d	b/t	s/d	$P_u(kN)$	$\Delta_u(mm)$	% variation in P_u	% variation in Δ_u
P_b	10				5400	5.9	–	–
	15				5250	13.8	3	134
	20	0.2	25	0.7	5050	25.3	7	329
	25				4750	40.7	12	590
	30				4450	61	18	934

Table 4.8: Effect of Overall Slenderness Ratio on Column P_d at $e/d=0.4$

Col^m	L/d	e/d	b/t	s/d	$P_u(kN)$	$\Delta_u(mm)$	% variation in P_u	% variation in Δ_u
P_c	10				3500	9.7	–	–
	15				3400	22.3	3	130
	20	0.4	30	0.7	3250	40.1	7	313
	25				3050	63.6	13	556
	30				2800	91	20	838

The axial load capacity is found to be higher for columns P_a or P_b as compared to column P_c . This is due to the presence of slender flange plates of column P_c and also a larger initial load eccentricity ratio ($e/d = 0.4$). Nevertheless, the average reduction in load carrying capacity of slender column P_c is similar to that in column P_a and P_b .

The effects of overall column slenderness ratio on PEC columns at a fixed load eccentricity ratio are presented in Fig. 4.7 to 4.9. The load to deflection responses for the columns with five different slenderness ratios 10, 15, 20, 25 and 30 are presented. Fig. 4.7 and 4.8 show the behaviour for PEC column with e/d ratio of 0.2 whereas Fig. 4.9 shows the behaviour with e/d ratio of 0.4.

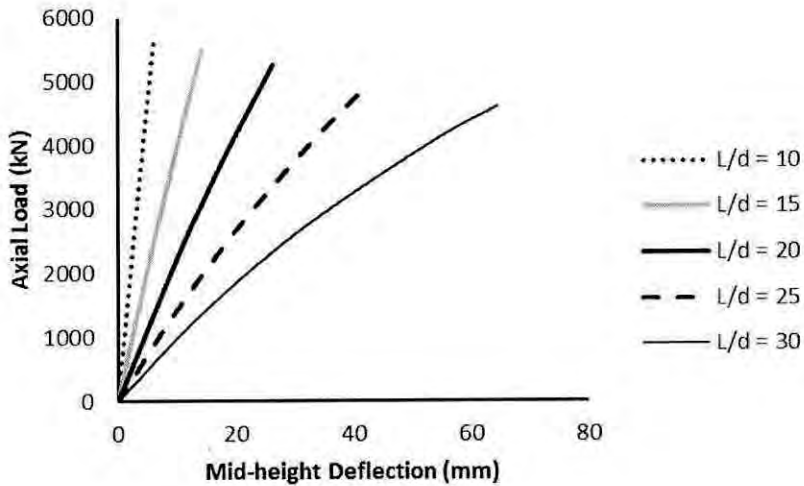


Fig. 4.7: Effect of L/d ratio on axial load to lateral deflection curve of column P_a with e/d ratio of 0.2

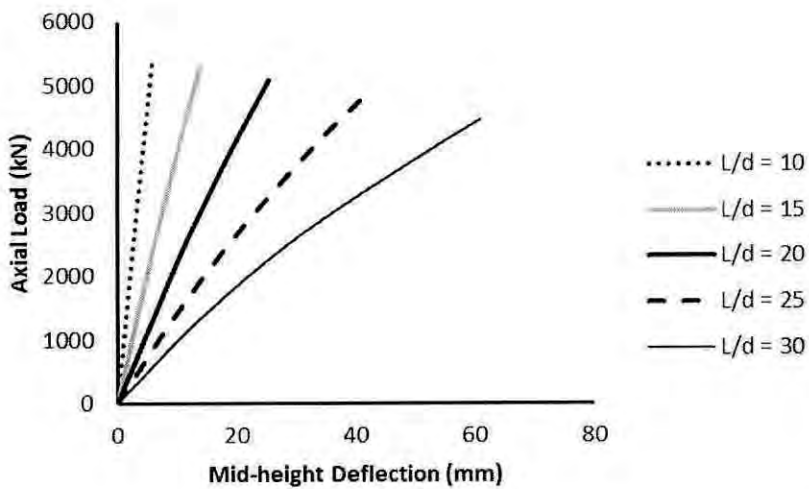


Fig. 4.8: Effect of L/d ratio on axial load to lateral deflection curve of column P_b with e/d ratio of 0.2

From these figures, it is clear that increase in the slenderness ratio increases the lateral deflection at mid height with a significant reduction in the load carrying capacity. It is also observed that for lower slenderness ratios (such as $L/d=10$), the load deflection response is linear as compared to that for L/d ratio of 30.

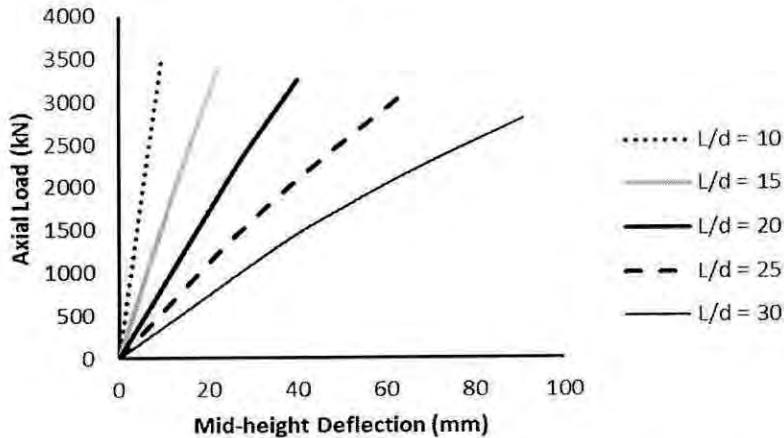


Fig. 4.9: Effect of L/d ratio on axial load to lateral deflection curve of column P_c with e/d ratio of 0.4

The effect of overall column slenderness ratio on the ultimate axial load and corresponding deflection for the three different types of columns are shown in Fig. 4.10 and 4.11 respectively.

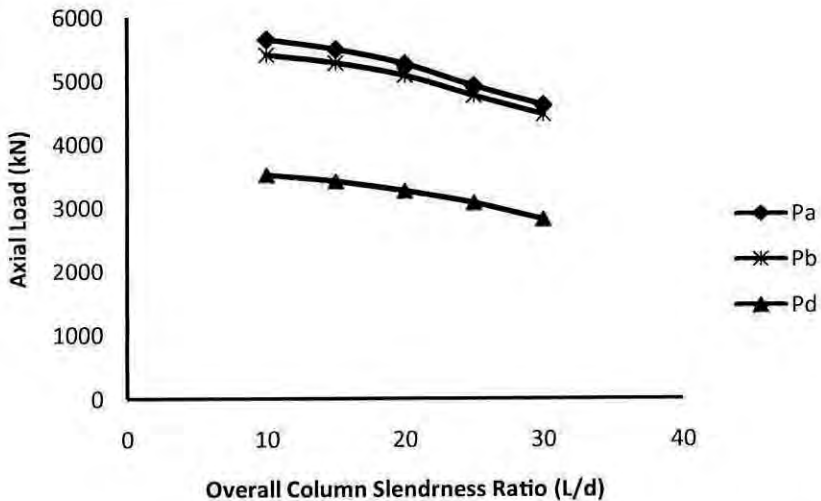


Fig. 4.10: Effect of overall column slenderness ratio on axial capacity of PEC column

The axial load carrying capacity is lower in column P_d compared to P_a or P_b as the column has higher flange plate slenderness ratio. However, the effect of L/d ratio on axial load and mid-height deflection of the three columns shows similar graphical pattern. Increase in the deflection at the ultimate point is higher in column with higher flange plate slenderness ratio (column P_d) as shown in Fig 4.11.

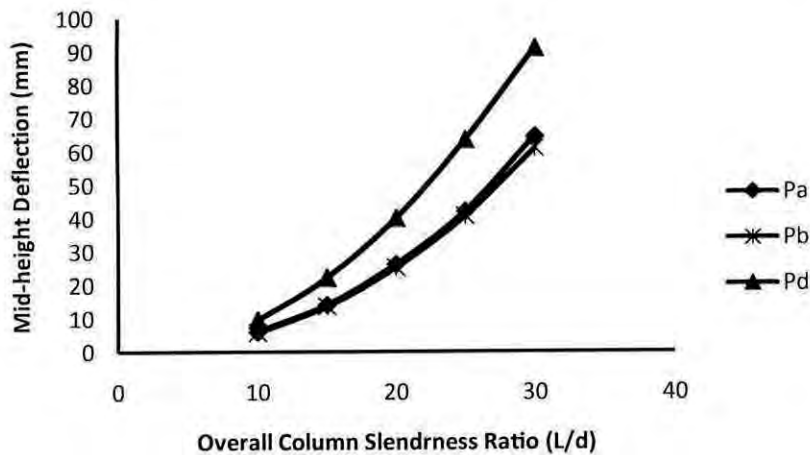


Fig. 4.11: Effect of overall column slenderness ratio on mid-height deflection of PEC column

4.2.3 Effect of Flange Plate Slenderness Ratio (b/t)

The flange plate slenderness ratio is defined as the ratio of the half-width of the flange, b , to its thickness, t . This parameter is varied between 25 and 35, with an intermediate value of 30. The ultimate capacity of a PEC column is significantly affected by this parameter, since it controls the occurrence of local instability in the flange plate of the column. Table 4.9 and 4.10 shows the effect of flange plate slenderness (b/t) ratio on the behaviour of slender partially encased composite column. Increasing b/t from 25 to 30 and 25 to 35 causes a reduction of 11% and 19% respectively in the axial load capacity of column P_a which is analysed with $e/d=0.2$ and $L/d=20$. The average reduction in the axial capacity is 10%. At the same time, lateral deflection is increased by 16% and 25% respectively for b/t ratio of 30 and 35 as compared to the deflection in column with b/t ratio of 25. The average increment in lateral deflection becomes 12% in the selected range of flange plate slenderness ratio.

Table 4.9: Effect of Flange Plate Slenderness (b/t) Ratio on Column P_a

Col^m	e/d	L/d	b/t	s/d	$P_u(kN)$	$\Delta_u(mm)$	% variation in P_u	% variation in Δ_u
P_a			25		5250	26.3	–	–
	0.2	20	30	0.5	4650	30.4	11	16
			35		4250	32.9	19	25

Table 4.10: Effect of Flange Plate Slenderness (b/t) Ratio on Column P_b

Col^m	e/d	L/d	b/t	s/d	$P_u(kN)$	$\Delta_u(mm)$	% variation in P_u	% variation in Δ_u
P_b			25		4000	49	–	–
	0.3	25	30	0.7	3500	56.5	13	15
			35		3100	59.7	29	22

Again, for column P_b , an increase in the b/t ratio by 5 and 10 decreases the ultimate load capacity by 13% and 29% and increases the deflection by 15% and 22% respectively. Both of the analysis results show that reduction in ultimate load capacity and increase in deflection accelerated with the increase in flange plate slenderness ratio. For this slender column, the load carrying capacity drops with an average value of 12%. At the same condition, lateral deflection increases by 11%.

The effects of flange plate slenderness ratio on PEC columns at a fixed load eccentricity ratio and slenderness ratio are presented in Figs 4.12 and 4.13. The axial load to lateral deflection curves for columns with three different flange plate slenderness ratios 25, 30 and 35, subjected to an initial load-eccentricity ratio of 0.2 and L/d of 20 are shown in Fig. 4.12. This figure shows significant reduction in strength and stiffness with the increasing value of b/t ratio. Similar behaviour is also observed (Fig. 4.13) for column P_d with $e/d=0.3$ and $L/d=25$.

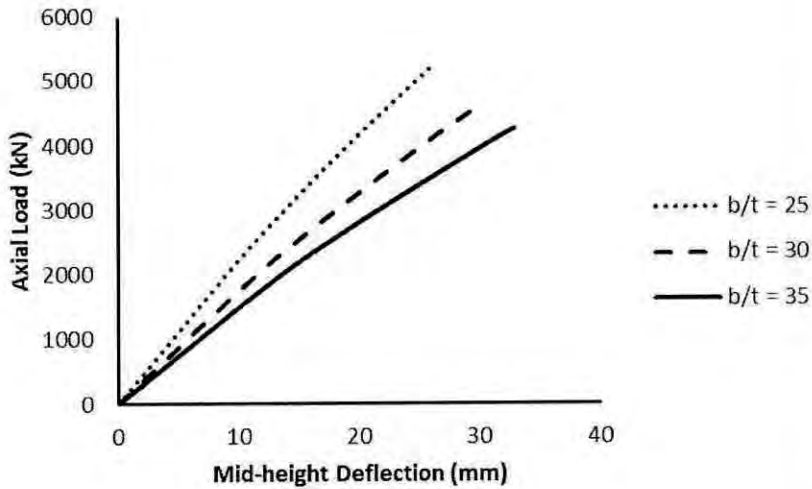


Fig. 4.12: Effect of b/t ratio on axial load to lateral deflection curve of column P_a with e/d 0.2 and L/d 20

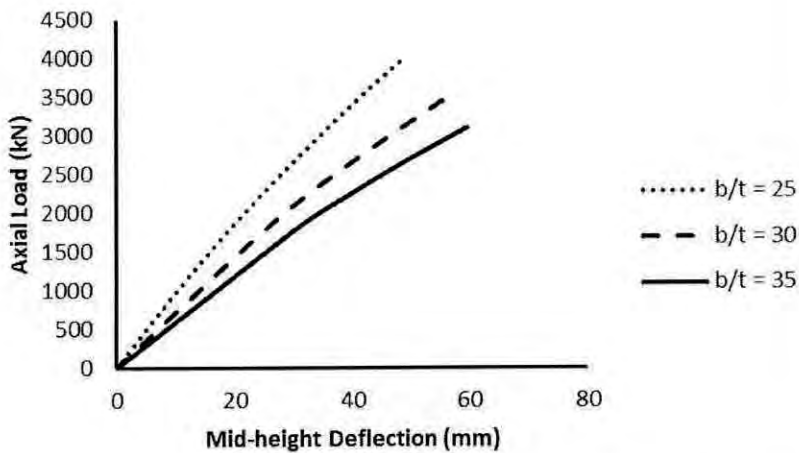


Fig. 4.13: Effect of b/t ratio on axial load to lateral deflection curve of column P_b with e/d 0.3 and L/d 25

4.2.4 Effect of Link Spacing to Depth Ratio (s/d)

Local flange buckling in a PEC column takes place in the unsupported length of the flange plate, i.e., in the flange panel between two successive links. Therefore, link spacing is clearly an important parameter affecting the behaviour of PEC columns. The effect of link spacing is studied by varying the ratio of link spacing, s , to the column cross-section, d . Two values of s/d ratio 0.5 and 0.7 are studied in the parametric study. As shown in Table 4.9, changing the s/d ratio from 0.5 to 0.7 has insignificant effect on the peak load. The

ultimate capacity of axial load drops only 5% when the link spacing to depth ratio is varied within the selected range. The lateral deflection of the reference column is affected by only 3% by changing the s/d ratio from 0.5 to 0.7.

Table 4.11: Effect of Link Spacing to Depth Ratio on Column P_b

Col^m	e/d	L/d	b/t	s/d	$P_u(kN)$	$\Delta_u(mm)$	% variation in P_u	% variation in Δ_u
P_b	0.2	15	25	0.5	5500	14.2	—	—
				0.7	5250	13.8	5	3

The effects of link spacing-to-depth ratio on PEC columns at a fixed load eccentricity ratio and slenderness ratio are presented in Fig. 4.14. The load to deflection curves for the columns with two different link spacing-to-depth ratios 0.5 and 0.7, subjected to an initial load eccentricity ratio of 0.2 and slenderness ratio 15 is shown. It can be clearly seen that the two graphs coincide, i.e. variation in ultimate capacity of axial load and lateral deflection is negligible with the change in the link spacing-to-depth ratio.

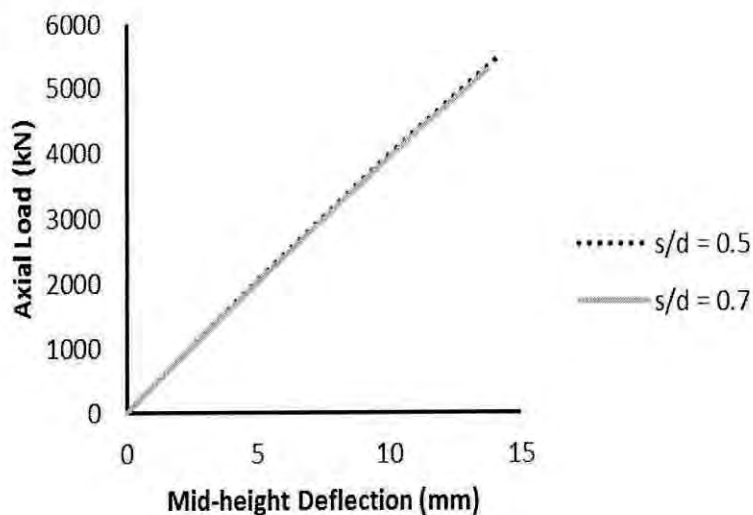


Fig.4.14: Effect of s/d ratio on axial load to lateral deflection curve of P_b column with e/d 0.2 and L/d 15

4.2.5 Effect of Slenderness Ratio on P-M Curve

The effects of overall slenderness ratio on the load-moment curve of column P_b are shown in Fig. 4.15. In order to study the variation of strength, partially encased composite columns of slenderness ratio 5, 15, 20, 25 and 30 are selected.

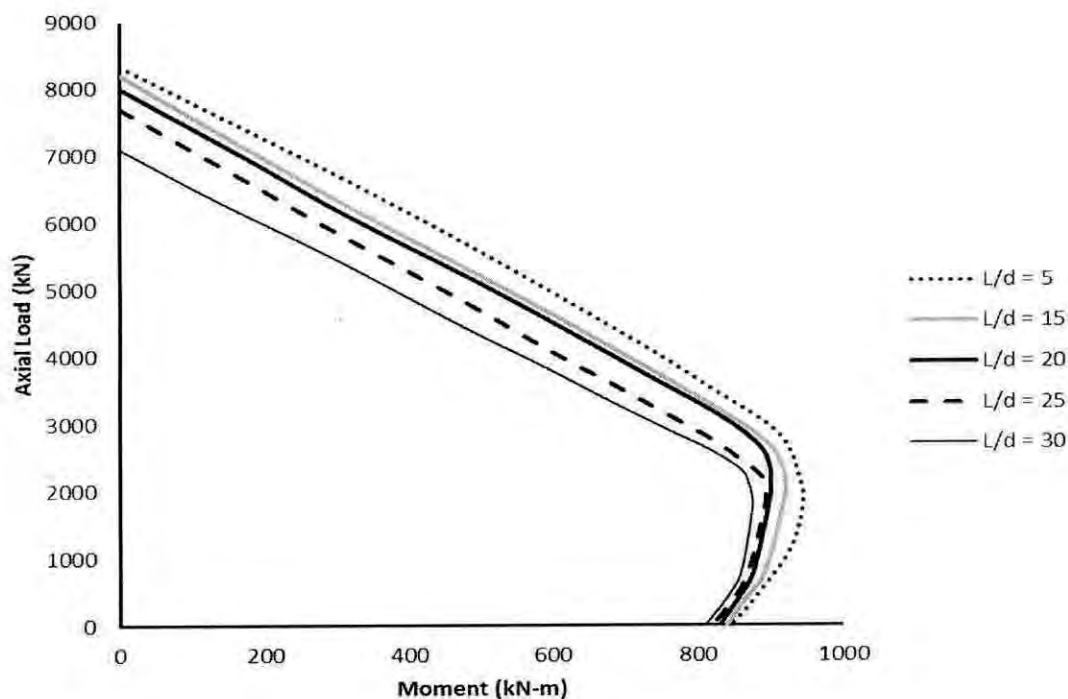


Fig. 4.15: Effect of overall column slenderness ratio on interaction diagram of slender PEC column.

From the interaction diagrams, it can be clearly seen that the area of the failure envelope reduces significantly with the increase of the overall slenderness ratio of PEC column. As the column gets slender, strength as well as ductility of the column reduces. Besides, considerable reduction in strength is found in compression zone as compared to the same in tension zone of the five interaction diagrams. From a short column ($L/d = 5$) to a slender column ($L/d = 15$), an average reduction of 7% is noted. However, as the column slenderness ratio increases from 15 to 20, only 3% average drop in strength is found. On the other hand, as mentioned above, a significant drop in strength is found when slenderness ratio is varied from 20 to 25. An average reduction rate of 8% is found in such condition. Finally, strength of slender PEC column decreases with an average value of 9%

as the slenderness of column is turned from 25 to 30. These amounts are noted in compression zone of slender PEC column. On the other hand, reduction in strength is insignificant in tension zones of slender PEC column. Moreover, for a short column, balanced point is obtained at a comparatively earlier stage than a slender column. As the column becomes more slender, the formation of balanced point occurs at a later stage. Consequently, tension zone reduces as the composite columns become more slender.

4.2.6 Effect of Flange Plate Slenderness Ratio on P-M Curve

The effects of flange plate slenderness ratio on the load-moment curve of partially encased composite columns are illustrated in Fig. 4.16. A specific slenderness ratio of 25 is taken to conduct this parametric study. Three different flange plate slenderness ratios ($b/t = 25$, $b/t = 30$, $b/t = 35$) are selected to observe the influence of this parameter on the failure envelope of slender partially encased composite column.

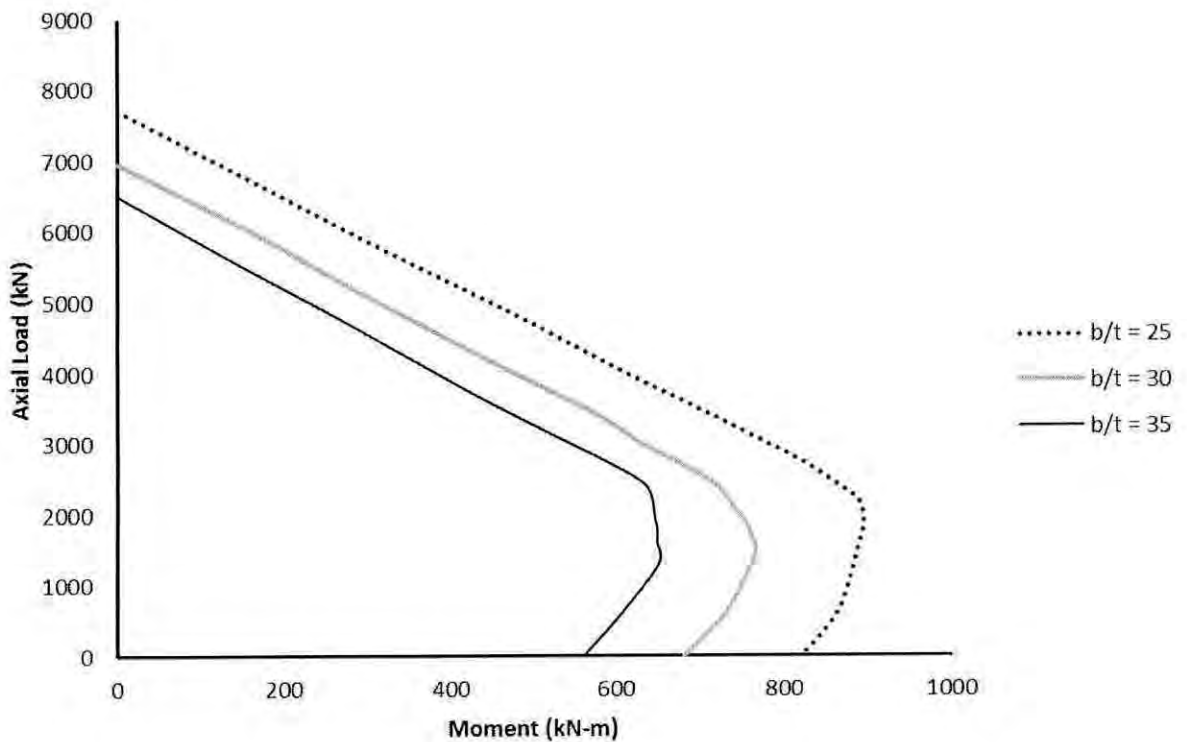


Fig.4.16: Effect of flange plate slenderness ratio on interaction diagram of slender PEC column.

The interaction diagrams of the reference column $P_b(L/d = 25$ and $s/d = 0.7)$ with variable flange plate slenderness ratios are shown in Fig. 4.16. From the Fig. 4.16, it is obvious that

111294

a significant reduction in failure envelope is found with the increase of the flange plate slenderness ratio of slender PEC column. An average reduction in strength of 15% is noted in compression zone, when the flange plate slenderness ratio is varied from 25 to 30. Moreover, by changing the flange plate slenderness ratio from 30 to 35, average drop in strength is observed as nearly 15%. Similarly, in tension zone strength of slender column decreases with an average value of 16% as b/t ratio is varied from 25 to 30. When b/t ratio is varied from 30 to 35, a similar reduction in average strength is found as noted in compression zone.

4.2.7 Effect of Concrete Strength on P-M Curve

The effects of concrete strength on the load-moment interaction diagram of partially encased composite columns are illustrated in Fig. 4.17.

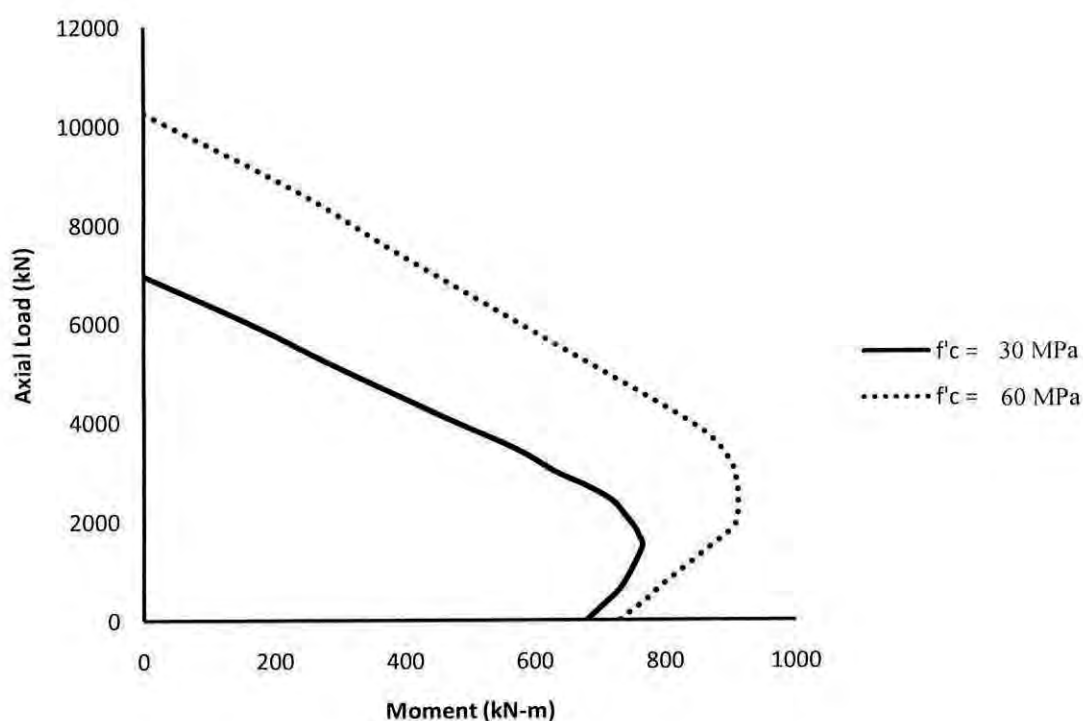


Fig. 4.17: Effect of concrete strength on interaction diagram of slender PEC column.

Among the reference columns, P_d type column ($b/t = 30$, $s/d = 0.7$) is selected to study the influence of this material parameter. Overall column slenderness ratio is fixed at 25. Normal strength concrete of $f'_c = 30$ MPa and high strength of concrete $f'_c = 60$ MPa are selected to observe the overall effect of this parameter on the failure envelope of this

specific slender partially encased composite column. The increase in the zone of failure envelope between the two load moment interaction diagrams is found quite significant with the increase of the concrete strength of such large extent. Additionally, a greater increase in strength is found in compression zone compared to that of the tension zone of the interaction diagrams for the increment of 30MPa in the strength of concrete. An average increase of 40% is noted in compression zone, when the concrete strength is varied from 30MPa to 60MPa. On the other hand, in tension zone, strength of slender column, P_d increases with an average amount of 8% as concrete is strengthened within the selected range. Besides, balanced point occurs at an earlier stage when concrete strength is 60MPa comparatively when the same is at 30MPa. Consequently, a larger area in tension zone is observed at 60MPa concrete strength compared to the area of tension zone for the concrete strength of 30MPa.

4.3 SUMMARY

The parametric study of slender PEC column for bending about strong axis is conducted using four types of geometric parameter and a single material parameter. The effects of these parameters are observed through the formulation of load deflection curve and the load moment interaction curve of reference slender PEC columns.

The axial capacity of a slender partially encased composite column is reduced significantly as the overall slenderness ratio increases, particularly for columns with slender plates. The capacity of the column is reduced by 20% when L/d ratio is increased from 10 to 30. This reduction is more pronounced in columns with larger link spacing. Increase in the slenderness ratio also increases the lateral deflection at mid height. Due to the second order deflection the load deflection curves for columns with higher slenderness ratios show nonlinear behaviour as compared to columns with lower slenderness ratio.

For the eccentrically loaded columns, load carrying capacity is found to drop significantly with an increase in eccentricity. A 20% reduction in the axial capacity is found by increasing the eccentricity ratio (e/d) from 0.1 to 0.2. About 50% reduction is observed when e/d ratio is increased to 0.5. The effect of the ratio of initial load eccentricity to the overall depth of the column cross-section is observed to increase the mid-height lateral

displacement of slender columns significantly and is found more pronounced for columns with higher L/d ratio.

Moreover, lateral deflection of slender column is increased when b/t ratio is increased within the three selected ranges. The axial capacity and deflection of the PEC column is observed to be slightly affected by the range of link spacing selected in this parametric study.

Among the selected parameters, slenderness ratio, flange plate slenderness ratio and concrete strength are varied to observe the influence of these parameters on P-M curve of slender PEC column. Decrease in strength is found with the increase of overall slenderness ratio and flange plate slenderness ratio. Again, failure envelope becomes smaller with the increase of overall slenderness ratio. It implies the ductility of slender PEC column decreases with the increase of the overall slenderness ratio. However, failure envelope becomes unaffected while varying the flange plate thickness ratio. As the strength of concrete increases from 30MPa to 60MPa, strength of slender PEC column is observed to increase by 40%.

PARAMETRIC STUDY ON PEC COLUMN
UNDER WEAK AXIS BENDING

5.1 INTRODUCTION

In the weak axis of the PEC column, lower stiffness is achieved due to the thin steel plate of the PEC column. Consequently, the failure of the PEC column under bending about this axis becomes brittle. To investigate the effects of the selected parameters on the behaviour of slender PEC columns under weak axis bending, a parametric study is conducted in a similar manner as conducted for the major axis bending.

5.2 DESIGN OF PARAMETRIC STUDY

Similar type of cross-section of slender PEC column as described in chapter 4 is selected. The geometric properties of four reference columns are shown in Table 4.1. Slenderness ratios (L/d) used in the study are 10, 15, 20, 25 and 30 whereas the load eccentricity ratios (e/d) used in this study are 0.1, 0.2, 0.3, 0.4 and 0.5. The flange plate slenderness ratios (b/t) are selected as 25, 30 and 35 and link spacing-to-depth ratios (s/d) are taken as 0.5 and 0.7. Two values of concrete strength (f_c') – 30MPa and 60MPa are taken into consideration. The influence of these parameters on the behaviour of PEC columns about weak axis bending are presented in the following sections.

5.2.1 Effect of Load Eccentricity Ratio (e/d)

The effects of column load eccentricity (e/d) ratio on the axial capacity and mid-height lateral deflection of the column are shown in Table 5.1 to 5.5. For column P_b with L/d ratio of 15, increasing in the e/d ratio from 0.1 to 0.2, 0.3, 0.4 and 0.5 decreases the ultimate load capacity by 27%, 44%, 55% and 63% respectively and increases the lateral

deflection by 39%, 56%, 64% and 67% respectively (Table 5.1). An average decrease of 22% is found for 10% increase in initial load eccentricity ratio of this slender PEC column. The mid-height lateral deflection increases with an average value of 15% with every 10% increment in load-eccentricity ratio.

In the weak axis bending of this specific type of slender PEC column, a higher declination (difference 7%) is observed in the load carrying capacity compared to that in the strong axis bending. Again, in case of PEC column P_b with L/d ratio of 25, increasing the e/d ratio from 0.1 to 0.2, 0.3, 0.4 and 0.5 decreases the ultimate load capacity by 29%, 45%, 55% and 61% and increases the deflection by 15%, 25%, 32% and 34% respectively (Table 5.2). For slenderness ratio 25, axial load carrying capacity of this slender PEC column decreases with an average rate of 21% and the lateral deflection increases at a rate of 8% for every 10% increment in the load eccentricity ratio. However, similar to strong axis bending, the change in lateral deflection of slender PEC column is significant within the range of load-eccentricity ratio of 0.1 to 0.2 for both slenderness ratios. Here, a larger decreasing rate (difference 7%) in load capacity of slender PEC column is found than that of major axis bending.

For column P_d with L/d ratio of 15 and 25, for an increment of 0.1 in load eccentricity ratio, the ultimate load capacity is reduced by 28%, 45%, 56%, 64% and 28%, 45%, 55%, 62% respectively. At the same time, mid-height lateral deflections of these PEC columns are increased by 36%, 50%, 60%, 61% and 24%, 31%, 36%, 40% respectively. At slenderness ratio 15, the average reduction rate in axial capacity is found 23% whereas for slenderness ratio 25, this rate is found as 21%. These rates are almost 9% and 5% greater than that are found from strong axis bending. The lateral deflection increases with an average rate of 14% and 10% for overall column slenderness ratio 15 and 25 respectively.

Again, for column P_a with L/d ratio of 25, increasing the e/d ratio from 0.1 to 0.2, 0.3, 0.4 and 0.5 decreases the ultimate load capacity by 28%, 45%, 55% and 61% and increases the deflection by 26%, 35%, 39% and 46% respectively (Table 5.5). Both of the analysis results show that reduction in ultimate load capacity and increase in lateral deflection accelerated with the increase in load eccentricity ratio. The ultimate capacity reduction

rate is quite same of that for column P_b , since the main distinguishing feature of these two columns is the spacing of transverse links. The average variation in axial capacity and lateral deflection is found as 21% and 11% for the increment in load eccentricity ratio of 0.1d.

Table 5.1: Effect of Load Eccentricity Ratio at $L/d = 15$

Col^m	e/d	L/d	b/t	s/d	$P_u(kN)$	$\Delta_u(mm)$	% variation in P_u	% variation in Δ_u
P_b	0.1				5800	10.4	–	–
	0.2				4250	14.5	27	39
	0.3	15	25	0.7	3250	16.2	44	56
	0.4				2600	17.0	55	64
	0.5				2150	17.4	63	67

Table 5.2: Effect of Load Eccentricity Ratio at $L/d = 25$

Col^m	e/d	L/d	b/t	s/d	$P_u(kN)$	$\Delta_u(mm)$	% variation in P_u	% variation in Δ_u
P_b	0.1				5050	34.9	–	–
	0.2				3600	40.1	29	15
	0.3	25	25	0.7	2800	43.7	45	25
	0.4				2300	46.0	55	32
	0.5				1950	46.9	61	34

Table 5.3: Effect of Load Eccentricity Ratio at $L/d = 15$

Col^m	e/d	L/d	b/t	s/d	$P_u(kN)$	$\Delta_u(mm)$	% variation in P_u	% variation in Δ_u
P_d	0.1				5300	12.4	–	–
	0.2				3800	16.8	28	36
	0.3	15	30	0.7	2900	18.6	45	50
	0.4				2350	19.8	56	60
	0.5				1900	20.0	64	61

Table 5.4: Effect of Load Eccentricity Ratio at $L/d = 25$

Col^m	e/d	L/d	b/t	s/d	$P_u(kN)$	$\Delta_u(mm)$	% variation in P_u	% variation in Δ_u
P _d	0.1				4440	38.3	—	—
	0.2				3200	47.3	28	24
	0.3	25	30	0.7	2450	50.0	45	31
	0.4				2000	52.0	55	36
	0.5				1700	53.6	62	40

Table 5.5: Effect of Load Eccentricity Ratio at $L/d = 25$

Col^m	e/d	L/d	b/t	s/d	$P_u(kN)$	$\Delta_u(mm)$	% variation in P_u	% variation in Δ_u
P _a	0.1				5150	32.8	—	—
	0.2				3700	41.2	28	26
	0.3	25	25	0.5	2850	44.3	45	35
	0.4				2300	45.6	55	39
	0.5				2000	47.8	61	46

Figure 5.1 to 5.5 shows the relation between axial load and mid-height lateral deflection for the selected reference PEC columns when bending occurs about the weak axis of these columns.

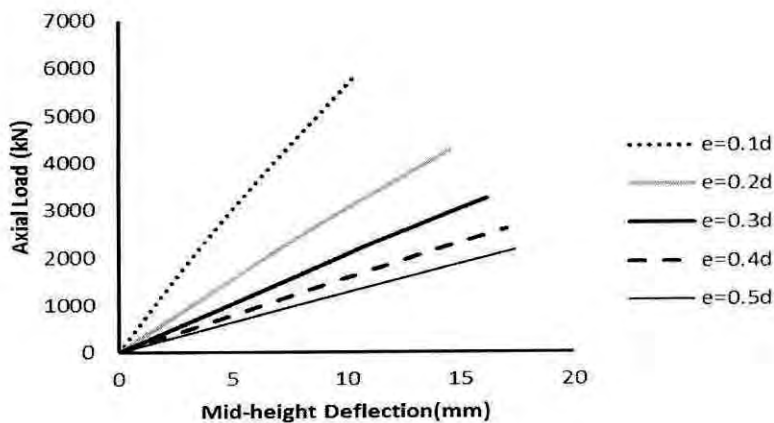


Fig. 5.1: Effect of e/d ratio on axial load to lateral deflection curve of column P_b with L/d ratio of 15

Figure 5.1, 5.2 and 5.5 demonstrates the load to deflection curves for column P_b and P_a (which has a b/t ratio of 25) with two different slenderness ratios ($L/d = 15$ and 25). On the other hand Fig. 5.3 and 5.4 show the similar curves for column P_d (b/t ratio of 30) for the similar ranges of L/d ratios.

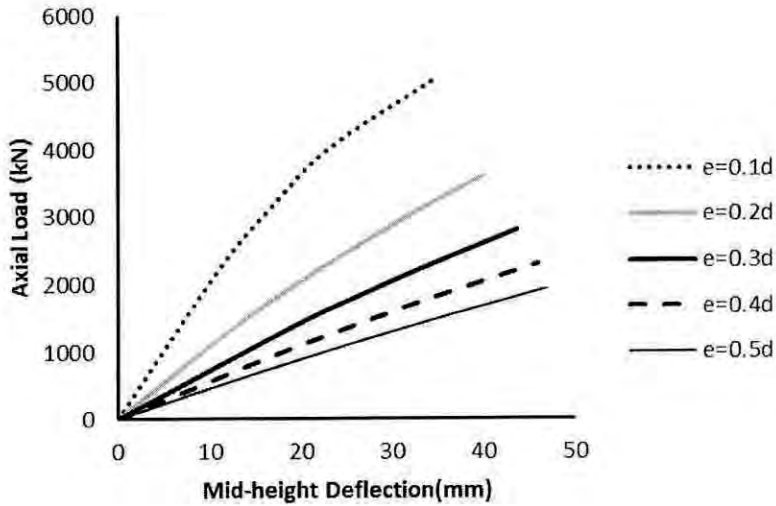


Fig. 5.2: Effect of e/d ratio on axial load to lateral deflection curve of column P_b with L/d ratio of 25

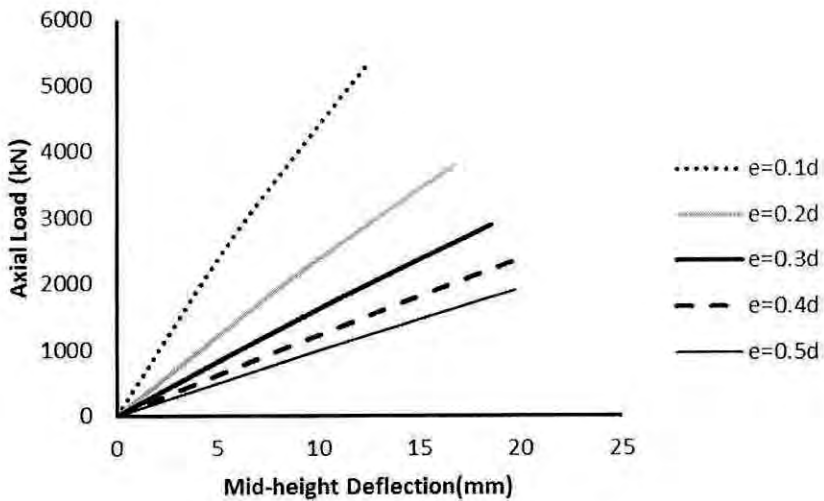


Fig. 5.3: Effect of e/d ratio on axial load to lateral deflection curve of column P_d with L/d ratio of 15

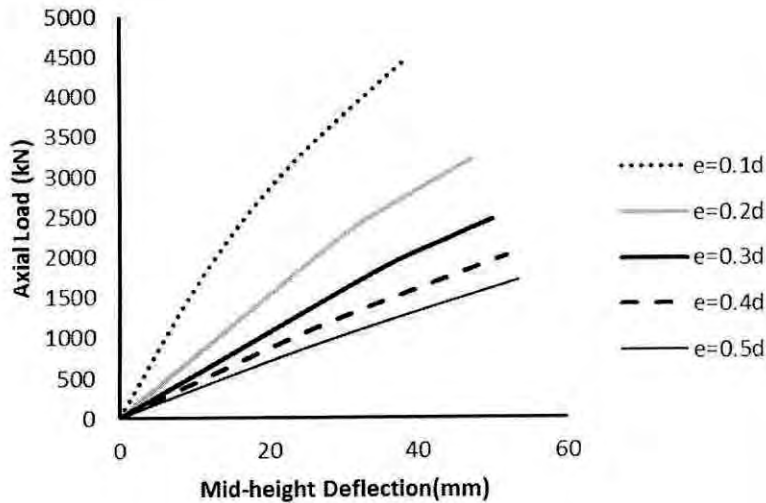


Fig. 5.4: Effect of e/d ratio on axial load to lateral deflection curve of column P_d with L/d ratio of 25

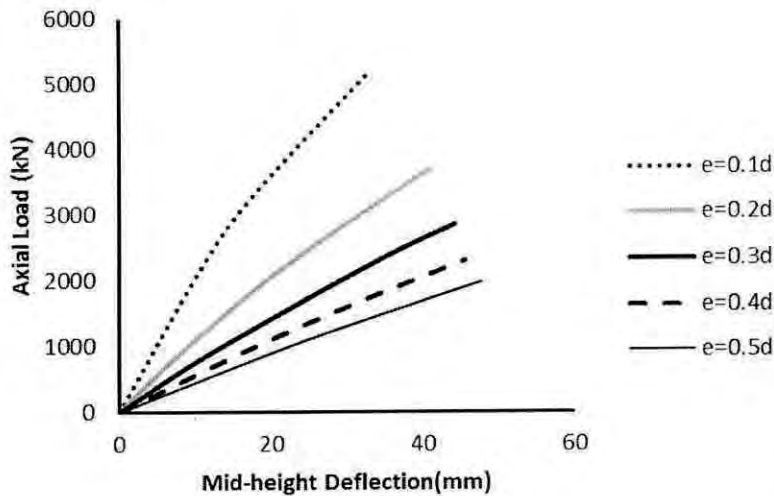


Fig. 5.5: Effect of e/d ratio on axial load to lateral deflection curve of column P_a with L/d ratio of 25

It is obvious from the study that the ultimate axial capacity of slender PEC column is significantly influenced by the amount of initial load eccentricity ratio. With the increase of the initial load eccentricity, the load-carrying capacity decreases significantly with an increase in the mid height lateral deflection of slender PEC column. In weak axis bending also, columns with higher slenderness ratio of 25, the load to deflection curves show relatively nonlinear behaviour as compared to the curves for columns with L/d ratio of 15.

5.2.2 Effect of Overall Column Slenderness Ratio (L/d)

Tables 5.6 to 5.8 show the influence of overall column slenderness (L/d) ratio on the behaviour of selected slender PEC columns. For column P_a (which has a s/d ratio of 0.5 and a b/t ratio of 25) if L/d ratio is increased by 5, 10, 15 and 20 the ultimate load capacity is reduced by 5%, 12%, 20% and 26% respectively (Table 5.6).

Again, for column P_b (which has a b/t ratio of 25 and s/d ratio of 0.7) an increase in the L/d ratio by 5, 10, 15 and 20 decreases the ultimate load capacity by 5%, 11%, 19% and 25% and increases the deflection by 123%, 293%, 509% and 776% respectively which are almost similar to column P_a (Table 5.7).

The average reduction rate in axial load capacity is found as 8% and 7% in column P_a and P_c with the selected increment of slenderness ratio of PEC column. Similar to the cases as described in the previous subsection, slight higher amount (only 2%) in the decreasing rate of load carrying capacity is found when bending occurs in weak axis instead of the major axis.

For column P_d , an increase in the L/d ratio by 5, 10, 15 and 20 reduces the ultimate load capacity by 5%, 12%, 21% and 30% respectively. Again, lateral deflections increased by 130%, 311%, 538% and 820% respectively (Table 5.8). Nevertheless, the average reduction in load carrying capacity of slender PEC column P_d is slightly higher (9%) as in column P_a or P_c .

Table 5.6: Effect of Overall Slenderness Ratio on Column P_a at $e/d=0.2$

Col^m	L/d	e/d	b/t	s/d	$P_u(kN)$	$\Delta_u(mm)$	% variation in P_u	% variation in Δ_u
P_a	10				4600	6.3	–	–
	15				4350	14.2	5	125
	20	0.2	25	0.5	4050	25.3	12	302
	25				3700	41.2	20	554
	30				3400	58.0	26	821

Table 5.7: Effect of Overall Slenderness Ratio on Column P_c at $e/d=0.3$

Col^m	L/d	e/d	b/t	s/d	$P_u(kN)$	$\Delta_u(mm)$	% variation in P_u	% variation in Δ_u
P_c	10				3150	8.2	–	–
	15				3000	18.3	5	123
	20	0.3	30	0.5	2800	32.2	11	293
	25				2550	49.9	19	509
	30				2350	71.8	25	776

Table 5.8: Effect of Overall Slenderness Ratio on Column P_d at $e/d=0.4$

Col^m	L/d	e/d	b/t	s/d	$P_u(kN)$	$\Delta_u(mm)$	% variation in P_u	% variation in Δ_u
P_d	10				4050	7.1	–	–
	15				3850	16.3	5	130
	20	0.4	30	0.7	3550	29.2	12	311
	25				3200	45.3	21	538
	30				2850	65.3	30	820

The effects of overall column slenderness ratio ($L/d = 10$ to $L/d = 30$) on PEC columns are presented in Fig. 5.6 to 5.8, remaining the load eccentricity ratio constant. Fig. 5.6 and 5.8 show the behaviour for PEC column with e/d ratio of 0.2 whereas Fig. 5.7 shows the behaviour with e/d ratio of 0.3.

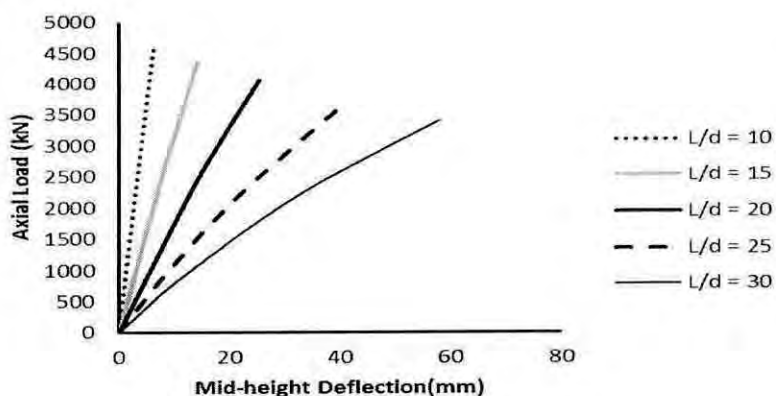


Fig. 5.6: Effect of L/d ratio on axial load to lateral deflection curve of column P_a with e/d ratio of 0.2

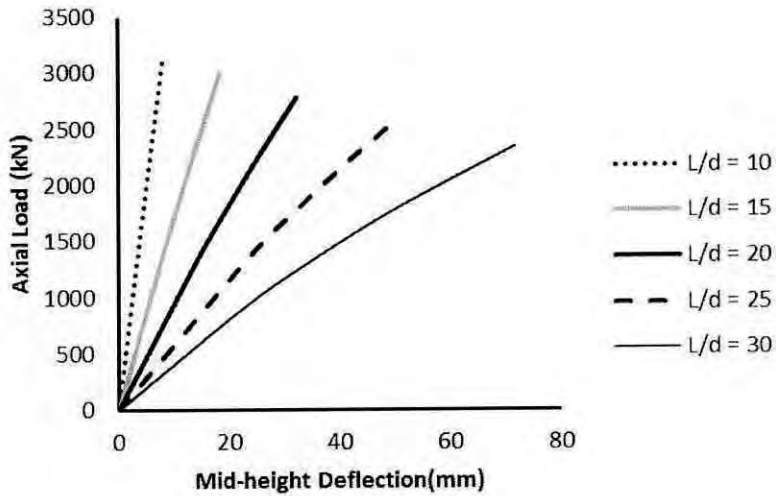


Fig. 5.7: Effect of L/d ratio on axial load to lateral deflection curve of column P_c with e/d ratio of 0.3

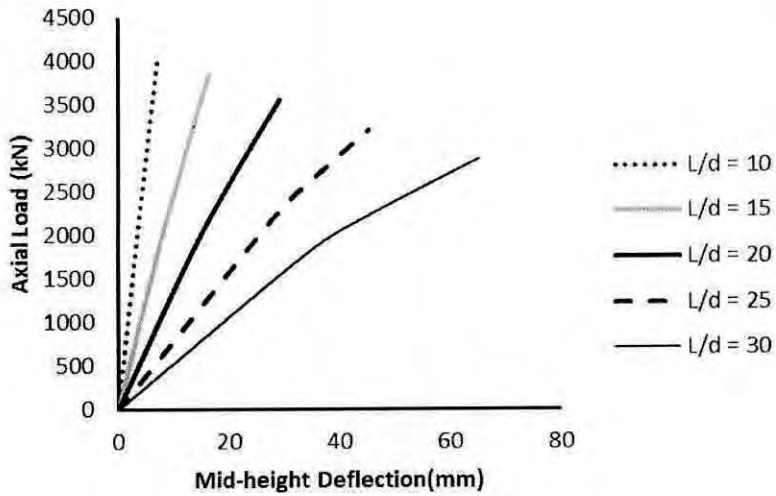


Fig. 5.8: Effect of L/d ratio on axial load to lateral deflection curve of column P_d with e/d ratio of 0.2

The nonlinear curves present an exponential increase in the mid-height lateral deflection of slender PEC column with the increase in the overall column slenderness ratios. In addition, drops in ultimate axial load capacity of PEC column is also manifested from the obtained curves.

The effect of overall column slenderness ratio on the ultimate axial load and corresponding deflection for the two different types of columns are shown in Fig. 5.9 and 5.10 respectively. The effect of L/d ratio on ultimate load and also on the lateral deflection at the mid-height of the columns shows similar trend.

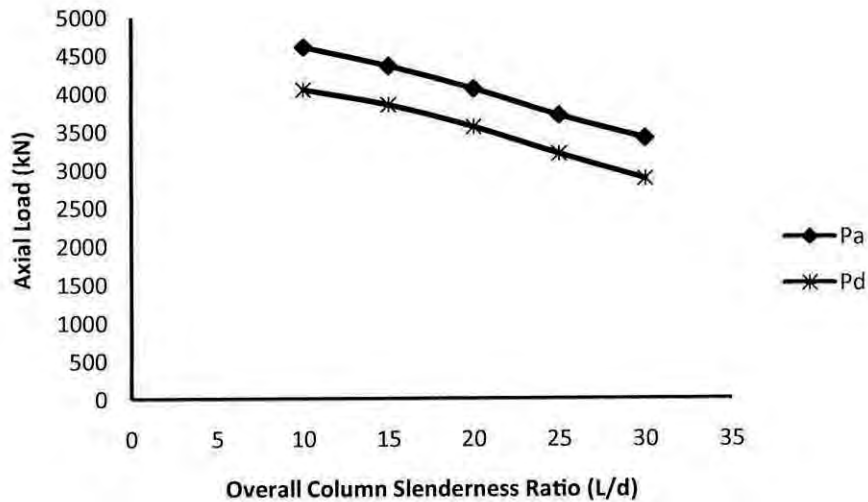


Fig. 5.9: Effect of overall column slenderness ratio on axial load capacity of PEC column

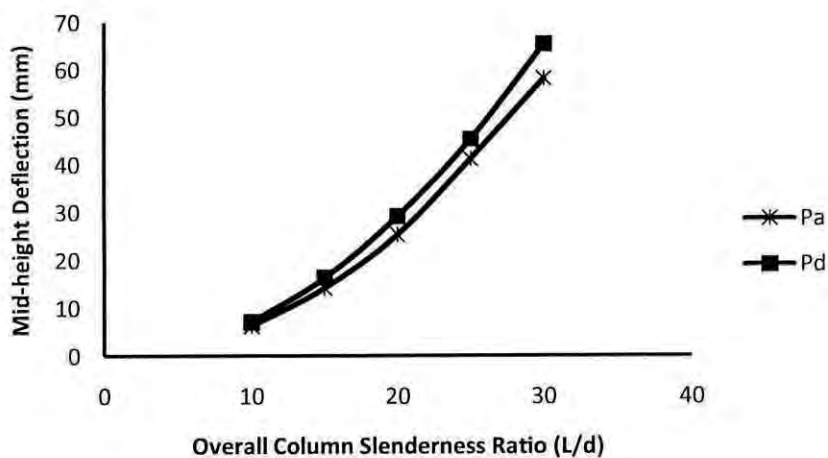


Fig. 5.10: Effect of overall column slenderness ratio on mid-height deflection of PEC column

5.2.3 Effect of Flange Plate Slenderness Ratio (b/t)

The effects of flange plate slenderness (b/t) ratio on the axial capacity and mid-height lateral deflection of slender PEC column are shown in Table 5.9 and 5.10, Increasing

b/t from 25 to 30 and 25 to 35 causes a reduction of 14% and 21% respectively in the axial load capacity of PEC column, P_b . The average reduction in the axial capacity is 12%. At the same time, lateral deflection is increased by 16% and 28% respectively (Table 5.9). The average increment in lateral deflection becomes 13% in the selected range of flange plate slenderness ratio. For the bending of slender column about in both strong and weak axis these average values are almost similar.

Again, for column P_c , an increase in the b/t ratio by 5 and 10 decreases the ultimate load capacity by 11% and 18% and increases the deflection by 13% and 22% respectively (Table 5.10). For this slender PEC column, the load carrying capacity is reduced with an average value of 10%. At the same condition, lateral deflection is increased by 11%.

Table 5.9: Effect of Flange Plate Slenderness (b/t) Ratio on Column P_b

Col^m	e/d	L/d	b/t	s/d	$P_u(kN)$	$\Delta_u(mm)$	% variation in P_u	% variation in Δ_u
P_b			25		3300	56.1	–	–
	0.2	30	30	0.7	2850	65.3	14	16
			35		2600	71.9	21	28

Table 5.10: Effect of Flange Plate Slenderness (b/t) Ratio on Column P_c

Col^m	e/d	L/d	b/t	s/d	$P_u(kN)$	$\Delta_u(mm)$	% variation in P_u	% variation in Δ_u
P_c			25		2850	44.3	–	–
	0.3	25	30	0.5	2550	49.9	11	13
			35		2350	54.1	18	22

The effects of flange plate slenderness ratio on PEC columns at a fixed load eccentricity ratio and overall column slenderness ratio are presented in Figs 5.11 and 5.12.

Figure 5.11 shows the behaviour of slender PEC column at initial load-eccentricity ratio of 0.2 and slenderness ratio 30, whereas Fig. 5.12 shows for the load eccentricity ratio of 0.3 and slenderness ratio of 25. With the increase of flange plate slenderness ratio, stiffness of

column is reduced. So, significant reduction in axial load capacity and increase in the mid-height lateral deflection of slender PEC column is observed from both of the curves.

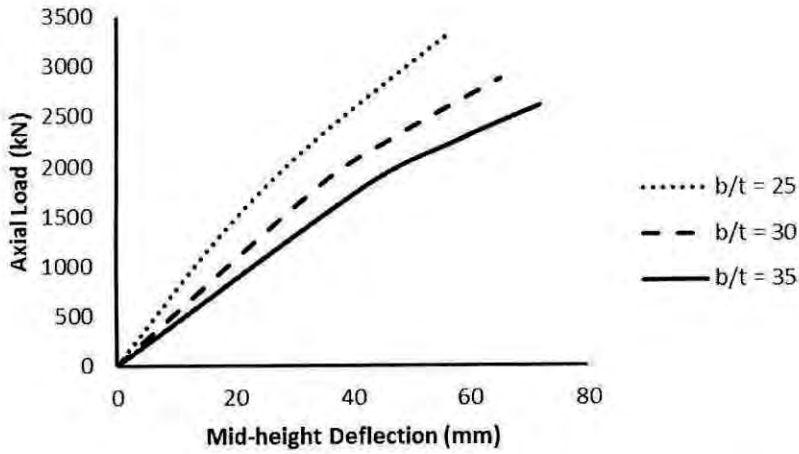


Fig. 5.11: Effect of b/t ratio on axial load to lateral deflection curve of column P_b with e/d 0.2 and L/d 30

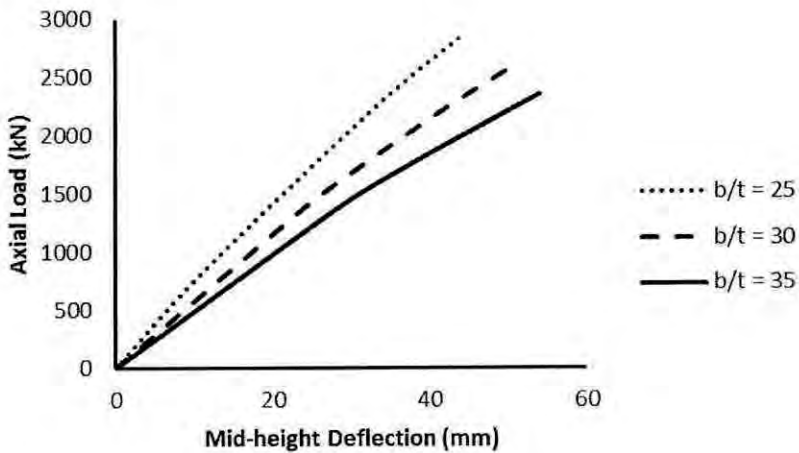


Fig. 5.12: Effect of b/t ratio on axial load to lateral deflection curve of column P_c with e/d 0.3 and L/d 25

5.2.4 Effect of Link Spacing to Depth Ratio (s/d)

Two values of link spacing to depth ratio (s/d)- 0.5 and 0.7 is studied in the parametric study. The ultimate capacity of axial load drops only 3% when the link spacing to depth

ratio has been varied within the range mentioned earlier. The lateral deflections of slender columns are affected with only 3% by the s/d ratios (Table 5.11).

Table 5.11: Effect of Link Spacing to Depth Ratio on Column P_b

Col^m	e/d	L/d	b/t	s/d	$P_u(kN)$	$\Delta_u(mm)$	% variation in P_u	% variation in Δ_u
P_b	0.2	25	25	0.5	3700	41.2	—	—
				0.7	3600	40.1	3	3

The effects of link spacing-to-depth ratio on PEC columns at a fixed load eccentricity ratio and slenderness ratio are presented in Fig. 5.13.

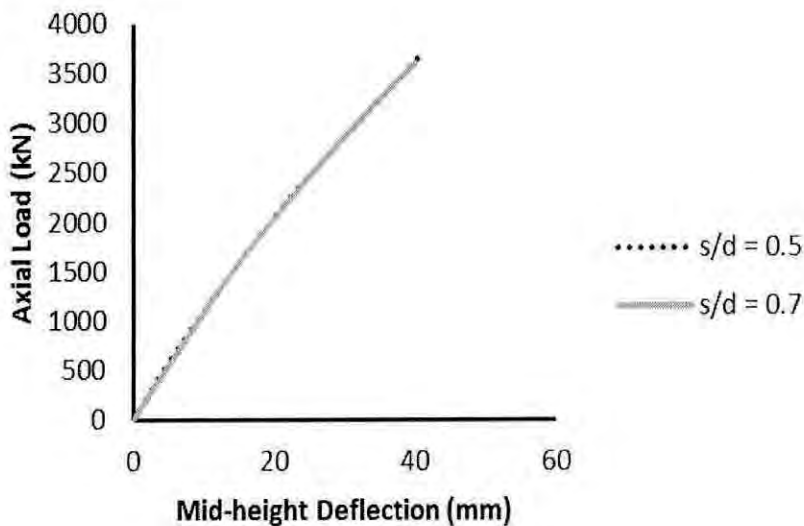


Fig. 5.13: Effect of link s/d ratio on axial load to lateral deflection curve of P_b column with e/d 0.2 and L/d 25

The load to deflection curves for the columns with two different link spacing-to-depth ratios 0.5 and 0.7, subjected to an initial load eccentricity ratio of 0.2 and slenderness ratio 25 is shown. It can be clearly seen that the two graphs coincide, i.e. consequence of spacing-to-depth ratio on ultimate capacity of axial load and lateral deflection is negligible.

5.2.5 Effect of Slenderness Ratio on P-M Curve

The effects of overall column slenderness ratio on the load-moment interaction diagram of PEC columns are shown in Fig. 5.14. PEC column, P_d is taken to conduct the study for the weak axis bending.

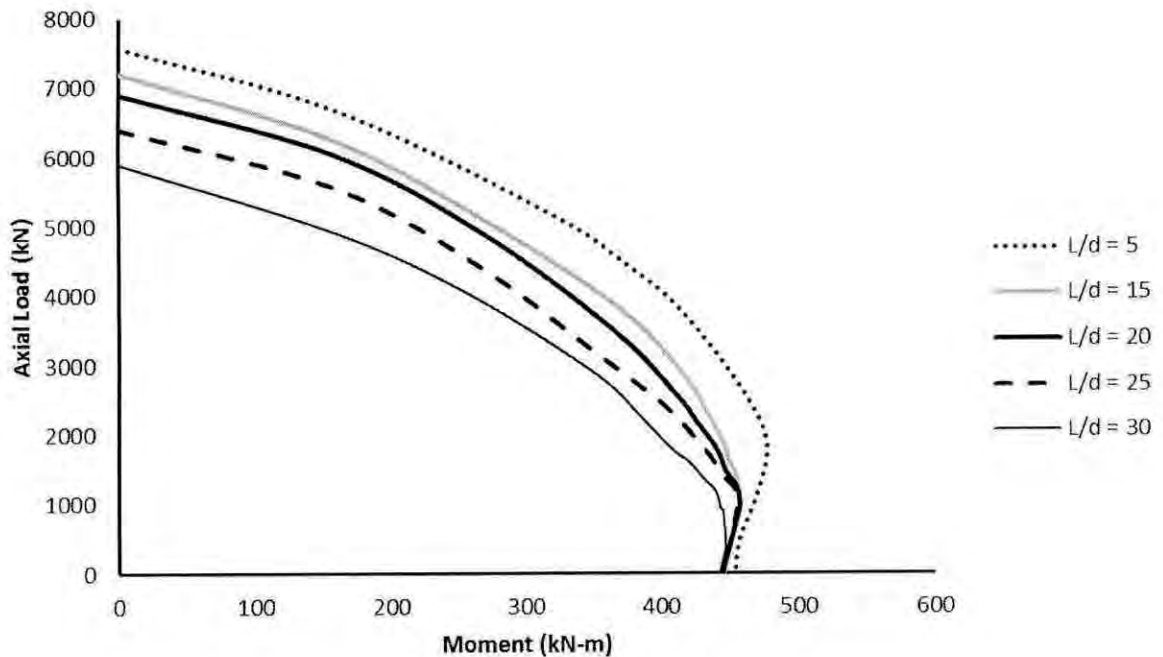


Fig. 5.14: Effect of overall column slenderness ratio on interaction diagram of slender PEC column.

The load-moment interaction diagrams show that the area of the failure envelope decreases significantly with the increase of the overall slenderness ratio of PEC column. With the increase of the overall column slenderness ratio, the PEC columns become brittle and this is clearly observed when weak axis bending is considered. In weak axis bending, a large gap is observed in the compression zones among the different slenderness ratios and it is found to be diminished at the end of the tension zone of any load-moment interaction diagram.

The strength reduction of PEC column is found to be insignificant in tension zone compare to that in the compression zone of the load-moment interaction diagram. In the compression zone of PEC column, in the range of a short column ($L/d = 5$) to a slender column ($L/d = 15$) an average reduction of 10% is observed. However, as column

slenderness ratio increase from 15 to 20, only 5% average reduction in strength is found. However, variation of column slenderness ratio from 20 to 25 shows a sharp decline in the strength of PEC column. In this case, an average reduction rate of 9% is found. Finally, strength of slender PEC column drops with an average value of 11% as the slenderness of column reaches to 30. Alike strong axis bending, here also balanced point occurs slightly at a later stage as the PEC columns become more slender.

5.2.6 Effect of Flange Plate Slenderness Ratio on P-M Curve

Fig. 5.15 illustrates the effects of flange plate slenderness ratio (b/t) on the load-moment curve of PEC columns. Reference slender PEC column P_d with a slenderness ratio of 30 is taken to study the influence of this parameter.

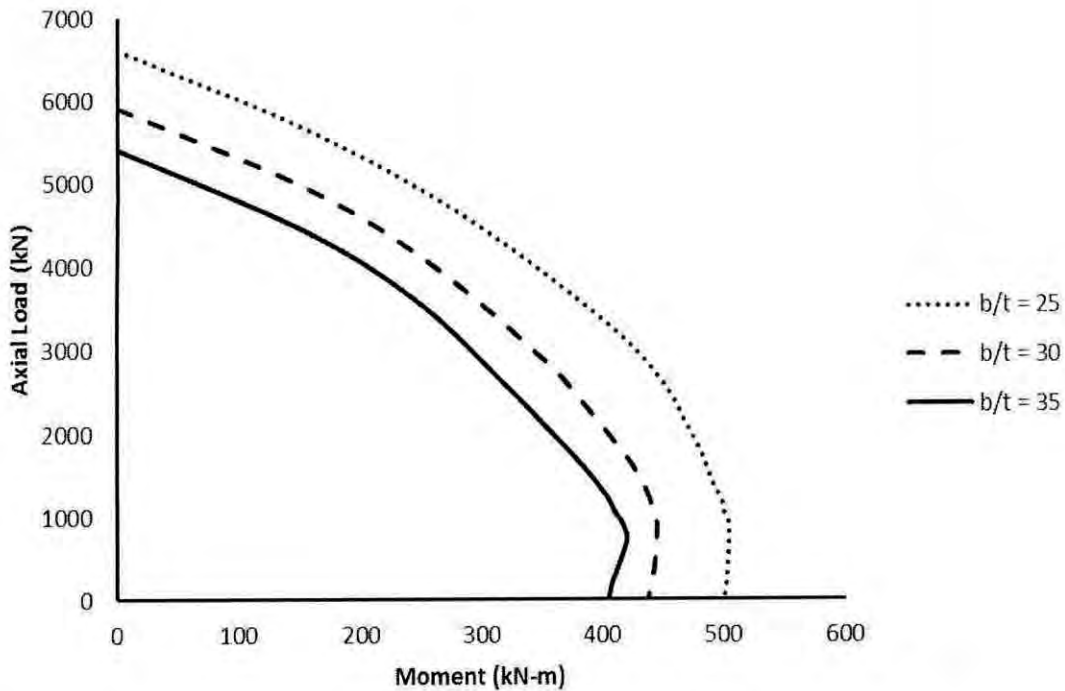


Fig. 5.15: Effect of flange plate slenderness ratio on interaction diagram of slender PEC column.

The interaction diagrams show a significant reduction in the zone of failure envelope with the increase of the flange plate slenderness ratio of PEC column. An average reduction of 17% is noted in compression zone, when the flange plate slenderness ratios increased from 25 to 30. Variation of flange plate slenderness ratio from 30 to 35, average drop in

strength is observed as nearly 16%. In tension zone, strength of slender PEC column decreases with an average amount of 12% as b/t ratio is varied from 25 to 30. When b/t ratio is increased from 30 to 35, comparatively a lower reduction in average strength (9%) is found as observed in compression zone. Besides, similar to strong axis bending, formation of balanced point occurs at a slight earlier stage as the flange plate slenderness ratio increases.

5.2.7 Effect of Concrete Strength on P-M Curve

The effects of concrete strength on the load-moment curve of partially encased composite columns are illustrated in Fig. 5.16.

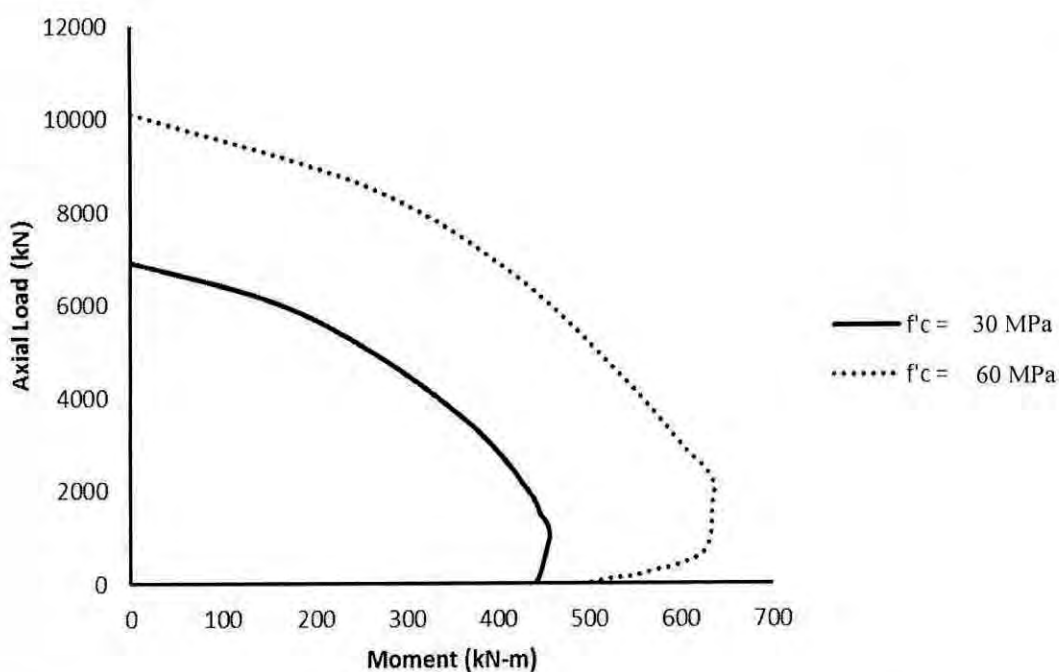


Fig. 5.16: Effect of concrete strength on interaction diagram of slender PEC column.

Among the reference columns, P_d type column is selected to study the influence of concrete strength. Overall column slenderness ratio is fixed at 20. Normal strength and high strength of concrete ($f'_c = 30$ MPa, $f'_c = 60$ MPa) are selected to observe the overall effect of this parameter on strength of slender PEC column. The area of the failure envelope is found to be increased considerably with the increase of the concrete strength. An average increase of 33% is found in compression zone, when the concrete strength is

varied within the selected range whereas in tension zone, an average increment of 19% is noted.

5.3 CONCLUSIONS

The parametric study of slender PEC column is conducted about the weak axis bending. Load deflection curves and load moment curves for slender PEC column constructed with a variety of geometric parameters selected are studied to determine the effect of this parameter on column behaviour.

Alike strong axis bending, the axial capacity of a slender partially encased composite column is reduced significantly with the increase in the load eccentricity ratio (e/d). The axial capacity drops in a greater amount in weak axis bending since lower stiffness is achieved here. Moreover, increasing the e/d ratio from 0.1 to 0.2 reduces the axial capacity by 28% whereas increasing the e/d ratio to 0.4 reduces the capacity by 62% as compared to the capacity corresponding to $e/d = 0.1$. These values are higher from that observed in major axis bending. Mid-height deflection is found to increase in a significant rate with the increase of e/d .

Overall slenderness ratio (L/d) influences the axial capacity of slender PEC column inversely. About 25% reduction in the axial capacity is observed by increasing the L/d ratio from 5 to 30. The decreasing rate is found almost similar as observed in strong axis bending. In addition, exponential increase in lateral deflection is observed with the increase in the slenderness ratio.

Flange plate slenderness ratio (b/t) is proved to be an important parameter in decreasing the load carrying capacity of slender PEC column subjected to weak axis bending. Increasing the b/t ratio from 25 to 35 decreases the axial load capacity by 20%. The average variation rate follows the trend of that found in major axis bending. Lateral deflection of slender column is increased significantly when b/t ratio is increased within this range. On the other hand, spacing of transverse links is found to have insignificant effect on the behaviour of slender PEC column.

Slenderness effect on load-moment curve is more significant from slenderness ratio of 25 or more. In the interaction diagram, a reduction in failure load in the compression zone is found to be around 45% when L/d ratio is increased from 5 to 30. The tension zone in the interaction diagram is observed to be comparatively much smaller. Use of high strength concrete (60MPa) results in 33% increase in strength of PEC column compared with normal strength concrete.

CONCLUSIONS AND RECOMMENDATIONS

6.1 GENERAL

The behaviour of slender partially encased composite (PEC) column under eccentric loading is studied numerically. The numerical tool is formulated using the Newmark's numerical iterative procedure. The load deflection curve and the load moment interaction diagram for slender PEC columns are established. The ultimate load carrying capacity, deflection at the ultimate point and bending moment capacity for slender PEC columns are estimated using the proposed method. The performance of this method is demonstrated by comparing the long column tests from published literature (Chicoine et al., 2000). The ultimate capacity of the test columns are compared to that obtained numerically. The proposed numerical method is observed to predict the experimental results with reasonable accuracy.

The numerical method presented is used to conduct an extensive parametric study on PEC columns under major and minor axis bending. The variable parameters included in the parametric study are initial load eccentricity ratio (e/d), overall column slenderness ratio (L/d), flange plate slenderness ratio (b/t), link spacing to depth ratio (s/d) and compressive strength of concrete (f'_c). The effects of these parameters are studied on the load to mid height deflection curve, ultimate load and maximum lateral deflection of PEC columns subjected to axial compression and bending. Moreover, the effects of these parameters on the load moment interaction curve of slender PEC column are studied. The major conclusions of the parametric study are included in the following section.

6.2 CONCLUSIONS

The numerical procedure developed is found to predict the ultimate load of slender PEC column with reasonable accuracy. From limited study about 90% accuracy is demonstrated on an average. Here, the parametric study is divided into two parts and the relevant conclusions are given below.

6.2.1 Parametric Study under Strong Axis Bending

The axial capacity of a partially encased composite column is reduced significantly as the overall slenderness ratio increases, particularly for columns with slender plates. About 20% reduction in axial capacity is observed by increasing the L/d ratios from 10 to 30. Effect of second order deflection on total deflection is found to be insignificant when L/d ratio is 10.

For the eccentrically loaded columns, load carrying capacity is found to drop significantly with an increase in eccentricity. Increasing the e/d ratio from 0.1 to 0.5 reduces the axial capacity by about 50%. The effect of the ratio of initial load eccentricity to the overall depth of the column cross-section is observed to increase the lateral displacement of slender columns significantly and is found more pronounced for columns with higher L/d ratio.

The lateral deflection of slender column is increased when b/t ratio is increased within the selected range. The axial capacity and deflection of the PEC column is observed to be slightly affected by the range of link spacing selected in this study.

Among the selected parameters, slenderness ratio, flange plate slenderness ratio and concrete strength are varied to observe the influence of these parameters on P-M curve of slender PEC column. Decrease in strength is found with the increase of slenderness ratio and flange plate slenderness ratio. When the slenderness ratio reaches to 25, the reduction in strength is more significant. At the same time, failure envelope becomes smaller with the increase of slenderness ratio. As the strength of concrete increases, strength of slender PEC column increases in large amount. The results showed that increasing the concrete strength from 30MPa to 60MPa enhances the column capacity 40%. Moreover, a smaller

tension zone is observed in the P-M curve as slenderness ratio and concrete strength increases.

6.2.2 Parametric Study under Weak Axis Bending

Similar to strong axis bending, the axial capacity of a slender partially encased composite column is reduced significantly with the increase in the load eccentricity ratio. The axial capacity drops in a greater amount in weak axis bending since lower stiffness is achieved here. About 62% reduction in the axial capacity is found by increasing the e/d ratio from 0.1 to 0.5. Mid-height deflection is found to increase at a significant rate with the increase of this parameter. Overall slenderness ratio influences the axial capacity of slender PEC column inversely. About 25% reduction in the axial capacity is observed by increasing the L/d ratio from 5 to 30.

Larger flange plate slenderness ratio is observed to be an important parameter in reducing the load carrying capacity. The average variation rate follows the trend of that found in major axis bending. Besides, lateral deflection of slender column is increased when b/t ratio is increased within this range. Moreover, spacing of transverse links is found to be insignificant on the behaviour of slender PEC column. In weak axis bending, the tension zone is observed to be comparatively much smaller than compression zone that is found in case of strong axis bending. Slenderness effect on load-moment curve is more significant for slenderness ratio of 25 or more. In addition, a greater increase in strength is found in compression zone compared to that of the tension zone of the interaction diagrams for the increment of 30MPa in the strength of concrete. An average increase of 33% is found in compression zone, when the concrete strength is changed from 30MPa to 60MPa whereas in tension zone, an average increment of 19% is noted.

6.3 DESIGN RECOMMENDATIONS

Based on the results of the parametric study the following design recommendations may be provided which are resembled to the design guidelines of Canadian steel design code (CSA-S16-09).

- i) Eccentricity of axial load has significant influence on the ultimate capacity of slender PEC column. From the analysis result, it is found that increase in the e/d

ration from 0.1 to 0.2 causes a significant drop (about 20%) in axial load. Therefore, to reduce the stability failure it is beneficial to keep the e/d ratio within 0.1.

- ii) Observing the effect of overall slenderness ratio (L/d) on the strength of PEC column it is recommended to maintain the slenderness ratio less than 25.
- iii) The impact of the selected parameter on slender PEC column is found to be more vulnerable for weak axis bending. In weak axis bending, the failure of slender PEC column is also observed to be brittle compared to PEC column in major axis bending. Behaviour under weak axis can be improved by the use of additional rebars or using high performance concrete (such as fibre reinforced concrete) in PEC columns.
- iv) Since a considerable decline in strength occurs at flange plate thickness ratio of 30 due to thinner flange plate, it is recommended to maintain the flange plate slenderness ratio less than 30.
- v) Concrete strength can improve the load carrying capacity of slender PEC column significantly. High strength concrete can be used in the design of slender PEC columns, however, the ductility of high strength concrete PEC columns under cyclic loading can be improved by confining the concrete or introducing high performance materials.
- vi) There is no significant benefit of utilizing lower link spacing in slender PEC columns; rather it increases the cost of construction. A link spacing less than 0.5 may not be used for slender PEC columns.

The findings of the current study can also be helpful in proposing design equations for increased lateral moment and reduced flexural stiffness for this composite section.

6.4 RECOMMENDATIONS FOR FUTURE RESEARCH

The numerical study is carried out for slender PEC column subjected to monotonic vertical loading only. Additional study may be carried out on the behaviour of PEC column subjected to cyclic horizontal loads.

The numerical study is conducted up to the peak load point for slender PEC column acting under eccentric loading condition. In future, post peak behaviour of these types of columns may be studied and analyzed by numerical simulations.

Material nonlinearity is not considered in formulating the load deflection response of slender PEC columns. The numerical method can be modified to include nonlinear material behaviour of concrete in future research.

REFERENCES

- AISC, (2005). American Institute of Steel Construction, Inc. "Code of Standard Practice for Steel Buildings and Bridges", One East Wacker Drive, Suite 3100, Chicago, Illinois.
- Begum, M., Driver, R.G. and Elwi, A.E. (2007). "Finite-Element Modelling of Partially Encased Composite Columns Using the Dynamic Explicit Method." ASCE Structural Journal, Vol. 133, 326-334.
- Begum, M. (2007). "Partially Encased Composite Columns: an Innovative Composite Structural System." Proceedings of New Technologies for Urban Safety of Mega Cities in Asia, Dhaka, Bangladesh.
- Bouchereau, R., and Toupin, J.-D. (2003). "Étude du Comportement en Compression-Flexion des Poteaux Mixtes Partiellement Enrobés." Report EPM/GCS-2003-03, Dept. of Civil, Geological and Mining Engineering, Ecole Polytechnique, Montreal, Canada.
- Chicoine, T., Tremblay, R., Massicotte, B., Yalcin, M., Ricles, J., and Lu, L.-W. (2000). "Test Programme on Partially-Encased Built Up Three-Plate Composite Columns." *Joint Report EPM/GCS No. 00-06*, February, Dept. of Civil, Geological and Mining Engineering, Ecole Polytechnique, Montreal, Canada – ATLSS Engineering Research Centre, No. 00-04, Lehigh University, Bethlehem, Pennsylvania, USA.
- Chicoine, T., Tremblay, R., Massicotte, B., Ricles, J., and Lu, L.-W. (2002). "Behaviour and Strength of Partially-Encased Composite Columns with Built Up Shapes." *Journal of Structural Engineering*, ASCE, Vol. 128 (3), 279-288.
- CSA., 2001. CSA S16-01, Limit States Design of Steel Structures, Canadian Standard Association, Toronto, ON.
- Dastfan, M. (2011), "Ductile steel plate shear walls with PEC columns", Ph. D. Thesis, Department of Civil and Environmental Engineering, University of Alberta, Alberta, AB, Canada.
- Deng, X., Dastfan, M., and Driver, R. G. (2008), "Behaviour of steel plate shear walls with composite columns", Proc., American Society of Civil Engineers Structures Congress, Vancouver, BC.
- Filion, I. (1998). "Étude Expérimentale des Poteaux Mixtes Avec Section d'acier de classe 4." Report n°. EPM/GCS-1998-06, Dept. of Civil, Geological and Mining Engineering, Ecole Polytechnique, Montreal, Canada.
- Mirza, S.A., and Tikka, T.K. (1999). "Flexural Stiffness of Composite Columns Subjected to Major Axis Bending." *ACI Structural Journal*, Vol. 96, 19-28.
- Mirza, S.A., and Tikka, T.K. (2005). "Equivalent Uniform Moment Diagram Factor for Composite Columns in Major Axis Bending." *ASCE Structural Journal*, Vol. 131, 569-581.

Newmark, N. M. (1943). "Numerical Procedures for Computing Deflections, Moments, and Buckling Loads." Trans. ASCE, 108, 1161-1234.

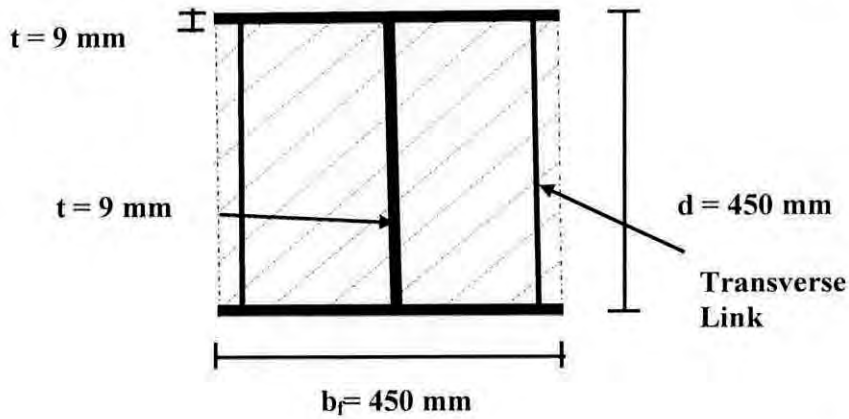
Prickett, B. S. and Driver, R. G. (2006). "Behaviour of Partially Encased Composite Columns Made with High Performance Concrete." Structural Engineering Report No 262, Dept. of Civil and Environmental Engineering, University of Alberta, AB, Canada.

Tremblay, R., Massicotte, B., Filion, I., and Maranda, R. (1998). "Experimental Study on the Behaviour of Partially Encased Composite Columns Made with Light Welded H Steel Shapes under Compressive Axial Loads." Proceedings of SSRC Annual Technical Session & Meeting, Atlanta, 195-204.

Wight, K.J. and MacGregor, J.G. (2009). "Reinforced Concrete: Mechanics and Design", 5th Edition, Pearson Prentice Hall, New Jersey, 540-550.

APPENDIX

A slender partially encased composite column of slenderness ratio (L/d) **25** is selected for the analysis. The cross-section of the column is **450 mm × 450 mm** in dimension. The following fig. shows in details the sectional properties of the column. In this analysis, flange plate slenderness ratio (b/t) and transverse link spacing to depth ratio (s/d) is selected as **25** and **0.7** respectively. Load eccentricity ratio of this eccentrically loaded column is selected as (e/d) **0.2**. Besides, 28 days cylindrical strength of concrete is taken as **30MPa**. Modulus of elasticity of steel (E_s) is selected as **200000MPa** and from the strength of concrete; modulus of elasticity of concrete (E_c) becomes **24862MPa**.



Moment of Inertia of steel section, $I_s = db_f^3/12 - [(d-t)*(b_f-2t)^3/12] = 4.6 \times 10^8 mm^4$

Moment of Inertia of concrete portion, $I_c = db_f^3/12 - I_s = 2.96 \times 10^9 mm^4$

Area of concrete, $A_c = (d-t)*(b_f-2t) = 190512 mm^2$

According to AISC (2005) effective flexural stiffness of composite column can be calculated as,

$$EI_{eff} = E_s I_s + C_1 E_c I_c$$

The co-efficient, C_1 is determined using the effective area of steel as follows:

$$C_1 = 0.1 + 2 \left(\frac{A_{se}}{A_c} + A_{se} \right)$$

Again,

$$A_{se} = (d - 2t + 2b_e)t$$

$$k = \frac{0.9}{\left(\frac{s}{b_f}\right)^2} + 0.2\left(\frac{s}{b_f}\right)^2 + 0.75, \quad \left(0.5 \leq \frac{s}{b_f} \leq 1\right)$$

$$= 2.68$$

$$\lambda_p = \frac{b}{t} \sqrt{\frac{12(1 - \nu_s^2)F_y}{\pi^2 E_s k}}$$

$$= 0.5$$

$$b_e = \frac{b_f}{(1 + \lambda_p^{2n})^{1/n}} \leq b_f$$

$$b_e = 416 \text{ mm}$$

$$A_{se} = 11376 \text{ mm}^2$$

$$C_I = 0.21$$

$$EI_{eff} = 1.1 \times 10^{14} \text{ N} - \text{mm}^2$$

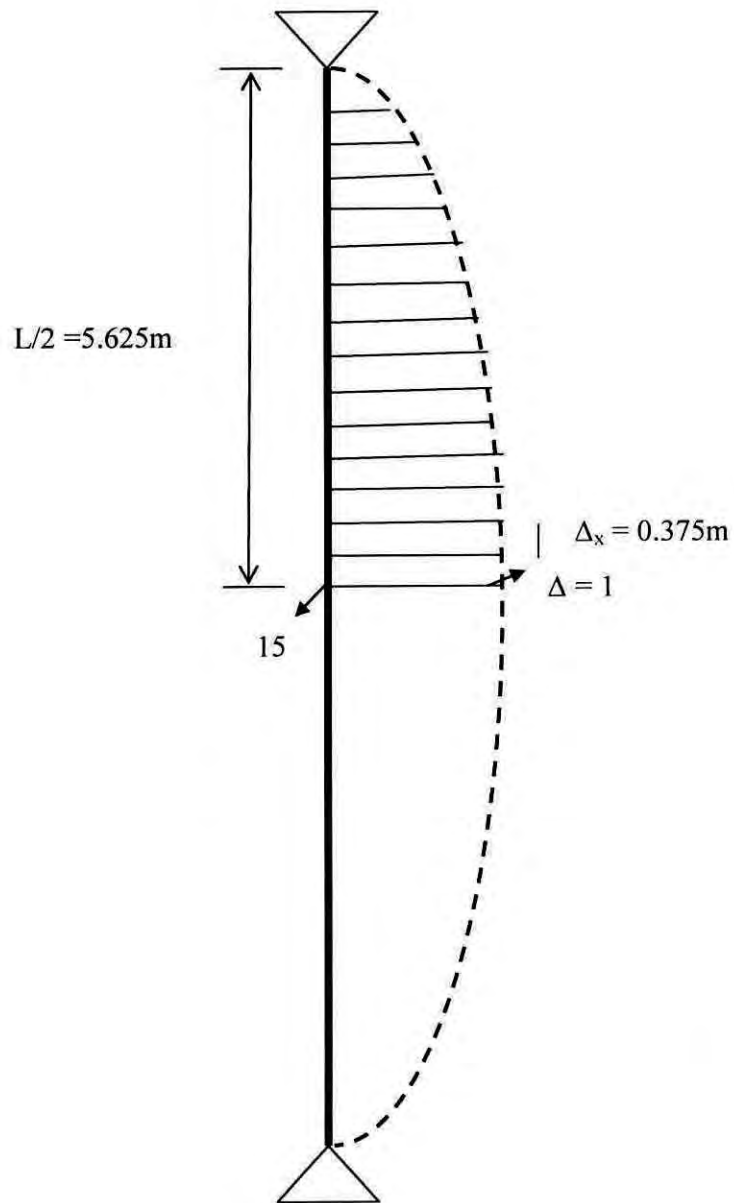


Fig.: Assumption of deflection in Newmark's method

Total moment at mid-height of column, $M = Pe + P\Delta = P(0.2 + 1)$

The values of deflections at other locations are determined by taking the deflected shape linear and corresponding moments are calculated.

Curvature at mid-height of column, $\phi = M/EI$

Determination of Equivalent Nodal Force:

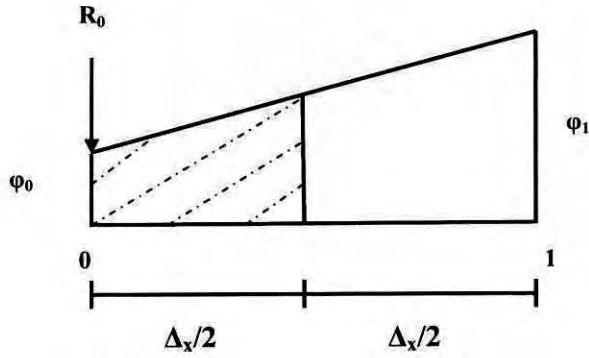


Fig.: Equivalent nodal force at extreme corner point

$$R_0 = \frac{1}{2} \left(\frac{\varphi_0 + \varphi_1}{2} \right) \left(\frac{\Delta_x}{2} \right)$$

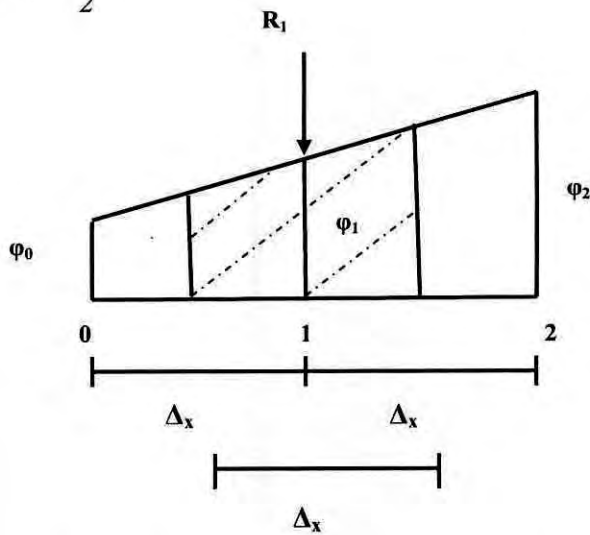


Fig.: Equivalent nodal force at interior point

$$R_1 = \frac{1}{2} \left(\frac{\varphi_0 + 2\varphi_1 + \varphi_2}{2} \right) (\Delta_x)$$

At mid-height of column,

$$R_{15} = \frac{1}{2} (\varphi_{14} + \varphi_{15}) (\Delta_x)$$

After determining equivalent nodal force, shear force diagram and bending moment diagram is drawn which are equivalent to the slope and deflection. The table A.1 to A.2 shows the result.

Calculation of Second order deflection using Newmark's Method

Table A.1: Calculation of second order deflection for an axial load of 1332 kN

Distance (m)	Initial Deflection (mm)	Total Moment (kN-m)	Curvature (per mm) (10^{-6})	Equivalent Nodal Force (10^{-4})	Slope	Deflection (mm)
0	0	122	0.99×10^{-6}	1.42	0.003	0
0.381	0.62	122.9	1×10^{-6}	1.91	0.0028	1.15
0.762	1.24	123.7	1.01×10^{-6}	1.92	0.0026	2.22
1.143	1.86	124.5	1.02×10^{-6}	1.94	0.0024	3.22
1.524	2.48	125.3	1.023×10^{-6}	1.95	0.0022	4.14
1.905	3.1	126.2	1.03×10^{-6}	1.96	0.002	5
2.286	3.72	127	1.04×10^{-6}	1.97	0.0018	5.77
2.667	4.34	127.8	1.043×10^{-6}	1.99	0.0016	6.47
3.048	4.96	128.7	1.05×10^{-6}	2	0.0014	7.09
3.429	5.58	129.5	1.06×10^{-6}	2.01	0.0012	7.64
3.81	6.2	130.3	1.063×10^{-6}	2.03	0.001	8.11
4.191	6.82	131.1	1.07×10^{-6}	2.04	0.0008	8.5
4.572	7.44	132	1.08×10^{-6}	2.05	0.0006	8.82
4.953	8.06	132.8	1.083×10^{-6}	2.07	0.0004	9.06
5.334	8.68	133.6	1.09×10^{-6}	2.08	0.0002	9.22
5.715	9.3	134.4	1.097×10^{-6}	2.08	0	9.3
6.096	8.68	133.6	1.09×10^{-6}	—	—	—

Table A.2: Calculation of second order deflection for an axial load of 2664 kN

Distance (m)	Initial Deflection (mm)	Total Moment (kN-m)	Curvature (per mm) (10^{-6})	Equivalent Nodal Force (10^{-4})	Slope	Deflection (mm)
0	0	244.1	1.99	2.85	0.0064	0
0.381	1.34	247.6	2.02	3.88	0.006	2.43
0.762	2.67	251.2	2.05	3.93	0.0056	4.72
1.143	4.01	254.8	2.08	3.99	0.0054	6.86
1.524	5.34	258.3	2.1	4.04	0.0052	8.84
1.905	6.68	261.9	2.14	4.1	0.0048	10.67
2.286	8.02	265.5	2.17	4.15	0.0044	12.35
2.667	9.35	269.0	2.19	4.21	0.004	13.86
3.048	10.69	272.6	2.22	4.26	0.0036	15.22
3.429	12.02	276.2	2.25	4.32	0.0031	16.41
3.81	13.36	279.7	2.28	4.37	0.0027	17.44
4.191	14.7	283.3	2.31	4.43	0.0022	18.3
4.572	16.03	286.9	2.34	4.48	0.0018	19
4.953	17.37	290.4	2.37	4.54	0.0013	19.52
5.334	18.7	294.0	2.4	4.59	0.0009	19.87
5.715	20.04	297.6	2.43	4.59	0	20.05
6.096	18.7	294.0	2.4	–	–	–

Table A.3: Calculation of second order deflection for an axial load of 3996 kN

Distance (m)	Initial Deflection (mm)	Total Moment (kN-m)	Curvature (per mm) (10^{-6})	Equivalent Nodal Force (10^{-4})	Slope	Deflection (mm)
0	0	366.1	2.98	4.3	0.01	0
0.381	2.17	374.8	3.06	5.89	0.0096	3.9
0.762	4.35	383.5	3.13	6.02	0.0091	7.58
1.143	6.52	392.2	3.2	6.16	0.0084	11.03
1.524	8.7	400.9	3.27	6.3	0.0078	14.24
1.905	10.87	409.6	3.34	6.43	0.0071	17.21
2.286	13.05	418.4	3.41	6.57	0.0065	19.94
2.667	15.22	427.1	3.48	6.7	0.0058	22.42
3.048	17.39	435.8	3.55	6.84	0.0051	24.64
3.429	19.57	444.5	3.62	6.97	0.0044	26.6
3.81	21.74	453.2	3.7	7.11	0.0037	28.3
4.191	23.92	461.9	3.77	7.24	0.003	29.73
4.572	26.09	470.6	3.83	7.38	0.0022	30.88
4.953	28.27	479.3	3.91	7.51	0.0015	31.75
5.334	30.44	488	3.98	7.65	0.0008	32.33
5.715	32.61	496.7	4.05	7.65	0	32.62
6.096	30.44	488	3.98	—	—	—

Table A.4: Calculation of second order deflection for an axial load of 5582 kN

Distance (m)	Initial Deflection (mm)	Total Moment (kN-m)	Curvature (per mm) (10^{-6})	Equivalent Nodal Force (10^{-4})	Slope	Deflection (mm)
0	0	511.4	4.17	6.03	0.016	0
0.381	3.38	530.3	4.33	8.39	0.015	5.96
0.762	6.76	549.2	4.48	8.68	0.014	11.59
1.143	10.14	568.1	4.63	8.97	0.013	16.9
1.524	13.52	587	4.79	9.27	0.012	21.86
1.905	16.9	605.9	4.94	9.56	0.011	26.47
2.286	20.28	624.9	5.1	9.85	0.01	30.72
2.667	23.66	643.8	5.25	10.14	0.009	34.59
3.048	27.04	662.7	5.41	10.44	0.008	38.07
3.429	30.42	681.6	5.56	10.74	0.007	41.16
3.81	33.8	700.5	5.71	11.03	0.006	43.83
4.191	37.18	719.4	5.87	11.32	0.005	46.09
4.572	40.56	738.3	6.02	11.61	0.004	47.92
4.953	43.94	757.2	6.18	11.91	0.002	49.3
5.334	47.32	776.1	6.33	12.2	0.001	50.23
5.715	50.7	795	6.48	12.2	0	50.7
6.096	47.32	776.1	6.33	–	–	–

Calculated moments at different axial load on slender PEC column to plot P-M curve:

Axial Load (kN)	Deflection (mm)	Moment (kN-m)
1332	9.3	134
2664	20.05	298
3996	32.62	497
5582	50.7	795

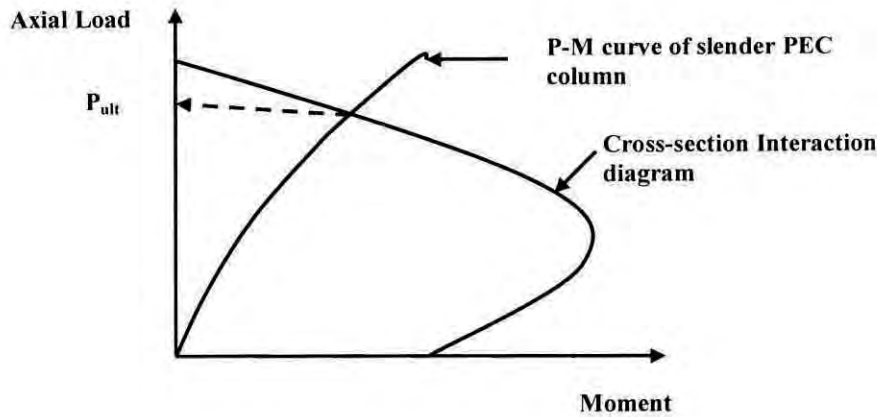


Fig: Determination of axial load capacity of slender PEC column

In a similar way as shown in the tables, deflection for P_{ult} is determined and Load-deflection curve is completed.

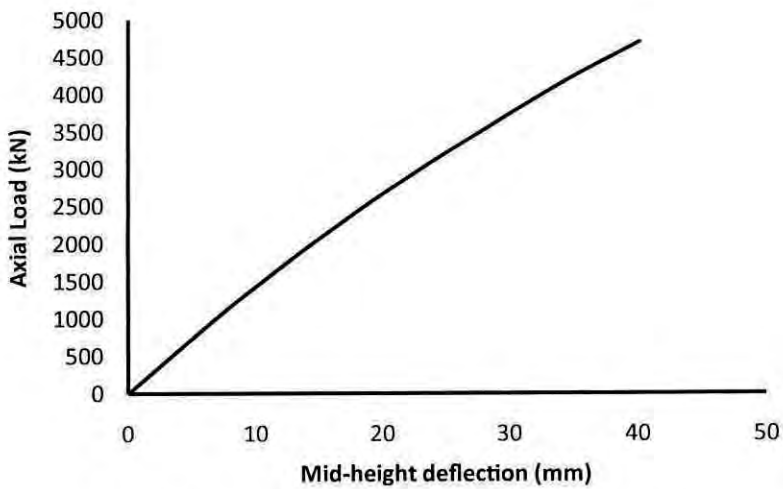


Fig.: Load-deflection response of PEC column

Formulation of interaction diagram for slender PEC column:

The load eccentricity ratios (e/d) are varied from 0.05 to 50. Then the following procedure is followed.

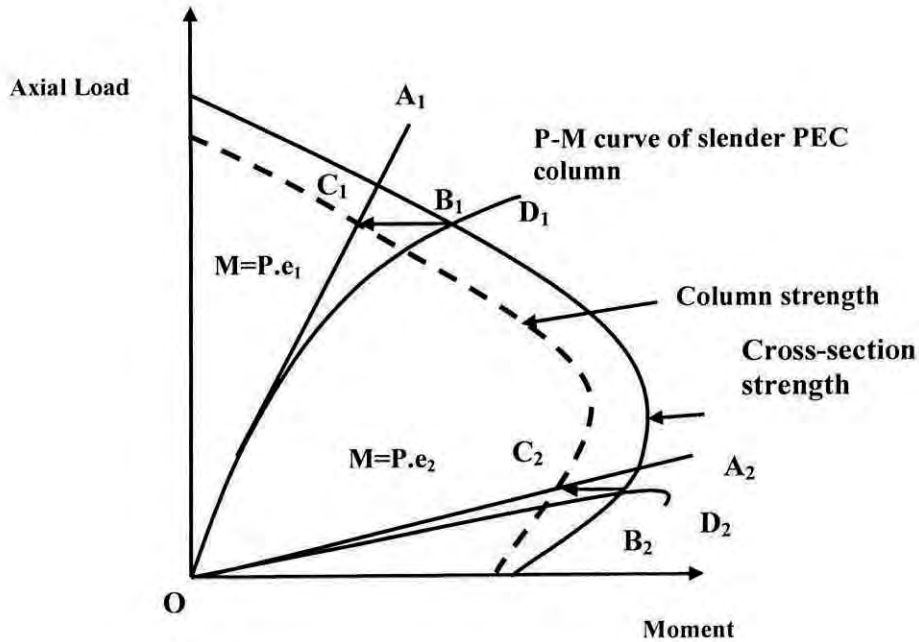


Fig.: Formation of interaction diagram for PEC column

For $e/d = 0.1$, the point C (308, 5800) and for $e/d = 0.8$ the point E (888, 2200) .

P-M curve at different eccentricities

Eccentricity is 5% of the depth of column

Load (kN)	Moment (kN-m)
0	0
2220	60
4440	143
6660	262
6850	274

Eccentricity is 10% of the depth of column

Load (kN)	Moment (kN-m)
0	0
2220	120
4440	286
5106	349
5900	432

Eccentricity is 20% of the depth of column

Load (kN)	Moment (kN-m)
0	0
1332	134
2664	298
3996	497
4700	620

Eccentricity is 30% of the depth of column

Load (kN)	Moment (kN-m)
0	0
1110	165
2220	359
3330	588
4000	746

Eccentricity is 40% of the depth of column

Load (kN)	Moment (kN-m)
0	0
888	173
1776	371
2664	595
3450	820

Eccentricity is 50% of the depth of column

Load (kN)	Moment (kN-m)
0	0
666	160
1332	336
1998	530
3007	863

Eccentricity is 60% of the depth of column

Load (kN)	Moment (kN-m)
0	0
666	192
1332	403
1998	636
2800	948

Eccentricity is 70% of the depth of column

Load (kN)	Moment (kN-m)
0	0
666	224
1110	386
1554	558
2400	919

Eccentricity is 80% of the depth of column

Load (kN)	Moment (kN-m)
0	0
666	256
1110	441
1776	741
2160	928

Eccentricity is 90% of the depth of column

Load (kN)	Moment (kN-m)
0	0
444	189
888	390
1332	605
2000	955

Eccentricity is 100% of the depth of column

Load (kN)	Moment (kN-m)
0	0
444	210
888	434
1332	672
1850	971

Eccentricity is 250% of the depth of column

Load (kN)	Moment (kN-m)
0	0
444	525
555	661
666	800
800	971

Eccentricity is 500% of the depth of column

Load (kN)	Moment (kN-m)
0	0
222	517
266	622
311	728
400	943

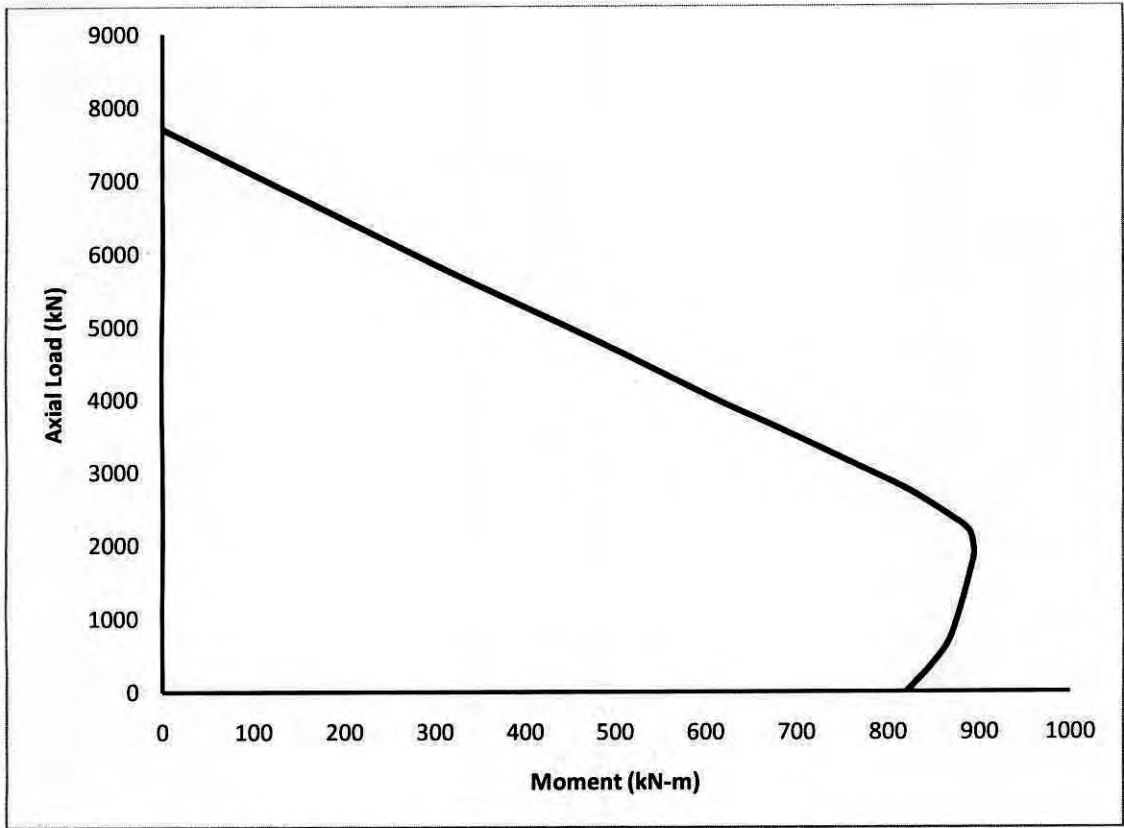


Fig.: Interaction diagram for slender PEC column

